

ALMA MATER STUDIORUM - UNIVERSITÀ DI BOLOGNA

SCHOOL OF ENGINEERING

*Department of
Electrical, Electronic, and Information Engineering
"Guglielmo Marconi"*

DEI

INGEGNERIA DELL'ENERGIA ELETTRICA

curriculum:

ELECTRICAL ENGINEERING

MASTER THESIS

in

Compatibilità Elettromagnetica Industriale M

**Misalignment Tolerant Model and Force Calculation in a
Resonator Array for Inductive Power Transfer**

**Presented by:
Mattia Simonazzi**

**Supervisor:
Prof. Leonardo Sandrolini**

**Co-supervisors:
Prof. Emeritus Ugo Reggiani
Dr. José Alberto**

**Academic Year 2018/2019
Session II**

*To those who have been close to me
in this journey of intellectual
and personal growth.*

Contents

Abstract	1
1 Introduction	3
1.1 Metamaterials	7
1.1.1 Analogy between relay coils and metamaterials	10
1.2 MIW	11
1.2.1 Circuit approach	14
1.2.2 Matching the transmission line	16
2 Misalignment Tolerant Model	19
2.1 Resonator array with a receiver	19
2.2 Receiver bigger than the array resonators	24
2.3 General case	26
2.4 More receivers	29
2.5 Parameters	34
2.5.1 Array Parameters	34
2.5.2 Mutual interactions	36

3	Inductance Calculation	39
3.1	Prototype	39
3.2	FEM Approach	40
3.2.1	Numerical Simulation	41
3.2.2	Results	44
3.3	Partial Inductance Approach	48
3.3.1	Analytical approach-Campbell Approach	52
3.3.2	Matlab Implementation	53
3.4	Result comparison	59
4	Current Calculation	61
4.1	Theoretical model	62
4.2	Numerical Implementation and Results	66
4.2.1	Input Variables	67
4.2.2	Simulation for low distance receiver	68
4.2.3	Simulation for large distance receiver	80
4.3	Conclusions	83
5	Experimental Verification	85
5.1	Experimental Setup	86
5.1.1	Power Source	87

<i>CONTENTS</i>	iii
5.1.2 Measurements Instrumentation	87
5.1.3 Array	88
5.2 Results	92
6 Force Calculation	101
6.1 Introduction	101
6.2 Forces of electromagnetic origin	102
6.2.1 Virtual work approach	104
6.2.2 Magnetic field generated by the array	107
6.2.3 Final formulation for the calculation of the fore action on the receiver	109
6.3 Numerical model	110
6.4 Results	112
7 Conclusions	121
7.1 Future perspective	123
Acknowledgments	125
Bibliography	127

List of Figures

1.0.1 Resonant coils with an intermediate coil acting as a relay.	5
1.0.2 Resonant coils forming a two-dimensional metamaterial.	6
1.0.3 Traditional apparatus for the wireless transmission of power.	6
1.1.1 Negative and positive refraction of an EM wave incident on a surface.	8
1.1.2 Split ring resonators as pipe (a), in printed circuit (b) and as complementary variety (c).	9
1.1.3 Three dimensional metamaterial structure.	10
1.1.4 Equivalent circuit of a 1-D structure of relay resonators.	11
1.2.1 Four-poles: “T model” equivalent circuit for a transmission line.	13
1.2.2 Four-poles: model for two coupled R-L-C circuits	13
2.1.1 Array of coupled resonators with a receiver over them.	20
2.1.2 Equivalent circuit of a resonator array with a receiver of the same dimension of the cells.	22
2.2.1 Resonator array with a receiver which is twice the size of the resonators.	24

2.2.2 Equivalent circuit of a resonator array with a receiver which is twice the size of an array cell.	26
2.3.1 General case: resonator array with a receiver which covers all the cells.	27
2.3.2 Equivalent circuit for the general case of a resonator array with a receiver which covers all the cells.	29
2.4.1 Example: resonator array with two receivers of different size.	30
2.4.2 Equivalent circuit for the case of more receiver fed by the resonator array.	34
3.2.1 Model of the system in Maxwell environment.	42
3.2.2 Plot of the mesh on the object forming constituting the apparatus.	44
3.2.3 Mutual inductance between a cell and a receiver moving over it.	46
3.2.4 Comparison of the mutual inductance between a cells and a receiver moving over it	47
3.2.5 Mutual inductance coefficient.	48
3.3.1 Representation of the coil in Matlab environment.	54
3.3.2 Representation of the receiver coil in different positions.	55
3.3.3 Mutual inductance coefficients as a function of the x displacement for different values of z : $z = 10mm$ for the first plot, $z = 40mm$ for the second plot and $z = 90mm$ for the third.	57
3.3.4 Mutual inductance for the extended x domain.	58
4.2.1 Magnitude of the current in the first resonator of the array.	69
4.2.2 Magnitude of the current in the first resonator of the array in small scale.	69

4.2.3 Magnitude of the current in the second resonator of the array. 70

4.2.4 Magnitude of the current in the third resonator of the array. 71

4.2.5 Magnitude of the current in the fourth resonator of the array. 72

4.2.6 Magnitude of the current in the fifth resonator of the array. 73

4.2.7 Magnitude of the current in the sixth resonator of the array. 74

4.2.8 Magnitude of the current in the receiver circuit. 75

4.2.9 Comparison of the receiver current with the currents of an array with 6 resonators for $z = 10mm$ 77

4.2.10 Comparison of the receiver current with the currents of an array with 8 resonators $z = 10mm$ 79

4.2.11 Comparison of the receiver current with the currents of an array with 6 resonators $z = 40mm$ 81

4.2.12 Comparison of the receiver current with the currents of an array with 6 resonators $z = 90mm$ 82

5.0.1 Representation of the resonator array with a receiver. 86

5.1.1 Resonator prototype: stranded wire wound around square wood block. 89

5.1.2 Experimental setup of an array of six resonators connected to the signal generator and loaded with an identical resonator acting as a receiver, placed over the last but one element. 90

5.2.1 Comparison of the measured and calculated currents for the first resonator of the array. 93

5.2.2 Comparison of the measured and calculated currents for the first resonator of the array.	93
5.2.3 Comparison of the measured and calculated currents for the third resonator of the array.	95
5.2.4 Comparison of the measured and calculated currents for the fourth resonator of the array.	96
5.2.5 Comparison of the measured and calculated currents for the fifth resonator of the array.	97
5.2.6 Comparison of the measured and calculated currents for the sixth resonator of the array.	97
5.2.7 Comparison of the measured and calculated currents for the receiver.	98
6.3.1 Representation of the coil exploited in the simulation.	110
6.4.1 Force on the receiver along the x direction as function of the receiver displacement with a discretization for the current element of $0.5mm$	115
6.4.2 Force on the receiver along the y direction as function of the receiver displacement with a discretization for the current element of $0.5mm$	116
6.4.3 Force on the receiver along the z direction as function of the receiver displacement with a discretization for the current element of $0.5mm$	117
6.4.4 Force on the receiver along the x direction as function of the receiver displacement with a discretization for the current element of $0.1mm$	118
6.4.5 Force on the receiver along the y direction as function of the receiver displacement with a discretization for the current element of $0.1mm$	119
6.4.6 Force on the receiver along the z direction as function of the receiver displacement with a discretization for the current element of $0.1mm$	120

Abstract

In this work, an inductive power transfer (IPT) system composed of an array of multiple magnetically coupled resonant inductors (cells) has been considered, allowing to increase the transmission distance or consider the misalignment between the emitter and receiver coils. The analysis of the arrays can be carried out with the theory of magneto-inductive waves (MIW) or with circuit theory, whereas this second approach has been followed. The impedance matrix of the resonator array has been modelled for different receiver shape and dimension. Moreover, it has and expressed as a function of the space improving the accuracy of the model. This latter has been exploited to calculate all the currents and voltages of the system. In first approximation, only the displacement in the MIW propagation direction has been considered, whereas the contribution of the receiver is expressed as a defect and becomes a function of the space as the mutual inductances between the circuits vary according to the receiver position. The self- and mutual inductance coefficients have been evaluated for each circuit of the system by applying the partial inductance methods, whose formulas have been implemented in Matlab environment. These results have been validated by means of magnetostatic FEM analysis of the system using the software Ansys Maxwell. Experimental measurements on a prototype of a 1-D resonator array have been performed, confirming the calculated values of the currents and as a consequence, of the mutual inductances. The last part of the thesis is devoted to the calculation of the mechanical forces of electromagnetic origin experienced by the receiver that covers the array, as a result of the interaction between the whole magnetic field - generated by all the array cells - and the current circulating in the receiver. These forces have been theoretically discussed first, with

a subsequent implementation the calculation in Matlab environment and an analysis of the obtained results.

Chapter 1

Introduction

From the beginning of the studies in electrical engineering science, the transmission and distribution of the electrical energy without any physical connection has represented a great technological challenge, giving life to several inventions and patents. For a long time, wireless power transfer (WPT) was considered to be not viable and against a background of disbelief it was not until the end of the twentieth century that real commercial WPT systems appeared [1]. An extended review of the history is presented in [2]. The origin can be considered Maxwell's "Treatise on Electricity and Magnetism", published in 1873 [3], where he predicted that power could be transmitted from one point to another in free space by means of electromagnetic waves, and then Hertz validated Maxwell's equations with his subsequent experiment. At the early beginning of the previous century, the famous Nikola Tesla started to perform other experiments for the transmission of electrical power from one point to another without wires and, furthermore, he patented a systems for transmitting electrical energy between two coils [4] which was based on magnetic resonance. Originally, one purpose was to employ the "invention on an industrial scale as, for instance, for lighting distant cities or districts from places where cheap power is obtainable". Wireless power transfer (WPT) systems can be indeed used for large number of purposes, ranging from electrical vehicle charging to powering portable medical devices and electronic equipment. The technology has continued to evolve including more powerful systems, operating under difficult

conditions in worldwide applications. Among all the possible applications, the most popular ones are related to recharge batteries in vehicular technology [5], to power and recharge implantable medical devices [6] or Radio-Frequency Identification (RFID) systems [7], or mobile appliances such as portable computers or mobile phones [8]. Moreover, these systems have the advantage of being capable of transferring power even in harsh environments with water, dust or dirt and allow the bypass of electrical contact. In general, the applications can be addressed to direct wireless powering of stationary or dynamic devices or automatic wireless charging of portable/movable devices. In the former applications power is supplied directly to the electrical devices, whereas in the latter a battery storing energy is necessary. WPT systems can be divided mainly in two categories: far-field (radiative) and near-field (non-radiative) systems. Far-field WPT or microwave power transfer (MPT) usually refers to systems that are capable to cover long distances (up to tens of km) and operate at frequencies from 1 to 300 GHz. With this technique, the amount of the transmitted power is still very small and this is also due to the electro-magnetic radiated fields physiological effects. Near-field WPT systems use inductive coupling to transfer power through distances from a few mm [9] to a few meters [10] and usually operate at frequencies from tens of kHz [11] up to a few MHz [12]. The amount of power transmitted by these WPT systems ranges from tens of mW [9] up to tens of kW [11], depending on the kind of applications. This technology exploits inductive coupling to transfer power and the main principle is based on resonant coils which resonate at the same frequency and are magnetically coupled. The resonance condition for the coils is essential being the magnetic coupling between two air-core coils intrinsically weak [13]. Generally, it can be obtained by arranging capacitance in series or in parallel with the coil inductance and then the exchange of energy (and thus the efficiency) between the circuits can in this way be raised, while the dissipation of power is limited. Moreover, introducing intermediate coils between the emitter and receiver an high power transmission efficiency can be achieved, as well as a longer distance can be covered [14], resulting in the so called “relay resonators systems” shown in figure 1.0.1. To date, different approaches are used by researchers for analyzing WPT systems: in particular the coupled mode theory (CMT) or the circuit theory (CT) are the most used to explain the main topics generally

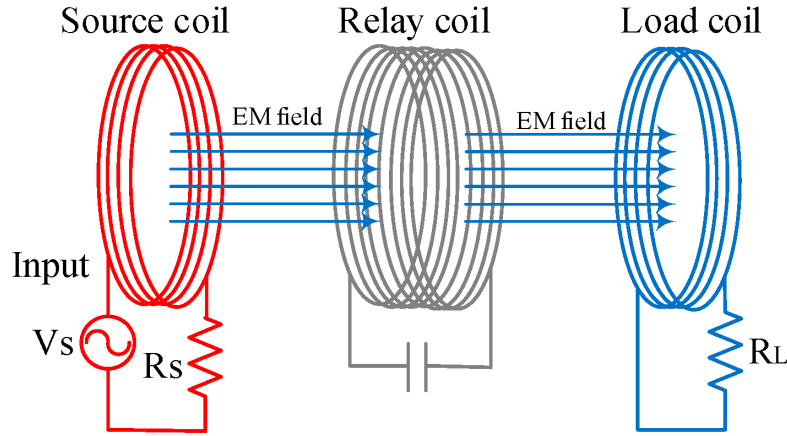


Figure 1.0.1: Resonant coils with an intermediate coil acting as a relay.

investigated, for example, frequency splitting, impedance matching and optimization design [15, 16, 17, 18]. The first approach is in general suitable for the study of the transmission of energy between two resonators (this approach was originally applied in the microwave field). The CT approach, on the contrary, is widely used by researchers and engineers as it is more straightforward being based on the mutual inductance model [19]. Anyway, in the last years, a novel type of wave propagation has been experimentally and analytically studied, known as magneto-inductive wave (MIW), which is supported by magnetic metamaterials structures acting as waveguides for it [20, 21]. The magnetic metamaterials are, in general, periodic arrays of resonant elements (also called metamaterial cells) and are composed of L-C series resonant circuits which are magnetically coupled each other in different arrangements (planar or axial), all of them tuned to a common resonant frequency. Usually, metamaterials are used for telecommunication technologies and data transfer systems but very recently prof. C.J. Stevens applied the MIW and metamaterials theory to WPT systems, due to their low losses in a wide bandwidth propagation [22, 23]. There is a direct analogy between metamaterials and the relay coils mentioned before, being both approached with the same theory, which is fully treated in the following. The resulting systems can extend the powered area and allow different configurations in which complicated geometries are required as well as feeding of more loads at the same time. In figure 1.0.2 it is possible to see an extension of resonant relay coils arranged on different rows which are in turn coupled to each other and

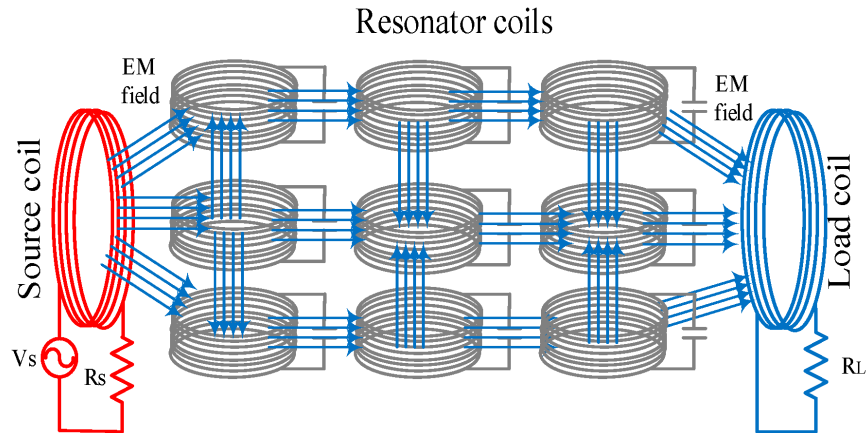


Figure 1.0.2: Resonant coils forming a two-dimensional metamaterial.

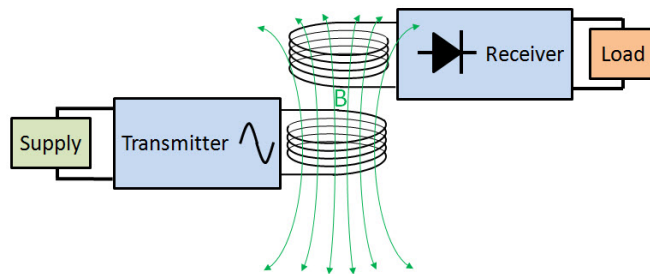


Figure 1.0.3: Traditional apparatus for the wireless transmission of power.

then forming a two-dimensional metamaterial structure. A typical IPT system, as described in [1] and depicted in figure 1.0.3, is composed of a power source, usually a power converter that picks power from the grid and converts it into a high frequency current (usually from tens to hundreds of kHz) that feeds the emitter (track) coil. The magnetic time-varying near field produced by the emitter coil is then picked up by the receiver (pickup) coil and the current induced in the pickup coil can be used to feed a load and, if needed, converted to DC or to another frequency. Moreover, the emitter and receiver coils are compensated and tuned to a certain resonant frequency, where the type of compensation depends on whether the resonance of the RLC circuit of the emitter and receiver coils is a parallel or series one.

1.1 Metamaterials

Metamaterials are artificial materials that can achieve electromagnetic properties that do not occur naturally, especially for what concerns the magnetic permeability μ_{eff} (response to a magnetic field) and the electric permittivity ε_{eff} (response to an electric field). Indeed, these two parameters can reach negative values simultaneously, thereby leading to a negative index of refraction for the electromagnetic field. These media support electromagnetic wave propagation in which the phase velocity is antiparallel to the direction of energy flow, and other unusual electromagnetic effects such as the reversal of the Doppler effect and Cerenkov radiation. The theoretical properties of metamaterials were first described in the 1960s by Victor Veselago [24], a Russian physicist who focused on the purely theoretical (at the time) concept of negative index materials. The refraction index is function of the frequency and it is generally defined as:

$$n_{eff}(\omega) = \sqrt{\varepsilon_{eff}(\omega)\mu_{eff}(\omega)} \quad (1.1.1)$$

where $\varepsilon_{eff}(\omega)$ is the effective electric permittivity as function of the frequency and $\mu_{eff}(\omega)$ is the effective magnetic permeability as function of the frequency. Both these physical quantities are defined as complex functions in order to incorporate the nonideal behavior of the real materials, that is affected by electric and magnetic hysteresis losses. In particular, for natural materials, these parameters are usually positive, with some exception for certain type of metals, such as gold or silver, that are characterised by a negative electric permittivity ε_{eff} . Since an electromagnetic wave can propagate only if the refraction index is real, then, in the natural matter, it is possible to have transmission if both ε_{eff} and μ_{eff} are positive – if one of them is negative, n_{eff} would be imaginary and the propagation of EM wave does not occur. Instead, Victor Veselago studies reported the effect of the simultaneous presence of negative ε_{eff} and μ_{eff} , proving that in those case the transmission of electromagnetic radiation was possible, being n_{eff} real. The negative root must be chosen for n_{eff} , leading to an antiparallel group and phase velocity, characteristic that can be easily visualized in the representation of figure 1.1.1. Considering the impact of an electromagnetic wave coming from a common material with a negative refraction index material a negative reflection occurs,

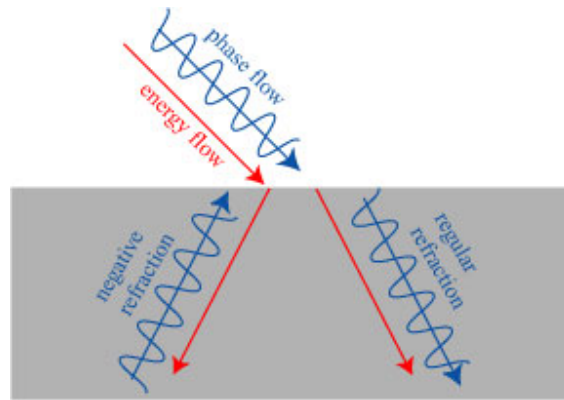


Figure 1.1.1: Negative and positive refraction of an EM wave incident on a surface.

being the direction of the Poynting vector and the wave vector laying on opposite directions. In figure 1.1.1 it is shown the behavior of the wave and group velocity in case of both regular and negative refraction with the related inversion of the energy flow [21]. Furthermore, being the reflection index negative, the refraction angle will change according to the direction of propagation of the wave (described by the wave vector) and the orientation of the electric and magnetic fields. Observing the phenomena from a macroscopic point of view, it is possible to observe that an EM wave is refracted on the same side of the normal entering material. For the sake of completeness, it must be noticed that metamaterial properties lead to other interesting and uncommon effects, namely:

- Doppler effect is reversed, meaning that a reduction of the frequency for a light source which is approaching to the observer occurs.
- Cherenkov radiation points the other way.

Unfortunately, for a long time no physical experience has been performed, due to the lack of presence of materials with the above-mentioned properties. Only theoretical investigation has been done, preparing the basis for a revolution in the science of materials. These concepts became a reality in the turn of the century. In 1996, John B. Pendry (et. al.) proposed that a periodic array of copper wires with a specific radius and spacing produces an electromagnetic response of negative ε materials. Three years later, he further proposed

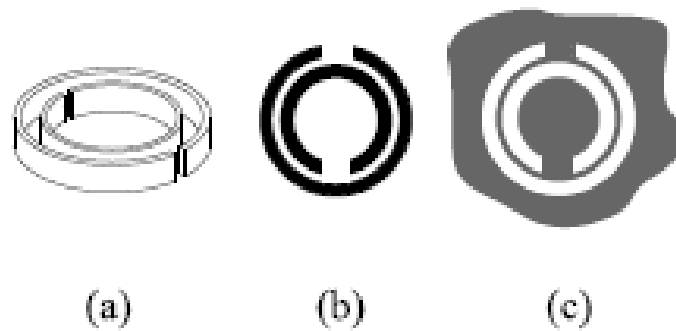


Figure 1.1.2: Split ring resonators as pipe (a), in printed circuit (b) and as complementary variety (c).

that a periodic array of split ring resonators (SRRs) would have a frequency band where μ is negative. It is now possible to understand how metamaterials are created. Basically, they are composed of electrical resonators laid on planes and arranged in such a way to form a periodic structure of pairs of elements, in which one array element produces a negative ϵ and the other array element produces a negative μ [25]. The precise shape, geometry, size, orientation and arrangement of those patterns gives them smart properties capable of manipulating electromagnetic waves: by blocking, absorbing, enhancing, or bending waves, to achieve benefits that go beyond what is possible with conventional materials. They are made from assemblies of multiple elements fashioned from composite materials such as metals and plastics, resulting in structures as reported in figure 1.1.3. The materials are usually arranged in repeating patterns, at scales that are smaller than the wavelengths of the phenomena they influence. The associated magnetic field pattern from the SRR is dipolar. By having splits in the rings, the SRR unit can be made resonant at wavelengths much larger than the diameter of the rings; that is, there is no half-wavelength requirement for resonance, as would be the case if the rings were closed. The purpose of the second split ring, inside and whose split is oriented opposite to the first, is to generate a large capacitance in the small gap region between the rings, lowering the resonant frequency considerably and concentrating the electric field. The periodic arrays are made from assemblies of multiple elements fashioned from composite materials such as metals and plastics and can behave as an effective medium for electromagnetic scattering when the wavelength is much longer than both the element

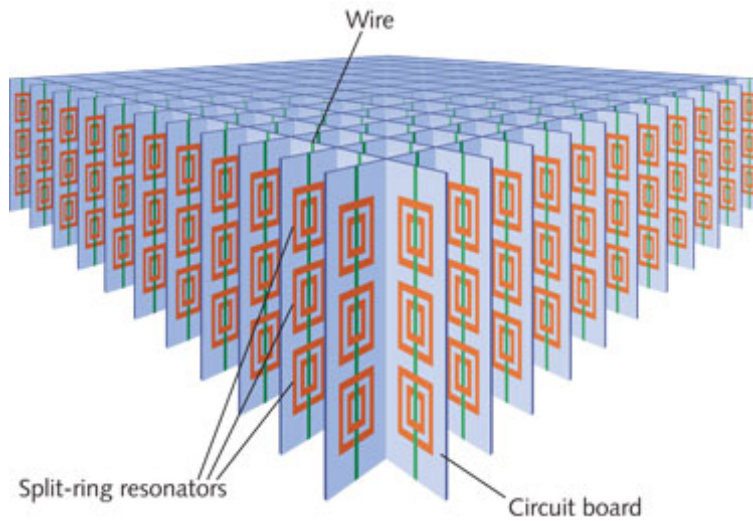


Figure 1.1.3: Three dimensional metamaterial structure.

dimension and lattice spacing, namely at scales that are smaller than the wavelengths of the phenomena they influence. An example medium is a three-dimensional array of intersecting thin straight wires, for which propagating modes follow a dispersion relation analogous to that of a neutral plasma.

1.1.1 Analogy between relay coils and metamaterials

As it has been mentioned in the introduction of this chapter 1, in the IPT systems usually additional resonant circuits are introduced between the transmitter and receiver coils, in order to increase the power reaching the load, for a certain distance. In order to better understand the phenomena that arise in this particular structures, let us consider what happen when an electromagnetic field hits the surface of these materials. A time-varying magnetic field applied parallel to the axis of the rings induces currents that, depending on the resonant properties of the unit, produce a magnetic field that may either oppose or enhance the incident field. This purpose can be clearly reached by means of different apparatuses, as are each series coupled resonating circuits, independent on the real geometry and shape. These resonating loops can be made of split ring resonators as well as common coils closed on a proper capacitor so that the resonant condition is achieved. The only difference states in the

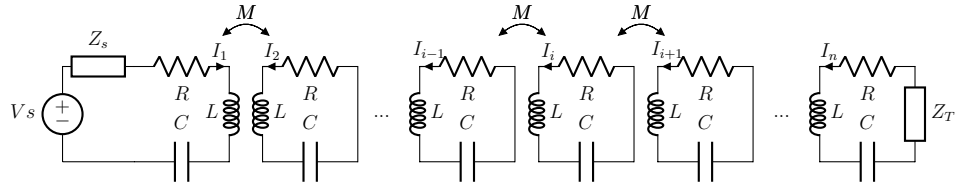


Figure 1.1.4: Equivalent circuit of a 1-D structure of relay resonators.

magnitude of the physical phenomena involved. Indeed, two electromagnetic systems can be considered equivalent if and only if they can be represented by the same electric circuit [26], meaning that the effective electromagnetic behavior is described by the same physical law. It is then possible to state that relay coil systems and metamaterial structures are equivalent, wheres their general circuit representation is reported in figure 1.1.4.

1.2 MIW

Magnetoinductive waves (MIW) resulted as a by-product of the research on metamaterials. As mentioned before, the magnetic elements used in the first realization of negative refraction were split-ring resonators that could be modeled as LC circuits, provided the dimensions are small relative to the free-space wavelength. We shall also assume that the separation of the elements is also much smaller than the wavelength. This is often referred to as the quasi-static approximation. The simplest and most common realization of an LC circuit as a metamaterial element is a capacitively loaded loop, as shown in the various figures before. Two such loops close to each other are coupled to each other due to the magnetic field of one loop threading the other loop and inducing a current in it. The presence of such coupling leads to waves that were called MIW by Shamonina et al. [21]. They belong to the category of slow waves that propagate at a velocity less than that of light.

In order to understand the origin of this phenomena, it is important to consider the mutual interaction between the split ring resonators that form the lattice structure. Basically, the incident magnetic field induces a voltage in the resonators according to the Faraday's law and then they produce a magnetic flux, which link to the near SRRs. The resulting effect is

an interaction of the first order that is possible to model considering the equivalent circuits. In particular, two coupled resonant circuits can be seen as a four-pole element in which the input and output quantities are the voltage and current in the first and second (coupled) resonator, respectively. The relationship between the input and output quantities is defined by the electromagnetic properties of the four-pole, that are those of the two coupled circuits. This results in relations of the type:

$$V_{out} = e^{-jkd}V_{in} \quad (1.2.1)$$

$$I_{out} = e^{-jkd}I_{in} \quad (1.2.2)$$

where k is the propagation constant and d can be regarded as the physical length of a unit. These relations state that for the same interval the phase of the quantities always change by the same amount and thus, if we have a chain of four-poles, the phase change between the output and input quantities is of the same factor e^{-jkd} . This behaviour corresponds to the one of a wave, meaning that the variables that describe the four-pole are effectively voltage and current waves. At this point, it must be noticed that the metamaterial is composed of a series of magnetic coupled circuits and then, in this frame, it can be considered a chain of four-poles, each with the same properties. In it easy to understand that the system variables, namely the voltage and the current of the circuit, change in the resonator that composes the chain as the wave propagates along this, as proved by the equation 1.2.1 and 1.2.2. The wave, anyway, cannot propagate freely in the entire space, but it bumps regularly into obstacles presented by the resonant circuit, making in this way the metamaterial acting as a waveguide. It is now intuitive to associate the four-pole chain to a transmission line, being this latter seen as a series of four-poles along which an EM wave in TEM configuration can propagate. Thanks to the circuit representation, it is possible to state that the whole phenomenon developed along the resonator array is well described considering a loaded transmission line, then, once the equivalent circuit of the resonating element is defined and knowing how it is coupled with the plane wave, then the model can be found. The only difference between a transmission

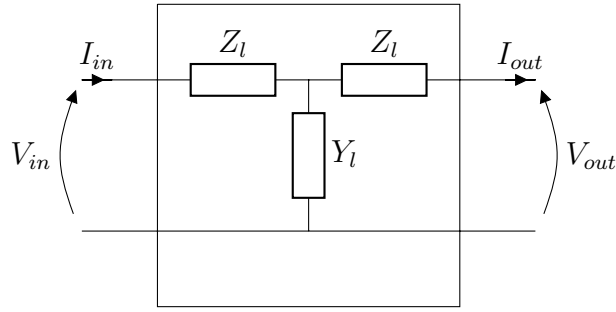


Figure 1.2.1: Four-poles: “T model” equivalent circuit for a transmission line.

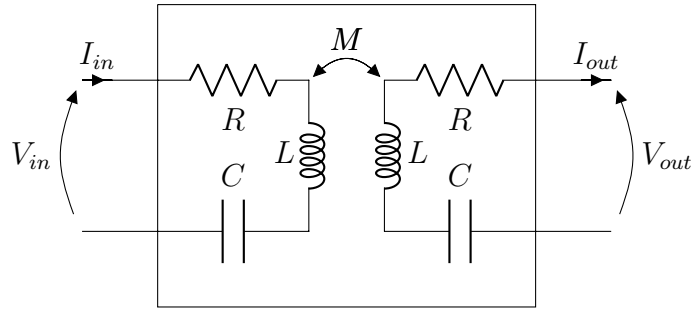


Figure 1.2.2: Four-poles: model for two coupled R-L-C circuits

line and a metamaterial structure states in the configuration of the four-pole considered. Indeed, for the former, the traditional model assumes a section of the transmission line to be described by the well known circuit called “T model”, which is composed of two impedances representing the transversal and longitudinal parameters of the line as shown in figure 1.2.1, whereas, for the latter, the circuit is the one representing the resonators that compose the metamaterial, shown in figure 1.2.2.

The negative refraction effect is analogous to wave propagation in a left-handed transmission line, and these structures have been used to verify some of the effects described here. In order to allow these materials to present the above described characteristics for a certain range of physical phenomena, they must resonate at the frequency of the incident radiation which is possible to express in terms of electric parameters. The simplest elements that propagate this wave are capacitively loaded metallic loops that usually compose the array. Then, the resonant frequency of the elements, which can be simply regarded as LC circuits, is expressed by the relation:

$$f_{res} = \frac{1}{2\pi\sqrt{LC}} \quad (1.2.3)$$

where L is the inductance of the loop and C is the capacitance of the loading capacitor. The resonant frequency becomes a design criterion for these materials, since it defines the wavelength of the radiations at which the metamaterial shows its particular properties.

1.2.1 Circuit approach

As a step forward, it is important to analyze the mutual interaction between the split ring resonators that form the lattice structure in order to complete the model. For this purpose, a circuit approach has been followed, representing the chain of coupled loops by means of an equivalent circuit, allowing the whole behavior of the apparatus to be fully described. In this frame it is important to underline that the mutual coupling between nonadjacent cells has been neglected, being this latter much weaker with respect to the coupling between consecutive resonators of the array. The reference circuit is the one reported in figure 1.1.4, in which it may be seen that the magnetic field created by the i^{th} element will also thread the $(i - 1)^{\text{th}}$ and $(i + 1)^{\text{th}}$ elements, causing the propagation of the above described wave. The phenomena can be modeled by means of circuit analysis, namely applying the Kirchhoff's voltage law to the i^{th} element and neglecting all the mutual interactions between nonadjacent cells, thereby holding:

$$j\omega M_{i,i-1}\hat{I}_{i-1} + \hat{Z}\hat{I}_i + j\omega M_{i,i+1}\hat{I}_{i+1} = 0 \quad (1.2.4)$$

where

$$\hat{Z} = R + j\omega L + \frac{1}{j\omega C} \quad (1.2.5)$$

is the proper impedance of each loop. In particular, L represents the self-inductance of the loop, whereas C is the whole capacitance of the resonator. The interaction of this circuit with the others forming the metamaterial structure has been taken into account through the mutual inductances between the coils, described by the coefficients M , where:

- $M_{i,i-1}$ is the mutual inductance between the elements $i - 1$ and i
- $M_{i,i+1}$ is the mutual inductance between the elements i and $i + 1$

The values of these parameters depend only on the geometry of the windings and their position in space, representing the key indicator for the quality of the power transmission. They have been fully described and calculated in [27].

The solution of the equation that expresses the wave traveling along the metamaterial is, in term of a generic cell current i , assumed to be:

$$\hat{I}_i = \hat{I}_1 e^{-\hat{k}(i-1)d} \quad (1.2.6)$$

where \hat{I}_1 is the value of the current flowing in the first cell and d is the periodic distance between two adjacent cells. The propagation constant \hat{k} is defined as $\hat{k} = \beta - j\alpha$, where α and β are the attenuation and phase constants, respectively, and they could also be expressed in terms of electrical parameters. In particular, the attenuation per cell represents the wave reduction along the metamaterial and assumes the form:

$$\alpha = \frac{1}{d} \sinh^{-1} \left(\frac{1}{\eta \frac{2M}{L} Q} \right) \quad (1.2.7)$$

in which $\frac{2M}{L}$ is the coupling coefficient and $Q = \frac{(\omega_0 L)}{R}$ is the quality factor of each resonator. The quantity η represents the number of spatial dimensions occupied by the lattice. The phase constant is expressed through the dispersion equation that, for the propagation of MI waves is:

$$\cos(\beta d) = \left(\frac{\omega_0^2 - \omega^2}{\frac{2M}{L} \omega_0^2} \right) \quad (1.2.8)$$

From this formula, it is possible to derive the bandwidth in which the wave propagation is achieved with very low losses. Furthermore, it is possible to state that the group velocity, $\frac{d\omega}{dk}$, is always positive and at the band edge the group velocity is zero, as it is for all waves on discrete structures. Note also that there is a lower cutoff frequency below which the MI

wave cannot propagate. The pass band is within the range

$$\frac{\omega_0}{\sqrt{1 + \eta \frac{2M}{L}}} < \omega < \frac{1}{\sqrt{1 - \eta \frac{2M}{L}}} \quad (1.2.9)$$

This kind of waves, namely the ones that characterize coupled circuits, can also be electrical, considering obviously capacitive couplings. The sign of the mutual inductance M determines the type of magneto-inductive wave propagation in the array: axial configuration involves forward waves with phase and group velocities in the same direction (given by $M > 0$). On the contrary, planar configuration involves backward waves with opposite directions of the phase and group velocities (given by $M < 0$).

1.2.2 Matching the transmission line

According to the discussion just made, MI waves can propagate along an array whether it is axial or planar. We may therefore regard such arrays as transmission lines, despite unusual dispersion relations. Now the focus is on the possibility to match that transmission line, namely to absorb all the incident power by means of a proper termination impedance, allowing the wave to travel from source to load without reflections [28]. In order to obtain the exact value for the matching impedance, the Kirchhoff's equation for the last element of the array in presence of the additional termination impedance \hat{Z}_T must be resorted, and then it holds:

$$j\omega M_{n,n-1} \hat{I}_{n-1} + \hat{Z} \hat{I}_n + \hat{Z}_T \hat{I}_n = 0 \quad (1.2.10)$$

According to (1.2.6), the relation between the currents \hat{I}_{n-1} and \hat{I}_n is expressed as:

$$\hat{I}_n = \hat{I}_{n-1} e^{-\hat{k}d} \quad (1.2.11)$$

From the dispersion relation (1.2.8) it is now possible to derive the expression for the angular frequency as:

$$\omega = \frac{\omega_0}{\sqrt{1 + \frac{2M}{L} \cos(\hat{k}d)}} \quad (1.2.12)$$

and then the termination impedance for the matching of the line is found.

$$\hat{Z}_T = j\omega M e^{-\hat{k}d} \quad (1.2.13)$$

becoming purely real and equal to $Z_T = \omega_0 M$ in resonant condition ($f = f_0$). Under this condition, the maximum power can be delivered by the MI wave to the last cell at the resonant frequency, thereby avoiding a standing wave. It is interesting to notice that the terminal impedance is not a real constant as it is for a classic coaxial line, but it is a complex and frequency-dependent quantity.

Chapter 2

Misalignment Tolerant Model

In this chapter the mathematical model of an array of coupled resonator in presence of a receiver will be derived. Indeed, According to the circuit model reported in the previous introduction, a metamaterial can be described by means of a proper electric circuit, allowing all the electric parameters to be studied. The presence of a receiver will modify this model and additional terms must be included in the impedance matrix, as it is reported in the following paragraphs. Furthermore, the possibility of the receiver to move along the resonator array led to a definition of the parameters that depends on the position. This is the reason why we defined the model as “misalignment tolerant”. Different situations have been analyzed, depending on the dimension of the receiver circuit.

2.1 Resonator array with a receiver

The first situation described is related to a metamaterial on which a receiver of the same shape and dimension of the resonant cells is placed, as it is shown in figure 2.1.1. This solution allows the model for the system to be simply described when the receiver is perfectly aligned with one of the element of the array, whereas for misaligned positions at maximum two cells at a time are covered. Following the circuit approach it is possible to derive an equivalent

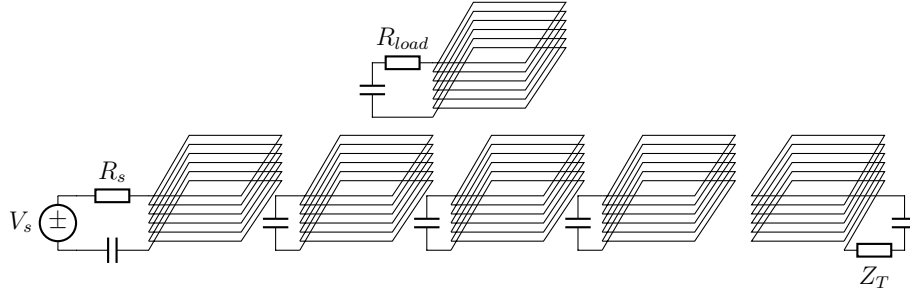


Figure 2.1.1: Array of coupled resonators with a receiver over them.

circuitual model represented in Fig.2.1.2 for the description of the system and then, in order to define it, the voltage and current Kirchhoff laws have been applied. The mutual coupling between nonadjacent cells of the array has been neglected, as 1.2.1. In the same way, the mutual interaction between the metamaterial and the receiver has been considered only for near cells, namely for those resonators that face the receiver circuit. This leads to a new terms to appear only in the correspondent position of the equation system reported below. For the sake of generality, an intermediate position has been assumed for the receiver resonator. In a sinusoidal steady-state, the resulting system of equations has the expression of:

$$\begin{aligned}
-\hat{V}_s + R_s \hat{I}_1 + \hat{Z} \hat{I}_1 + j\omega M_{1,2} \hat{I}_2 &= 0 \\
j\omega M_{2,1} \hat{I}_1 + \hat{Z} \hat{I}_2 + j\omega M_{2,3} \hat{I}_3 &= 0 \\
&\vdots \\
j\omega M_{i-1,i-2} \hat{I}_{i-2} + \hat{Z} \hat{I}_{i-1} + j\omega M_{i-1,i} \hat{I}_i &= 0 \\
j\omega M_{i,i-1} \hat{I}_{i-1} + \hat{Z} \hat{I}_i + j\omega M_{i,i+1} \hat{I}_{i+1} + j\omega M_{i,r} \hat{I}_r &= 0 \\
j\omega M_{i+1,i} \hat{I}_i + \hat{Z} \hat{I}_{i+1} + j\omega M_{i+1,i+2} \hat{I}_{i+2} + j\omega M_{i+1,r} \hat{I}_r &= 0 \\
j\omega M_{i+2,i+1} \hat{I}_{i+1} + \hat{Z} \hat{I}_{i+2} + j\omega M_{i+2,i+3} \hat{I}_{i+3} &= 0 \\
&\vdots \\
j\omega M_{n,n-1} \hat{I}_{n-1} + \hat{Z} \hat{I}_n + \hat{Z}_T \hat{I}_n &= 0
\end{aligned} \tag{2.1.1}$$

with one additional KVL for the receiver circuit:

$$j\omega M_{r,i}\hat{I}_i + j\omega M_{r,i+1}\hat{I}_{i+1} + \hat{Z}_r\hat{I}_r = 0 \quad (2.1.2)$$

where $\hat{Z}_r = \hat{Z} + R_{load}$ is the impedance of the receiver resonator. The receiver current is obtained from (2.1.2) as follows:

$$\hat{I}_r = -j\omega \frac{M_{r,i}}{\hat{Z}_r} \hat{I}_i - j\omega \frac{M_{r,i+1}}{\hat{Z}_r} \hat{I}_{i+1} \quad (2.1.3)$$

In order to refer the equations only to the array currents and show the receiver impedance contribution seen from the nearest cell, the receiver current \hat{I}_r has been substituted in the system (2.1.1), leading to

$$\begin{aligned} -\hat{V}_s + R_s\hat{I}_1 + \hat{Z}\hat{I}_1 + j\omega M_{1,2}\hat{I}_2 &= 0 \\ j\omega M_{2,1}\hat{I}_1 + \hat{Z}\hat{I}_2 + j\omega M_{2,3}\hat{I}_3 &= 0 \\ &\vdots \\ j\omega M_{i-1,i-2}\hat{I}_{i-2} + \hat{Z}\hat{I}_{i-1} + j\omega M_{i-1,i}\hat{I}_i &= 0 \\ j\omega M_{i,i-1}\hat{I}_{i-1} + \hat{Z}\hat{I}_i + \omega^2 \frac{M_{i,r}^2}{\hat{Z}_r} \hat{I}_i + j\omega M_{i,i+1}\hat{I}_{i+1} + \omega^2 \frac{M_{i,r}M_{r,i+1}}{\hat{Z}_r} \hat{I}_{i+1} &= 0 \\ j\omega M_{i+1,i}\hat{I}_i + \omega^2 \frac{M_{i,r}M_{r,i+1}}{\hat{Z}_r} \hat{I}_i + \hat{Z}\hat{I}_{i+1} + \omega^2 \frac{M_{i+1,r}^2}{\hat{Z}_r} \hat{I}_{i+1} + j\omega M_{i+1,i+2}\hat{I}_{i+2} &= 0 \\ j\omega M_{i+2,i+1}\hat{I}_{i+1} + \hat{Z}\hat{I}_{i+2} + j\omega M_{i+2,i+3}\hat{I}_{i+3} &= 0 \\ &\vdots \\ j\omega M_{n,n-1}\hat{I}_{n-1} + \hat{Z}\hat{I}_n + \hat{Z}_T\hat{I}_n &= 0 \end{aligned} \quad (2.1.4)$$

The receiver impedance contributions are then expressed as

$$\hat{Z}_{d_i} = \omega^2 \frac{M_{i,r}^2}{\hat{Z}_r} \quad (2.1.5)$$

$$\hat{Z}_{d_{i+1}} = \omega^2 \frac{M_{i+1,r}^2}{\hat{Z}_r} \quad (2.1.6)$$

$$\hat{Z}_{d_{i,i+1}} = \hat{Z}_{d_{i+1,i}} = \omega^2 \frac{M_{i,r}M_{r,i+1}}{\hat{Z}_r} \quad (2.1.7)$$

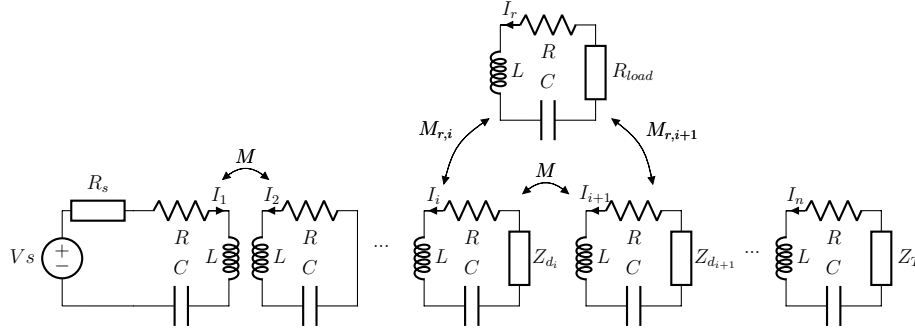


Figure 2.1.2: Equivalent circuit of a resonator array with a receiver of the same dimension of the cells.

According to the matrix formulation

$$\hat{\mathbf{V}} = \hat{\mathbf{Z}}_{\mathbf{m}} \hat{\mathbf{I}} \quad (2.1.8)$$

where $\hat{\mathbf{V}} = [\hat{V}_s \ 0 \ \dots \ 0]^T$ with \hat{V}_s the phasor of the supply voltage of the emitter coil and $\hat{\mathbf{I}}$ is the complex vector of the currents flowing in the cells, the impedance matrix $\hat{\mathbf{Z}}_{\mathbf{m}}$ becomes:

$$\hat{\mathbf{Z}}_{\mathbf{m}} = \begin{bmatrix} \hat{Z} + R_s & j\omega M & & \dots & 0 & \dots & 0 \\ j\omega M & \hat{Z} & j\omega M & \dots & 0 & \dots & 0 \\ \vdots & \vdots & \ddots & \dots & \vdots & \dots & \vdots \\ 0 & 0 & j\omega M & \hat{Z} + \hat{Z}_{d_i} & j\omega M + \hat{Z}_{d_{i,i+1}} & 0 & 0 \\ 0 & \dots & 0 & j\omega M + \hat{Z}_{d_{i+1,i}} & \hat{Z} + \hat{Z}_{d_{i+1}} & j\omega M & 0 \\ \vdots & \dots & \vdots & \dots & \vdots & \ddots & \vdots \\ 0 & \dots & 0 & \dots & 0 & j\omega M & \hat{Z} + \hat{Z}'_T \end{bmatrix} \quad (2.1.9)$$

The matrix described in (2.1.9) can be split in the sum of two contributions, as reported in (2.1.10).

$$\hat{\mathbf{Z}}_{\mathbf{m}} = \hat{\mathbf{Z}}_{\text{array}} + \hat{\mathbf{Z}}_{\mathbf{d}} \quad (2.1.10)$$

In particular, the first term of the sum $\hat{\mathbf{Z}}_{\text{array}}$ represents the the impedance matrix of the array of resonator without the receiver circuit, whereas the second matrix $\hat{\mathbf{Z}}_{\mathbf{d}}$ incorporates

only to the defect impedance introduced by the receiver placed above the metamaterial. The result of the sum $\hat{\mathbf{Z}}_{\mathbf{m}}$ corresponds to the impedance matrix of the whole system inclusive of the source and termination impedances. As it is possible to see in (2.1.9), the original matrix has been modified only in the terms that correspond to the cells that are covered by the receiver, meaning that the dimension of this latter defines the number of additional defects that must be taken into account.

$$\hat{\mathbf{Z}}_{\text{array}} = \begin{bmatrix} \hat{Z} + R_s & j\omega M & 0 & 0 & 0 & \cdots & 0 \\ j\omega M & \hat{Z} & j\omega M & 0 & 0 & \cdots & 0 \\ \vdots & \cdots & \ddots & \vdots & \vdots & \cdots & 0 \\ 0 & 0 & j\omega M & \hat{Z} & j\omega M & 0 & 0 \\ \vdots & \cdots & \vdots & \vdots & \ddots & \cdots & 0 \\ 0 & \cdots & 0 & 0 & j\omega M & \hat{Z} & j\omega M \\ 0 & \cdots & 0 & 0 & 0 & j\omega M & \hat{Z} + \hat{Z}'_T \end{bmatrix} \quad (2.1.11)$$

$$\hat{\mathbf{Z}}_{\mathbf{d}} = \begin{bmatrix} 0 & \cdots & 0 & 0 & 0 & 0 & \cdots & 0 \\ \vdots & \cdots & \ddots & \ddots & \vdots & \vdots & \cdots & \vdots \\ 0 & \cdots & 0 & \hat{Z}_{d_i} & \hat{Z}_{d_{i,i+1}} & 0 & \cdots & 0 \\ 0 & \cdots & 0 & \hat{Z}_{d_{i+1,i}} & \hat{Z}_{d_{i+1}} & 0 & \cdots & 0 \\ \vdots & \cdots & \vdots & \ddots & \ddots & \vdots & \cdots & \vdots \\ 0 & \cdots & 0 & 0 & 0 & 0 & \cdots & 0 \end{bmatrix} \quad (2.1.12)$$

It is easy to understand that bigger or multiple receivers can increase the complexity of the system and the model must be adapted to the new configuration. As proof, an analysis of a mono-dimensional metamaterial with a larger receiver is reported.

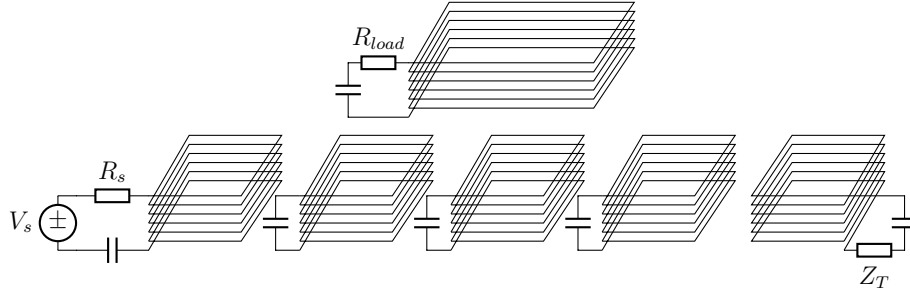


Figure 2.2.1: Resonator array with a receiver which is twice the size of the resonators.

2.2 Receiver bigger than the array resonators

Usually, in order to increase the power transmitted to the load, the geometry of the receiver is extended, whereas the surface described by the coil becomes wider, allowing more flux link to that circuit. In the following case, the dimension of the receiver has been doubled, thereby making it able cover 3 cells of the array in case of intermediate position, as represented in figure 2.2.1. The model has been obtained following the usual circuit approach, and the system modifies as follows:

$$\begin{aligned}
 -\hat{V}_s + R_s \hat{I}_1 + \hat{Z} \hat{I}_1 + j\omega M_{1,2} \hat{I}_2 &= 0 \\
 j\omega M_{2,1} \hat{I}_1 + \hat{Z} \hat{I}_2 + j\omega M_{2,3} \hat{I}_3 &= 0 \\
 &\vdots \\
 j\omega M_{i-1,i-2} \hat{I}_{i-2} + \hat{Z} \hat{I}_{i-1} + j\omega M_{i-1,i} \hat{I}_i &= 0 \\
 j\omega M_{i,i-1} \hat{I}_{i-1} + \hat{Z} \hat{I}_i + j\omega M_{i,i+1} \hat{I}_{i+1} + j\omega M_{i,r} \hat{I}_r &= 0 \\
 j\omega M_{i+1,i} \hat{I}_i + \hat{Z} \hat{I}_{i+1} + j\omega M_{i+1,i+2} \hat{I}_{i+2} + j\omega M_{i+1,r} \hat{I}_r &= 0 \\
 j\omega M_{i+2,i+1} \hat{I}_{i+1} + \hat{Z} \hat{I}_{i+2} + j\omega M_{i+2,i+3} \hat{I}_{i+3} + j\omega M_{i+2,r} \hat{I}_r &= 0 \\
 j\omega M_{i+3,i+2} \hat{I}_{i+2} + \hat{Z} \hat{I}_{i+3} + j\omega M_{i+3,i+4} \hat{I}_{i+4} &= 0 \\
 &\vdots \\
 j\omega M_{n,n-1} \hat{I}_{n-1} + \hat{Z} \hat{I}_n + \hat{Z}_T \hat{I}_n &= 0
 \end{aligned} \tag{2.2.1}$$

For the receiver circuit it holds

$$j\omega M_{r,i}\hat{I}_i + j\omega M_{r,i+1}\hat{I}_{i+1} + j\omega M_{r,i+2}\hat{I}_{i+2} + \hat{Z}_r\hat{I}_r = 0 \quad (2.2.2)$$

Substituting the receiver current \hat{I}_r in the resonator's KVL equations and arranging the system, the new impedance matrix $\hat{\mathbf{Z}}''_{\mathbf{m}}$ is found. Now the receiver affects 3 cells, that must encompass the impedance defect in their circuit representations expressed as follows:

$$\hat{Z}_{d_i} = \omega^2 \frac{M_{i,r}^2}{\hat{Z}_r} \quad (2.2.3)$$

$$\hat{Z}_{d_{i+1}} = \omega^2 \frac{M_{i+1,r}^2}{\hat{Z}_r} \quad (2.2.4)$$

$$\hat{Z}_{d_{i+2}} = \omega^2 \frac{M_{i+2,r}^2}{\hat{Z}_r} \quad (2.2.5)$$

$$\hat{Z}_{d_{i,i+1}} = \hat{Z}_{d_{i+1,i}} = \omega^2 \frac{M_{i,r}M_{r,i+1}}{\hat{Z}_r} \quad (2.2.6)$$

$$\hat{Z}_{d_{i+1,i+2}} = \hat{Z}_{d_{i+2,i+1}} = \omega^2 \frac{M_{i+1,r}M_{r,i+2}}{\hat{Z}_r} \quad (2.2.7)$$

Again it is possible to exploit the partition made in 2.1 that allow the representation of the matrix $\hat{\mathbf{Z}}''_{\mathbf{m}}$ as a sum of the contribution given by the naked array and the matrix with the defects due to the presence of the receiver. Then, it follows

$$\hat{\mathbf{Z}}''_{\mathbf{m}} = \hat{\mathbf{Z}}_{\mathbf{array}} + \hat{\mathbf{Z}}''_{\mathbf{d}} \quad (2.2.8)$$

where $\hat{\mathbf{Z}}_{\mathbf{array}}$ is the same reported in (2.1.11), being the array of resonator unchanged. Instead, the defect impedances depends on the receiver coil geometry, which is now increased

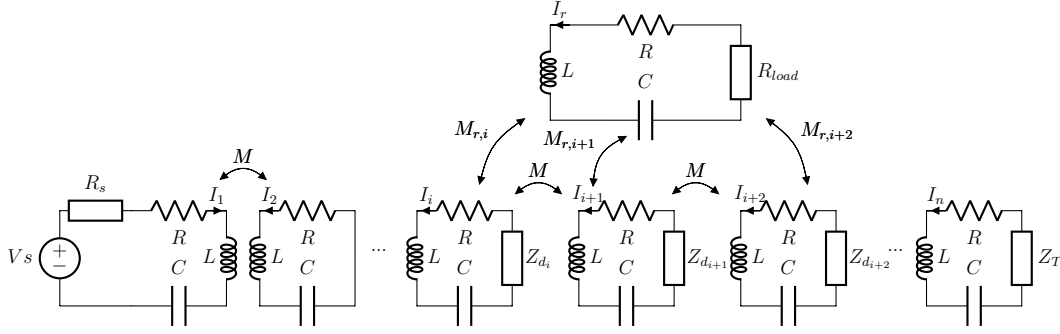


Figure 2.2.2: Equivalent circuit of a resonator array with a receiver which is twice the size of an array cell.

with respect to the previous case, leading to

$$\hat{\mathbf{Z}}_d'' = \begin{bmatrix} 0 & \cdots & 0 & 0 & 0 & 0 & 0 & \cdots & 0 \\ \vdots & \cdots & \ddots & \ddots & \vdots & \vdots & \vdots & \cdots & \vdots \\ 0 & \cdots & 0 & \hat{Z}_{d_i} & \hat{Z}_{d_{i,i+1}} & 0 & \vdots & \cdots & 0 \\ 0 & \cdots & 0 & \hat{Z}_{d_{i+1,i}} & \hat{Z}_{d_{i+1}} & \hat{Z}_{d_{i+1,i+2}} & 0 & \cdots & 0 \\ 0 & \cdots & \vdots & 0 & \hat{Z}_{d_{i+2,i+1}} & \hat{Z}_{d_{i+2}} & 0 & \cdots & 0 \\ \vdots & \cdots & \vdots & \vdots & \vdots & \ddots & \ddots & \cdots & \vdots \\ 0 & \cdots & 0 & 0 & 0 & 0 & 0 & \cdots & 0 \end{bmatrix} \quad (2.2.9)$$

Other defects terms have to be added in case of further magnetic interaction for the resonators, resulting in a more complicated equivalent circuit shown in figure 2.2.2. In this perspective the limit case has been analyzed, with a general model proposed for a receiver circuit that covers - and then interacts - with each cell.

2.3 General case

For the sake of generality the most general situation which refers to an array completely covered by the receiver circuit, shown in figure 2.3.1, has been reported in the following. As

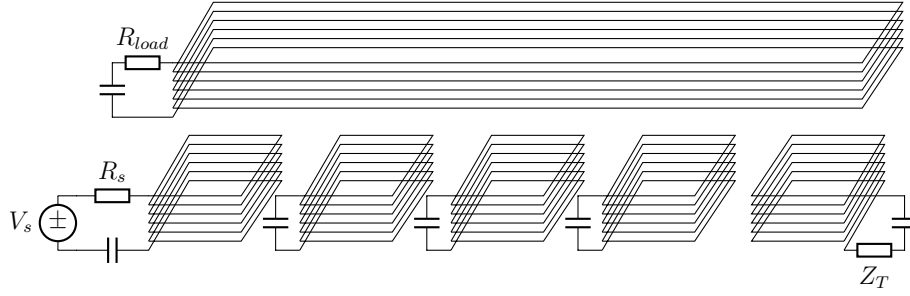


Figure 2.3.1: General case: resonator array with a receiver which covers all the cells.

a consequence, each Kirchoff's voltage equation for the cells must include the interaction of the correspondent element with the receiver, as reported in (2.3.1):

$$\begin{aligned}
 -\hat{V}_s + R_s \hat{I}_1 + \hat{Z} \hat{I}_1 + j\omega M_{1,2} \hat{I}_2 + j\omega M_{1,r} \hat{I}_r &= 0 \\
 j\omega M_{2,1} \hat{I}_1 + \hat{Z} \hat{I}_2 + j\omega M_{2,3} \hat{I}_3 + j\omega M_{2,r} \hat{I}_r &= 0 \\
 &\vdots \\
 j\omega M_{i,i-1} \hat{I}_{i-1} + \hat{Z} \hat{I}_i + j\omega M_{i,i+1} \hat{I}_{i+1} + j\omega M_{i,r} \hat{I}_r &= 0 \\
 &\vdots \\
 j\omega M_{n,n-1} \hat{I}_{n-1} + \hat{Z} \hat{I}_n + \hat{Z}_T \hat{I}_n + j\omega M_{n,r} \hat{I}_r &= 0
 \end{aligned} \tag{2.3.1}$$

The receiver equation has the form of:

$$j\omega M_{r,1} \hat{I}_1 + \dots + j\omega M_{r,i} \hat{I}_i + \dots + j\omega M_{r,n} \hat{I}_n + \hat{Z}_r \hat{I}_r = 0 \tag{2.3.2}$$

and then the receiver current holds:

$$\hat{I}_r = -j\omega \frac{M_{r,1}}{\hat{Z}_r} \hat{I}_1 - \dots - j\omega \frac{M_{r,i}}{\hat{Z}_r} \hat{I}_i - \dots - j\omega \frac{M_{r,n}}{\hat{Z}_r} \hat{I}_n \tag{2.3.3}$$

The impedance matrix of the whole system $\hat{\mathbf{Z}}_{\mathbf{m}}'''$ has been still reported as sum of the array impedance matrix and the defects matrix, whereas this latter is strongly increased in size

due to the dimension of the receiver, resulting in

$$\hat{\mathbf{Z}}_{\mathbf{m}}''' = \hat{\mathbf{Z}}_{\text{array}} + \hat{\mathbf{Z}}_{\mathbf{d}}''' \quad (2.3.4)$$

$$\hat{\mathbf{Z}}_{\mathbf{d}}''' = \begin{bmatrix} \hat{Z}_{d_1} & \hat{Z}_{d_{1,2}} & \cdots & \cdots & \cdots & \cdots & \cdots & \hat{Z}_{d_{1,n-1}} & \hat{Z}_{d_{1,n}} \\ \hat{Z}_{d_{2,1}} & \hat{Z}_{d_2} & \cdots & \cdots & \cdots & \cdots & \cdots & \hat{Z}_{d_{2,n-1}} & \hat{Z}_{d_{2,n}} \\ \vdots & \vdots & \cdots & \vdots & \vdots & \vdots & \cdots & \vdots & \vdots \\ \hat{Z}_{d_{i,1}} & \hat{Z}_{d_{i,2}} & \cdots & \hat{Z}_{d_{i,i-1}} & \hat{Z}_{d_i} & \hat{Z}_{d_{i,i+1}} & \cdots & \hat{Z}_{d_{i,n-1}} & \hat{Z}_{d_{i,n}} \\ \vdots & \vdots & \cdots & \vdots & \vdots & \vdots & \cdots & \vdots & \vdots \\ \hat{Z}_{d_{n-1,1}} & \hat{Z}_{d_{n-1,2}} & \cdots & \cdots & \cdots & \cdots & \cdots & \hat{Z}_{d_{n-1,n-1}} & \hat{Z}_{d_{n-1,n}} \\ \hat{Z}_{d_{n,1}} & \hat{Z}_{d_{n,2}} & \cdots & \cdots & \cdots & \cdots & \cdots & \hat{Z}_{d_{n,n-1}} & \hat{Z}_{d_{n,n}} \end{bmatrix} \quad (2.3.5)$$

where

$$\hat{Z}_{d_i} = \omega^2 \frac{M_{i,r}^2}{\hat{Z}_r} \quad i = 1, \dots, n \quad (2.3.6)$$

$$\begin{cases} \hat{Z}_{d_{i-n,i}} = \hat{Z}_{d_{i,i-n}} = \omega^2 \frac{M_{i-n,r} M_{r,i}}{\hat{Z}_r} \\ \vdots \\ \hat{Z}_{d_{i-1,i}} = \hat{Z}_{d_{i,i-1}} = \omega^2 \frac{M_{i-1,r} M_{r,2}}{\hat{Z}_r} \\ \hat{Z}_{d_{i,i+1}} = \hat{Z}_{d_{i+1,i}} = \omega^2 \frac{M_{i,r} M_{r,i+1}}{\hat{Z}_r} \\ \vdots \\ \hat{Z}_{d_{i+n,i}} = \hat{Z}_{d_{i,i+n}} = \omega^2 \frac{M_{i,r} M_{r,i+n}}{\hat{Z}_r} \end{cases} \quad i = 1, \dots, n \quad (2.3.7)$$

The general case approached in this section considers a receiver which interacts with all the cells forming the array and then each circuit presents an additional impedance. Differently than the cases treated before, the resulting impedance matrix for the whole system $\hat{\mathbf{Z}}_{\mathbf{m}}'''$ appears full of terms, as it is for the defects matrix shown in (2.3.5). The equivalent circuit referred to the whole apparatus is reported in figure 2.3.2, for which the resonator has been represented large as the entire array, just in order to give the idea of a fully covered structure.

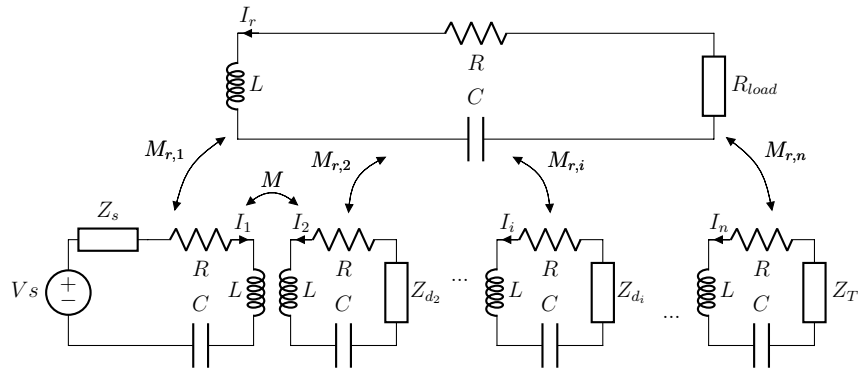


Figure 2.3.2: Equivalent circuit for the general case of a resonator array with a receiver which covers all the cells.

Furthermore, it must be noticed that the defect impedances now affects all the resonators of the array, resulting in a modified topology. The increase in the mutual interaction between receiver and array can make the impedance matrix not symmetric anymore, losing the property of tridiagonality. As a remark, it is interesting to recall that the solution of the system (2.1.8) for $\hat{\mathbf{Z}}_m$ that belongs to the family of Toeplitz matrices can be expressed in a closed form, according to [27]. The inserted defects reported in this paragraphs, that are mainly due to the presence of the receiver in intermediate positions, undermine the efforts made by Alberto et al. and the solution for the current in each cell is achievable only solving the system with the traditional approach, namely inverting the matrices numerically. All these considerations have been done for an array covered by a receiver of any size, but the same circuit model can be applied also in case of more receivers over the metamaterial.

2.4 More receivers

An interesting peculiarity that characterizes a metamaterial for wireless power transfer applications is the possibility to feed more receivers simultaneously. The general approach for the model of an array of coupled resonators covered by multiple receivers can be traced back to the case of a single receiver of size bigger than the resonating cell, namely the situation in which it can cover more elements at a time. As already mentioned in this chapter, the interaction between magnetically coupled coils is modeled by means of the addition of an

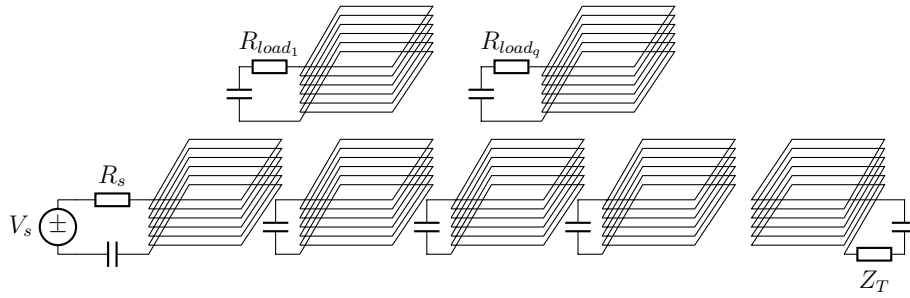


Figure 2.4.1: Example: resonator array with two receivers of different size.

impedance in their respective equivalent circuits, once the mutual inductance is known. In this way the whole equivalent electric circuit can be obtained and all the parameters of the apparatus can be studied solving relatively simple equations. Being the treatment similar to the previous cases, the general formulation is directly approached. The proposed analysis refers to an array of n resonating RLC loops over which q receiver circuits are placed. Some hypotheses must be enforced to ensure the practical feasibility of the system, but they do not affect the generality of the model. The main assumption that has been made defines the limit of the size of the receivers, namely the condition to avoid physical interference or overlapping. Indeed, assuming to have q receivers, the sum of their lengths must be equal to the maximum of the length of the array. Nevertheless, the sizes and the geometry of these circuits can be different from each other. Let now approach the formulation. As it is well known, the first step required for the modeling of the system is again the formulation of the voltage Kirchhoff's laws for the n cells of the array, that must encompass the voltage drop on the cell impedance and the mutual interaction with the adjacent elements of the metamaterial; in case of a receiver placed above the cell, a further mutual contribution must be added. Assuming the dimensions of all the q receivers are equal to those of a resonating element of the metamaterial, the KVL equation can be written as follows:

$$\begin{aligned}
-\hat{V}_s + R_s \hat{I}_1 + \hat{Z} \hat{I}_1 + j\omega M_{1,2} \hat{I}_2 &= 0 \\
j\omega M_{2,1} \hat{I}_1 + \hat{Z} \hat{I}_2 + j\omega M_{2,3} \hat{I}_3 &= 0 \\
&\vdots \\
j\omega M_{i-1,i-2} \hat{I}_{i-2} + \hat{Z} \hat{I}_{i-1} + j\omega M_{i-1,i} \hat{I}_i + j\omega M_{i-1,r} \hat{I}_{r_1} &= 0 \\
j\omega M_{i,i-1} \hat{I}_{i-1} + \hat{Z} \hat{I}_i + j\omega M_{i,i+1} \hat{I}_{i+1} + j\omega M_{i,r} \hat{I}_{r_1} &= 0 \\
j\omega M_{i+1,i} \hat{I}_i + \hat{Z} \hat{I}_{i+1} + j\omega M_{i+1,i+2} \hat{I}_{i+2} + j\omega M_{i+1,r} \hat{I}_{r_1} &= 0 \\
j\omega M_{i+2,i+1} \hat{I}_{i+1} + \hat{Z} \hat{I}_{i+2} + j\omega M_{i+2,i+3} \hat{I}_{i+3} + j\omega M_{i+2,r} \hat{I}_{r_1} &= 0 \\
&\vdots \\
j\omega M_{j-1,j-2} \hat{I}_{j-2} + \hat{Z} \hat{I}_{j-1} + j\omega M_{j-1,j} \hat{I}_j + j\omega M_{j-1,r} \hat{I}_{r_q} &= 0 \\
j\omega M_{j,j-1} \hat{I}_{j-1} + \hat{Z} \hat{I}_j + j\omega M_{j,j+1} \hat{I}_{j+1} + j\omega M_{j,r} \hat{I}_{r_q} &= 0 \\
j\omega M_{j+1,i} \hat{I}_j + \hat{Z} \hat{I}_{j+1} + j\omega M_{j+1,j+2} \hat{I}_{j+2} + j\omega M_{j+1,r} \hat{I}_{r_q} &= 0 \\
j\omega M_{j+2,j+1} \hat{I}_{j+1} + \hat{Z} \hat{I}_{j+2} + j\omega M_{j+2,j+3} \hat{I}_{j+3} + j\omega M_{j+2,r} \hat{I}_{r_q} &= 0 \\
&\vdots \\
j\omega M_{k-1,k-2} \hat{I}_{k-2} + \hat{Z} \hat{I}_{k-1} + j\omega M_{k-1,k} \hat{I}_k + j\omega M_{k-1,r} \hat{I}_{r_N} &= 0 \\
j\omega M_{k,k-1} \hat{I}_{k-1} + \hat{Z} \hat{I}_k + j\omega M_{k,k+1} \hat{I}_{k+1} + j\omega M_{k,r} \hat{I}_{r_N} &= 0 \\
j\omega M_{k+1,i} \hat{I}_k + \hat{Z} \hat{I}_{k+1} + j\omega M_{k+1,k+2} \hat{I}_{k+2} + j\omega M_{k+1,r} \hat{I}_{r_N} &= 0 \\
j\omega M_{k+2,k+1} \hat{I}_{k+1} + \hat{Z} \hat{I}_{k+2} + j\omega M_{k+2,k+3} \hat{I}_{k+3} + j\omega M_{k+2,r} \hat{I}_{r_N} &= 0 \\
&\vdots \\
j\omega M_{n,n-1} \hat{I}_{n-1} + \hat{Z} \hat{I}_n + \hat{Z}_T \hat{I}_n &= 0
\end{aligned} \tag{2.4.1}$$

where the indices i, j, k represent the resonators of the array on which the receiver is placed.

For this latter, the KVL equation holds:

$$j\omega M_{r_q, j - \frac{N_q}{2}} \hat{I}_{j - \frac{N_q}{2}} + \dots + j\omega M_{r_q, i-1} \hat{I}_{i-1} + j\omega M_{r_q, i} \hat{I}_i + j\omega M_{r_q, i+1} \hat{I}_{i+1} + \dots + j\omega M_{r_q, j + \frac{N_q}{2}} \hat{I}_{j + \frac{N_q}{2}} + \hat{Z}_{r_q} \hat{I}_{r_q} = 0 \quad (2.4.2)$$

where

$$\begin{cases} q = 1, \dots, N_q \\ j = 1, \dots, n \end{cases} \quad (2.4.3)$$

and then it leads to a current with the expression:

$$\hat{I}_{r_q} = -j\omega \frac{M_{r_q, d_{j - \frac{N_q}{2}}}}{\hat{Z}_r} \hat{I}_{d_{j - \frac{N_q}{2}}} - \dots - j\omega \frac{M_{r_q, j-1}}{\hat{Z}_r} \hat{I}_{j-1} - j\omega \frac{M_{r_q, j}}{\hat{Z}_r} \hat{I}_j - j\omega \frac{M_{r_q, j+1}}{\hat{Z}_r} \hat{I}_{j+1} - \dots - j\omega \frac{M_{r_q, j + \frac{N_q}{2}}}{\hat{Z}_r} \hat{I}_{j + \frac{N_q}{2}} \quad (2.4.4)$$

where

$$\begin{cases} q = 1, \dots, N_q \\ j = 1, \dots, n \end{cases} \quad (2.4.5)$$

considering that N_q is the number of array's cells covered by the receiver q . Following the procedure explained in paragraph 2.1, it is possible to rearrange the system of equations in matrix form and then obtain an impedance matrix \hat{Z}_m valid for the general case of q receivers, for which the contributions of the naked array and the defects impedance has been split again. Then, it holds:

$$\hat{Z}_m''' = \hat{Z}_{\text{array}} + \hat{Z}_d''' \quad (2.4.6)$$

where the matrix \hat{Z}_{array} is the same reported in (2.1.11), whereas the defect impedance matrix \hat{Z}_d''' assumes the form reported in (2.4.7).

$$\hat{\mathbf{Z}}_{\mathbf{m}}''' = \begin{bmatrix} 0 & \cdots & 0 & \cdots & \cdots & \cdots & \cdots & 0 & \cdots & \cdots & \cdots & 0 & \cdots & 0 \\ 0 & \cdots & \vdots & \cdots & \vdots & \cdots & 0 \\ 0 & \cdots & 0 & \hat{Z}_{d_{i,i-1}} & \hat{Z}_{d_i} & \hat{Z}_{d_{i,i+1}} & \hat{Z}_{d_{i+2}} & 0 & \cdots & \cdots & \cdots & 0 & \cdots & 0 \\ \vdots & \cdots & \vdots & \vdots & \ddots & \ddots & \ddots & \vdots & \vdots & \vdots & \vdots & \vdots & \cdots & \vdots \\ 0 & \cdots & 0 & \cdots & 0 & \hat{Z}_{d_{j,j-1}} & \hat{Z}_{d_j} & \hat{Z}_{d_{j,j+1}} & \hat{Z}_{d_{j+2}} & 0 & \cdots & 0 & \cdots & 0 \\ \vdots & \cdots & \vdots & \vdots & \vdots & \vdots & \ddots & \ddots & \ddots & \vdots & \vdots & \vdots & \cdots & \vdots \\ 0 & \cdots & 0 & \cdots & \cdots & \cdots & 0 & \hat{Z}_{d_{k,k-1}} & \hat{Z}_{d_k} & \hat{Z}_{d_{k,k+1}} & \hat{Z}_{d_{k+2}} & 0 & \cdots & 0 \\ \vdots & \cdots & \vdots & \cdots & \cdots & \cdots & \vdots & \cdots & \cdots & \cdots & \cdots & \vdots & \cdots & \vdots \\ 0 & \cdots & 0 & \cdots & \cdots & \cdots & 0 & \cdots & \cdots & \cdots & \cdots & 0 & \cdots & 0 \end{bmatrix} \quad (2.4.7)$$

The defect impedances are expressed as:

$$\hat{Z}_{d_j} = \omega^2 \frac{M_{j,r_q}^2}{\hat{Z}_r} \begin{cases} q = 1, \dots, N_q \\ j = 1, \dots, n \end{cases} \quad (2.4.8)$$

$$\hat{Z}_{d_{j,j+1}} = \hat{Z}_{d_{j+1,j}} = \omega^2 \frac{M_{j,r_q} M_{r_q,j+1}}{\hat{Z}_r} \begin{cases} q = 1, \dots, N_q \\ j = 1, \dots, n \end{cases} \quad (2.4.9)$$

$$\begin{cases} \hat{Z}_{d_{j-\frac{N_q}{2},j}} = \hat{Z}_{d_{j,j-\frac{N_q}{2}}} = \omega^2 \frac{M_{j-\frac{N_q}{2},r_q} M_{r_q,j}}{\hat{Z}_r} \\ \vdots \\ \hat{Z}_{d_{j-1,j}} = \hat{Z}_{d_{j,j-1}} = \omega^2 \frac{M_{j-1,r_q} M_{r_q,j}}{\hat{Z}_r} \\ \hat{Z}_{d_{j+1,j}} = \hat{Z}_{d_{j,j+1}} = \omega^2 \frac{M_{j+1,r_q} M_{r_q,j}}{\hat{Z}_r} \\ \vdots \\ \hat{Z}_{d_{j+\frac{N_q}{2},j}} = \hat{Z}_{d_{j,j+\frac{N_q}{2}}} = \omega^2 \frac{M_{j+\frac{N_q}{2},r_q} M_{r_q,j}}{\hat{Z}_r} \end{cases} \begin{cases} q = 1, \dots, N_q \\ j = 1, \dots, n \end{cases} \quad (2.4.10)$$

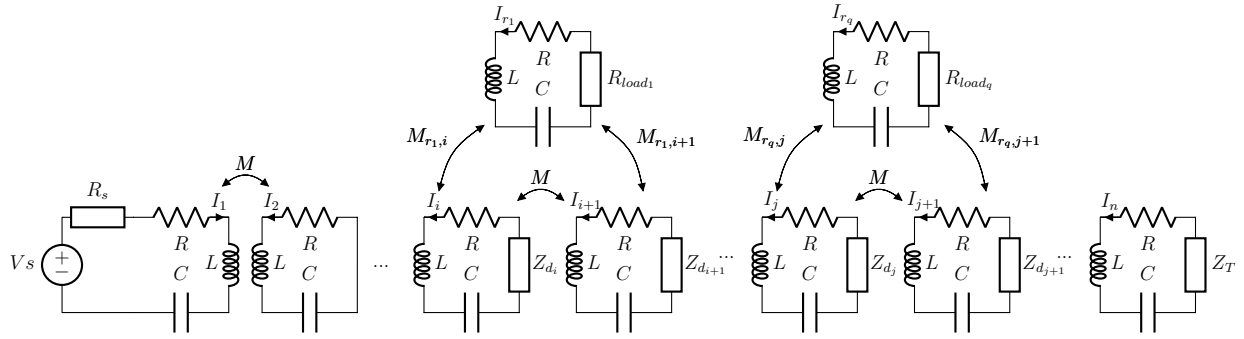


Figure 2.4.2: Equivalent circuit for the case of more receiver fed by the resonator array.

In order to better understand the meaning of (2.4.1) its correspondent circuit representation is reported 2.4.2. The models presented in this chapter characterize the interaction of a mono-dimensional metamaterial with one or more passive resonant circuits in the neighborhood and are necessary for the analysis of their performances. Anyway, the study must be completed with the description of the parameters involved in the equations, that often have a decisive impact on the whole performance.

2.5 Parameters

According to the equations that describe the systems reported in the paragraphs 2.1, 2.2, 2.3 and 2.4 the main parameters that affect the behavior of these systems are the pulse frequency ω , the impedance of the resonators \hat{Z} and the mutual inductance M between them. These variables are fixed depending on the application, whose goal is defined during the design. In order to properly engineer the apparatus, the physical meaning of each term must be fully understood, especially for the parameters whose impact is most severe.

2.5.1 Array Parameters

The first part to be discussed refers to the array. It is indeed composed of a series of magnetically coupled resonators and their impedance must be chosen according to the frequency

at which they must resonate. The element impedance can be written as

$$\hat{Z} = R + j\omega L + \frac{1}{j\omega C}$$

and the conditions for the parameters can be basically the following

- the resistance R is the only parameter that should affect the state variables of the system in resonant conditions, namely voltages and currents and depends on the electric and thermal capability of the system.
- the inductance L must be treated carefully, since the magnetic flux produced depends on it. This parameter depends only on the geometry of the inductor and different solutions can be chosen. Often the resonators are printed on a PCB and the value of the inductance is very complicated to be defined, as reported in; other times they can be wound in air or iron as classical solution for magnetic apparatus in electrical engineering systems. An hidden parameter that must be taken into account in the design and affects strongly the inductor is the quality factor. Indeed, it reports the amount of energy loss relative to the stored energy in the resonator, thereby indicating the damping effect of this latter in resonant conditions.

$$Q = \frac{\omega L}{R}$$

For our purpose it is clearly better to have high Q inductors.

- The capacitance C must be chosen in order to make the system resonate, according to

$$\omega = \frac{1}{\sqrt{LC}}$$

and then

$$C = \frac{1}{\omega^2 L}$$

It can be realized by means of a dielectric interspace on the copper lands in case of

printed circuits, as it is well explained in [28]; otherwise a capacitor can be soldered on the winding terminals realizing a series resonant circuit.

- The resonant pulse frequency $\omega = 2\pi f$ represents the angular frequency at which the magneto-inductive wave propagates and depends on the application. For the purpose of power transfer hundreds of kHz are usually chosen. Once the resonant frequency is defined, all the other parameters can be found consequently.

2.5.2 Mutual interactions

The second focus, for what concerns the parameters, must be done on the mutual inductances. Indeed, they are responsible for the magnetic mutual coupling of the resonant elements and the receiver, thus enabling the propagation of the wave and the transfer of the power. These inductances are again defined only on the basis of the geometry of the system and their evaluation cannot be simple, especially because of the divergent behavior of the Neumann integral. Furthermore, the value of these parameters is expressed as function of the distance between the coupled circuits, that in the case of power transfer applications, could vary during the operation. For these reasons, the analysis could become very complicated and it is necessary to resort to the basics of electromagnetism and circuit theory.

Mutual Inductance between adjacent cells A metamaterial mono-dimensional structure is constituted by coupled resonators of the same shape and the MI wave propagates through them thanks to the magnetic coupling. It is then important to maximize this coupling and this can be done by acting on the geometry of the system. Physically, the flux produced by a resonating cell must link to the adjacent one as much as possible, in order to allow the power to be fully transferred along the array element by element. Generally, once the geometry of the coils is chosen, they are placed closed to each other, and then the coupling is realized.

Mutual Inductance between the array and a receiver For what concerns the mutual coupling between the array and a receiver placed over the metamaterial, the model for the mutual inductance M requires a study which is even more complicated by the simultaneous presence of different cells of the array, whose interaction must be definitely taken into account. Furthermore, the model must consider the possibility of the receiver to move on the metamaterial and then the resulting function must depend on the absolute position x , taken with respect to an absolute cartesian coordinate system. This formulation leads to have all the derived parameters expressed as a function of the absolute position, namely all the quantities that depend on the mutual inductance $M(x)$. The definition of mutual inductance and its derivation has been proved in chapter 3 and considers the interaction of two currents, more exactly two electrically decoupled circuits. Being the resonators of the array magnetically coupled only, the electrical model corresponds to a series of separated electric circuits thereby making the definition of a mutual coefficient for the array - receiver system conceptually wrong. It is indeed necessary to define it for each couple of circuits, namely for the receiver and each cell of the metamaterial. Being the array composed of inductors of the same shape, the resulting system presents symmetries that allow the mutual coefficient M to be considered equal for each couple of currents, leading to significant savings in the computation effort. For the sake of completeness, the variation introduced by the spatial dependence of $M = M(x)$ in the general model for one receiver - presented in section 2.3 - has been reported below. However, it is possible to state that all the configurations reported in section 2.3 maintain the same formulation, except for the spatial dependent mutual contribution. With reference to the general formulation, it is possible to write:

$$\hat{\mathbf{Z}}_{\mathbf{m}}'''(x) = \hat{\mathbf{Z}}_{\text{array}} + \hat{\mathbf{Z}}_{\mathbf{d}}'''(x). \quad (2.5.1)$$

In (2.5.1)

$$\hat{\mathbf{Z}}_{\mathbf{d}}'''(x) = \begin{bmatrix} \hat{Z}_{d_1}(x) & \cdots & \cdots & \cdots & \cdots & \cdots & \hat{Z}_{d_{1,n}}(x) \\ \hat{Z}_{d_{2,1}}(x) & \cdots & \cdots & \cdots & \cdots & \cdots & \hat{Z}_{d_{2,n}}(x) \\ \vdots & \cdots & \vdots & \vdots & \vdots & \cdots & \vdots \\ \hat{Z}_{d_{i,1}}(x) & \cdots & \hat{Z}_{d_{i,i-1}}(x) & \hat{Z}_{d_i}(x) & \hat{Z}_{d_{i,i+1}}(x) & \cdots & \hat{Z}_{d_{i,n}}(x) \\ \vdots & \cdots & \vdots & \vdots & \vdots & \cdots & \vdots \\ \hat{Z}_{d_{n-1,1}}(x) & \cdots & \cdots & \cdots & \cdots & \cdots & \hat{Z}_{d_{n-1,n}}(x) \\ \hat{Z}_{d_{n,1}}(x) & \cdots & \cdots & \cdots & \cdots & \cdots & \hat{Z}_{d_{n,n}}(x) \end{bmatrix} \quad (2.5.2)$$

and

$$\hat{Z}_{d_i}(x) = \omega^2 \frac{M_{i,r}^2(x)}{\hat{Z}_r} \quad i = 1, \dots, n \quad (2.5.3)$$

$$\left\{ \begin{array}{l} \hat{Z}_{d_{i-n,i}}(x) = \hat{Z}_{d_{i,i-n}}(x) = \omega^2 \frac{M_{i-n,r}(x)M_{r,i}(x)}{\hat{Z}_r} \\ \vdots \\ \hat{Z}_{d_{i-1,i}}(x) = \hat{Z}_{d_{i,i-1}}(x) = \omega^2 \frac{M_{i-1,r}(x)M_{r,2}(x)}{\hat{Z}_r} \\ \hat{Z}_{d_{i,i+1}}(x) = \hat{Z}_{d_{i+1,i}}(x) = \omega^2 \frac{M_{i,r}(x)M_{r,i+1}(x)}{\hat{Z}_r} \\ \vdots \\ \hat{Z}_{d_{i+n,i}}(x) = \hat{Z}_{d_{i,i+n}}(x) = \omega^2 \frac{M_{i,r}(x)M_{r,i+n}(x)}{\hat{Z}_r} \end{array} \right. \quad i = 1, \dots, n \quad (2.5.4)$$

are continuous spatial-dependent functions. This formulation allows the parameters of the system to be completely defined for each position of the receiver and thus the state variables to be found resorting to the traditional circuit approach described in section 2.3. It is indeed possible to consider the system solved step by step, thereby approaching the calculation as a discrete spatial-variation, hypothesis that has been exploited for the numerical solution shown in the following chapters.

Chapter 3

Inductance Calculation

The inductance coefficients for a magnetic system can be identified as:

- self-inductance of a coil which refers to the amount of magnetic flux generated by the coil and linked to the same coil;
- mutual inductance between two coils that indicates the amount of magnetic flux generated by a coil and which links to the other one.

The general approach for the definition and calculation of these coefficients is based on the evaluation of the magnetic energy in the whole system - being this constituted by either one or two electric circuits - ensuring the right solution of the problem. Nevertheless, a large amount of geometries allow the formulation to be rearranged in easier expressions, assuming the current concentrated on the axis of the conductor. The introduction of this hypothesis leads to the definition of the Neumann's formula, as reported in [29].

3.1 Prototype

The magnetic system studied in this thesis is basically composed of 6 resonant L-C circuits placed one after the other in a line, thereby forming a series of relay coils that can be

considered a one-dimensional magneto-inductive waveguide, according to [26]. The coils are wound on square wood blocks and are terminated on a capacitance that allow the system to resonate at a certain frequency. Thanks to their geometry, the windings of adjacent resonators are magnetically coupled and the mutual inductance becomes the key parameter to be analyzed, being crucial in the definition of the model. In order to assess the correct value of the mutual coefficient, the real value for the geometric dimensions must be used in the following numerical analysis. The size of the coils is defined by the wood cores, that have a square base of 153mmx153mm and a width of 29mm. The wire has a total diameter of 2.97mm, where the section of the conductor is 3.31mm². A more detailed description of the system is reported in chapter 5

3.2 FEM Approach

According to the general definition of inductance coefficient, it is possible to find the self- and mutual inductance for a winding of any geometry by evaluating the total amount of the magnetic flux linked to the surface described by the coil. In case of the self-inductance coefficient of circuit, the definition can be expressed as:

$$L_i = \frac{\Phi_{i,i}}{I_i} \quad (3.2.1)$$

where Φ is the total magnetic flux penetrating the surface that is enclosed by the loop in which the current I circulates. Instead, for the calculation of the mutual coefficient we have:

$$M_{i,j} = M_{j,i} = \frac{\Phi_{i,j}}{I_j} \quad (3.2.2)$$

in which $\Phi_{i,j}$ corresponds to the amount of flux generated by the current circulating in the j -th loop which links to the surface bounded by the i -th circuit. For both cases the flux is defined as:

$$\Phi = \iint_S \bar{B} \cdot \hat{n} dS \quad (3.2.3)$$

and being

$$\bar{B} = \nabla \times \bar{A} \quad (3.2.4)$$

the Stockes' theorem can be applied, leading to

$$\Phi = \oint_l \bar{A} \cdot d\bar{l}. \quad (3.2.5)$$

This approach can be implemented only numerically, for example by means of finite element method software, that allow the Maxwell's equations to be integrated over any domain. It is indeed the complexity of this latter that requires the problem to be numerically solved, being the magnetic field spread over the entire volume of the system. This analysis has the important advantage to be very general, since it provides the vector potential \bar{A} for each point of the space that can lead to the magnetic flux Φ by means of the integration reported in (3.2.5).

3.2.1 Numerical Simulation

The software used for the numerical calculation is the academic version of Ansys Maxwell, one of the most popular and renowned FEM software available on trade. The first step required is the definition of the geometry of the system and these procedure requires to draw the model by means of the CAD tools that Maxwell provides. Another possible solution is to use a mechanical CAD and then export the model to the FEM software, being this program able to deal with several types of files, including the classical "STEP" files. In this phase of analysis also the material that composes the device under study must be defined, together with the electromagnetic properties of the surrounding space. The resulting model is shown in the figure 3.2.1. The type of solver needed for the analysis depends on the mathematical problem, which can vary according to the sources of the fields and the boundary conditions enforced. Being the coils of the apparatus built by using stranded wire, the skin effect can be considered negligible and then a stationary solution has been found setting the solver for the magnetostatic simulation. It is important to recall the fact that the mutual inductance

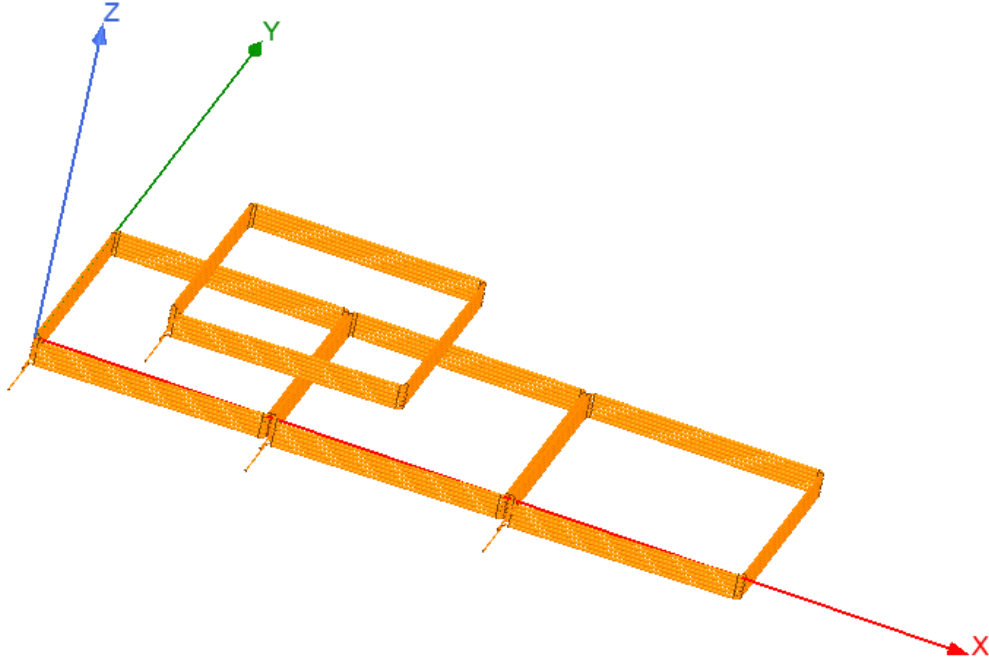


Figure 3.2.1: Model of the system in Maxwell environment.

coefficient is defined for pairs of coupled circuits, and then the metamaterial structure is characterized by as many coefficients as the number of circuits involved in the apparatus. Each mutual inductance coefficient is determined evaluating the amount of linked flux, that strictly varies depending on the facing surfaces of the coils, namely depending on the position of the receiver. In order to perform the correct calculation of $M(x)$ several solutions have been obtained for different positions of the receiver coil - along the resonators array - setting the “parametric simulation mode” that automatically changes the parameters of the system. In the considered case, only the distance of the receiver - defined as the distance between the first edge of the first resonator and the receiver - has been shifted, ranging from the value 0 to the entire length of the array. The value of the DC current circulating in the circuit does not affect the result and it has been set equal for each resonator, choosing a symbolic value. Note that the dimensions are measured with respect to a reference system whose origin is located in the first vertex of the first resonator on the left, as shown in the figure 3.2.1. The main parameters for the simulations are reported in table 3.2.1. The basic procedure implemented by a FEM code consists in the discretization of the whole

Table 3.2.1: Parameters for the simulations.

Simulation Parameters		Value	Unit
Solver	Magnetostatic	/	/
Excitation	Current	50	A
Simulation Setup	Max. Number of passes	8	/
	Percent Error	2	%
Parametric	X start	0	mm
	X max	312	mm
	X step	25	mm

domain in tetrahedrons in which the partial differential equations are solved and then the global solution is achieved interpolating the results obtained in each tetrahedral sub-domain. During the simulation the mesh is gradually thickened in order to increase the precision of the final result. Furthermore, the parametric approach allows the geometry to be automatically modified according to the settings and a FEM simulation is performed for each step. In order to understand the computational effort needed for this kind of calculation, it must be noticed that each step of the parametric analysis requires at least 3 hours to be completed, despite the computer was equipped with 16 GB of RAM memory and a “last generation” microprocessor. The results of the simulations are now presented and commented.

Mesh The mesh is automatically generated by the code and in this case no modifications in the settings were necessary. The resulting mesh has been plotted for each object involved in the system, namely the circuits and the region in the surrounds. As it is possible to guess, the portion of region where discontinuities in the geometry and/or in the material are present is characterized by a denser mesh, with smaller tetrahedrons in order to better approximate the shape of the object. The regions with highest number of discretizations are those that encompass the windings. Indeed, between coil loops the space becomes small and at the same time the interaction due to the magnetic field very large. This relentlessly leads to an high number of elements - and then of unknowns - that make the system very complex to be solved, with very long computational times. For example, for the mesh shown in figure 3.2.2, 971867 tetrahedrons were employed to model the whole system. It is then important to find

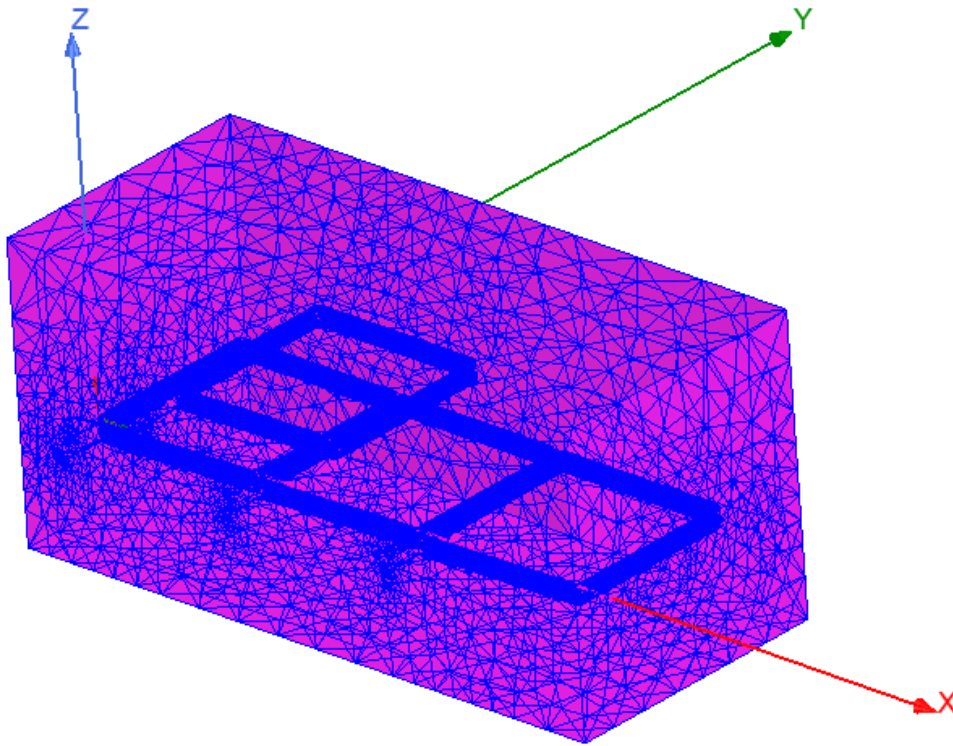


Figure 3.2.2: Plot of the mesh on the object forming constituting the apparatus.

a trade-off between the precision of the solution and the time required by the calculator to get the results.

3.2.2 Results

The results of the mutual inductance calculations for the system described in section 3.1 are now presented and discussed, highlighting their dependence on the position. First of all, it is important to recall that a mutual inductance is always defined for two coupled circuits - and then two currents - so, being this system composed of a series of independent resonating circuits, it is necessary to define as many coefficients as the coupled coils, one for each pair of them. According to chapter , the interaction between nonadjacent resonators can be neglected, thus the mutual coefficient between the array coils is constant in space and equal for each couple of them, whereas the mutual inductances between the receiver and each array cell vary in space with similar behaviour.

Table 3.2.2: Self-Inductance coefficients.

	$M_{I_1} [\mu H]$	$M_{I_2} [\mu H]$	$M_{I_3} [\mu H]$	$M_{I_{receiver}} [\mu H]$
Self-Inductance Coefficient	11.193	11.557	11.13	11.581

Table 3.2.3: Mutual inductance between the cells of the array.

$M [\mu H]$	I_1	I_2	I_3
I_1	11.193	-2.3143	-0.13741
I_2	-2.3143	11.557	-2.3201
I_3	-0.13741	-2.3201	11.130

Self-inductance Considering the self-inductance first, the values obtained from the simulations are reported in table 3.2.2. As it is possible to notice, the values differ, despite the the coils are identical. This is due to the numerical error, that is around 0.3 %. The value for the self-inductance experimentally measured is around $12.6 \pm 0.1 [\mu H]$, as reported in 5.

Mutual Inductance For what concerns the mutual inductance between the cells of the array, the results provided by the FEM analysis are summarised in table 3.2.3. It is interesting to notice that on the main diagonal there are the self inductance coefficients, while the other terms appear outside, creating the proper symmetry. Comparing the inductances of adjacent cells with those of nonadjacent ones, an important difference of more than one order of magnitude can be appreciated. Considering the first element as example, it is coupled with the second through a mutual inductance of $M_{1,2} = -2.3 \mu H$ and with the third through a mutual inductance of value $M_{1,3} = -0.137 \mu H$. Looking at these values, it is possible to notice that $M_{1,3}$ is 95% smaller than $M_{1,2}$ and then the approximation done in the circuit model - that consists in neglecting the nonadjacent interactions - is totally justified. These values validate also the ones assessed experimentally, as reported in 5. However, the most important result, that represents the original contribution to the study of these system, is represented by the definition of the mutual coefficients between the receiver and each cell of the array. Being this dependent on the position x of the receiver circuit along the array axis, the parametric FEM simulations provided the mutual inductance which is function

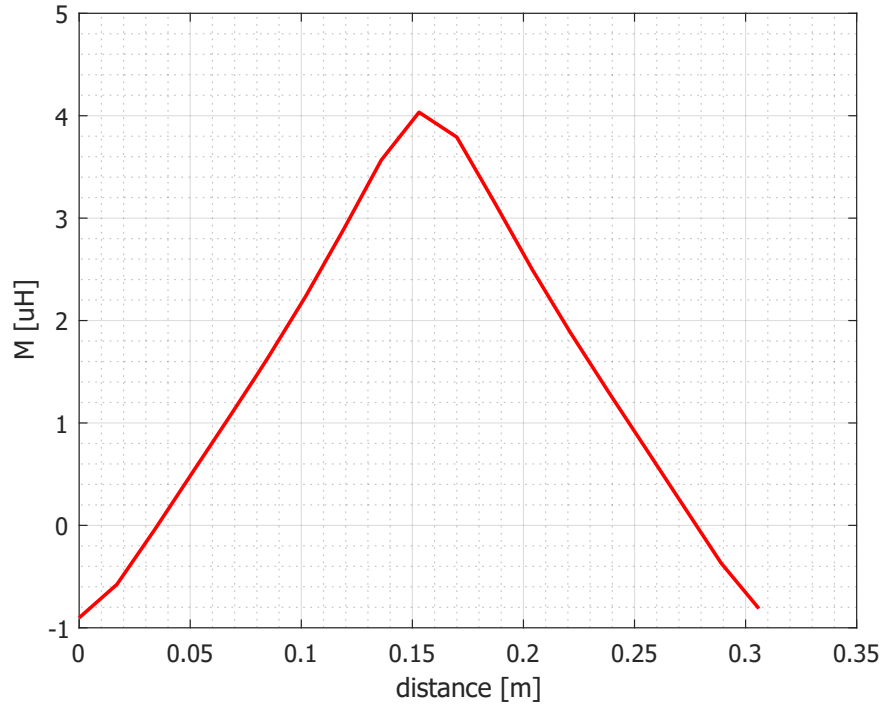


Figure 3.2.3: Mutual inductance between a cell and a receiver moving over it.

of the coordinate x and the height from the array z , namely $M_{i,r}(x, z)$; once the position z is fixed, the function reduces to $M_{i,r}(x)$. The misalignment in the y direction is not considered. In figure 3.2.3 the mutual inductance between the receiver and the second cell of the metamaterial for a distance $z = 30\text{mm}$ has been plotted, being this the most general case as the cell i^{th} interacts with other resonators of the array at both sides. The behaviour of the function $M_{2,r}(x)$ shows its maximum for the value 153mm of the coordinate x , namely when the receiver is perfectly aligned with the second cell. In this position the mutual inductance is $M_{2,r} = 4.2 \mu\text{H}$. Indeed, the majority of the flux produced by the resonating cell links to the circuit above it, and this happens for each pair of perfectly aligned circuits. As the receiver moves away from element, the mutual inductance decreases dramatically, until the displacement reaches the value of the length of the coils, namely when the receiver covers the next cell. At that time, the coupling could be considered negligible. The expected values can be predicted to be symmetric with respect to the other cells, being the structure of the apparatus periodic. Indeed, all the elements that form the array are identical. This

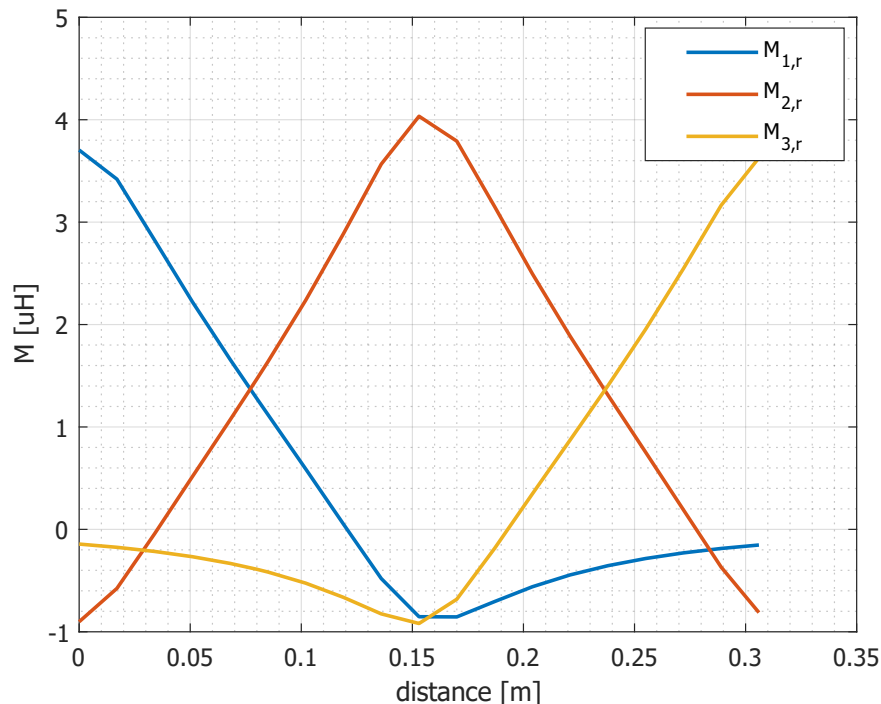


Figure 3.2.4: Comparison of the mutual inductance between a cells and a receiver moving over it .

peculiarity is verified by the behaviour of the other mutual inductance coefficients $M_{1,r}$ and $M_{3,r}$, as it is possible to observe in the figure where

1. the blue curve represents the coefficient $M_{1,r}$
2. the red curve the coefficient $M_{2,r}$
3. the yellow curve $M_{3,r}$

According to what predicted, the functions reflect the periodicity of the structure even if some inaccuracies occur, mainly due to numerical errors. The maximum value, indeed, reaches different values for each pair coupled circuits. The points of maximum, instead, occur for the same coordinate x . An interesting peculiarity to be discussed can be observed in figure 3.2.5, in which the mutual inductance between the first cell of the array and the receiver is reported. As it can be noticed, the value of $M_{3,r}(x)$ for the receiver moving out

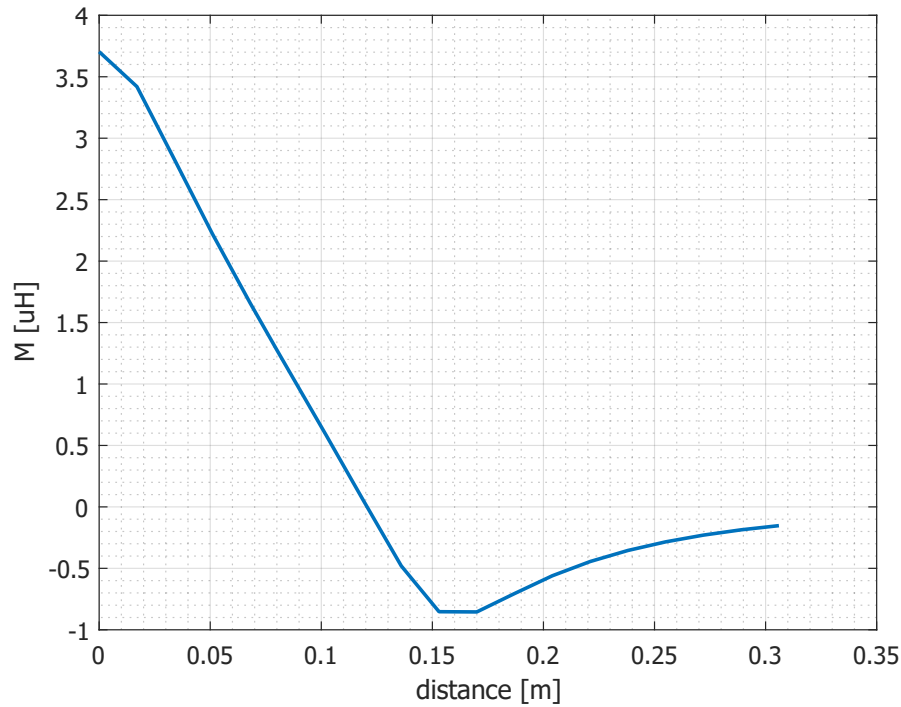


Figure 3.2.5: Mutual inductance coefficient.

the transmitter coil of the array changes its sign just some millimeters before going out from that area. Apparently, this result is not theoretically justified, being the current - and then the flux - signs unchanged. The reason can be found in the inversion of the flux entrance, which -in this case - across the surface bounded by the coil from the bottom to the top. As the receiver moves away from the resonator it is coupled with, the mutual inductance tends asymptotically to zero, as expected. For values of displacement comparable to the length of the coupled cell the interaction of the two circuits can be considered negligible compared to the one between adjacent element. This behavior repeats for each mutual inductance coefficient between the receiver and the array cells.

3.3 Partial Inductance Approach

The partial inductance calculation method solves all these problems. Indeed, it is enough to compute partial self- and mutual inductances for all conductor segments of concern, place

the partial self- and mutual inductances in those conductor segments, and “turn the crank” by simply analyzing the resulting circuit. Partial inductance is considered one of the most powerful tools to assess the inductance coefficients against both numerical results and closed form expressions. This approach could be considered an extension of the field approach, that has been explained in section 3.2, being easier to apply in case of complex electromagnetic environments. Basically, being the flux expressed through a line integral defined for closed lines, it is possible to state that the inductance is defined for closed paths only, namely closed loops. In this context, it is possible to rearrange the formulation assigning a so called “partial inductance” to a portion of the considered loop. This approach allows the evaluation of the integral (3.2.5) to be decoupled into n unique contributions attributable to specific sections of the loop perimeter - which has to be split into segments - thereby attributing specific contributions to the specific sections of the perimeter, according to [29]. Indeed, for the flux of a loop holds:

$$\begin{aligned}\Phi &= \oint_l \bar{A} \cdot \bar{dl} \\ &= \int_{l_1} \bar{A} \cdot \bar{dl} + \int_{l_2} \bar{A} \cdot \bar{dl} + \dots + \int_{l_n} \bar{A} \cdot \bar{dl}\end{aligned}\quad (3.3.1)$$

In this way the self-inductance coefficient becomes equal to:

$$\begin{aligned}L &= \frac{\Phi}{I} \\ &= \frac{\int_{l_1} \bar{A} \cdot \bar{dl}}{I} + \frac{\int_{l_2} \bar{A} \cdot \bar{dl}}{I} + \dots + \frac{\int_{l_n} \bar{A} \cdot \bar{dl}}{I}\end{aligned}\quad (3.3.2)$$

and then the partial self-inductance of a segment of a conductor is defined as:

$$L_i = \frac{\int_{l_i} \bar{A} \cdot \bar{dl}}{I_i}\quad (3.3.3)$$

whereas the partialmutual inductance between two different segments of a current loop is:

$$M_{i,j} = \frac{\int_{l_j} \bar{A} \cdot d\bar{l}}{I_i} \quad (3.3.4)$$

Self-Inductance In the case of a wound coil composed of multiple turns, it is possible to treat the coil as a series of independent straight wires of negligible diameter which are magnetically coupled one to the other, exploiting the partial inductance method above described. According to [30], the self-inductance contribution can be obtained as the sum of the mutual contributions between each pair of segments that compose the winding and the self-inductance of the single wire, as reported in the formula

$$L_{tot} = \sum_{i=1}^{N'} L_i + \sum_{i=1}^{N'} \sum_{j=1}^{N'} M_{i,j} \quad (3.3.5)$$

here N' is the number of segments in which the coil is divided. With this arrangement the mutual Neumann integral can be exploited for the calculations of $M_{i,j}$ and it is expressed as:

$$M_{i,j} = \frac{\mu_0}{4\pi} \int_{l_i} \int_{l_j} \frac{d\bar{l}_i \cdot d\bar{l}_j}{r_{ij}} \quad (3.3.6)$$

where the subscripts i and j indicate the two coupled segments of the coil and the quantity r_{ij} represents the magnitude of the euclidean distance between the two infinitesimal vector elements $d\bar{l}_i$ and $d\bar{l}_j$ of the coil.

For the partial-self-inductance the more general approach reported in section 3.2 must be resorted, being the Neumann formula applied to a single wire always divergent due the singularity of the distance vector r_{ii} . Namely:

$$L_i = \frac{\mu_0}{4\pi} \int_{l_i} \int_{l_i} \frac{d\bar{l}_i \cdot d\bar{l}_i}{r_{ii}} \rightarrow \infty \quad (3.3.7)$$

In the past century several scientific papers has proposed closed formulas to be directly applied, which have been derived from the definition reported in 3.2. In that case the linked flux has been evaluated for a surface that starts from the coil and extends endlessly, as described

in [29]. The approximation involved is basically related to the radius of the conductor, that must be much smaller compared with the length of the wire. The formula exploited in this work is reported in [?] and has the following expression:

$$L_i = \frac{\mu_0}{2\pi} l \left[\sinh^{-1}\left(\frac{l}{r_w}\right) - \sqrt{1 + \left(\frac{r_w}{l}\right)^2} + \frac{r_w}{l} \right] \quad (3.3.8)$$

where l is the length of the filament and r_w its radius. The formula has a general validity, since it directly results from the integration. Further simplifications are allowed introducing the hypothesis of a length of the segment which is much larger than the wire radius, namely $l \gg r_w$.

Mutual Inductance Calculation For the calculation of the mutual inductance coefficient between two wound coils, they can be considered made up of straight wires with negligible diameter as mentioned before. The mutual inductance is obtained by the sum of the partial mutual inductances $M_{i,j}$ between any segment i belonging to the first coil and any segment j of the second coil. Thus, it holds:

$$M_{tot} = \sum_{i=1}^{N'_1} \sum_{j=1}^{N'_2} M_{i,j} \quad (3.3.9)$$

where N'_1 and N'_2 are the numbers of segments in which the two coils are divided and the mutual Neumann formula for the coefficients $M_{i,j}$ is (3.3.6). The main difference between the two coefficients (i.e. self- and mutual inductance) lies in the pairs of coupled wires considered, that belong to the same winding for the case of self-inductance and to two different coupled coils for the mutual one. It must be also be noticed the absence of the partial-self-inductance coefficients in the calculation of the mutual inductance between two wound coils, as it can be easily guessed.

3.3.1 Analytical approach-Campbell Approach

Many books and scientific papers propose the calculation of self- and mutual inductance coefficients of coupled coils, but, of course, these coefficients strictly depend on geometry of the system. A general approach is then needed, allowing the computation to be performed for any shape of the winding as alternative to the classical and very complicated analytical calculations. The most general way for the representation of a coil is to split it into straight wires as mentioned before, leading to the necessity of a formula for the calculation of the mutual coefficient for any pair of wires of any lengths. Considering these latter as ordinary segments in a three dimensional space, the Neumann integral can be differentiated using geometric relationship written for the two segments, as it has been done by George A. Campbell in the publication [31]. Indeed, it states that the Neumann integral can be expressed as:

$$M = \cos(e) \int \int \frac{dS ds}{r} \quad (3.3.10)$$

where

$$r^2 = (Pp)^2 + S^2 - 2Ss \cos(e) + s^2 \quad (3.3.11)$$

With this notation, S and s are the points on the segments that have the algebraic projection on the other filament and are taken positive starting from the common perpendicular Pp ; e is the angle between the segments. The integral (3.3.10) can be in a directly integrable form as below:

$$\begin{aligned} M &= \cos(e) \int \int \left(D_S \frac{S}{r} + D_s \frac{s}{r} - \frac{(Pp)^2}{r^3} \right) dS ds = \\ &= \cos(e) \left(\left| S \int \frac{ds}{r} \right| + \left| s \int \frac{dS}{r} \right| - \frac{Pp}{\sin(e)} \int \int \frac{Pp}{r^3} \sin(e) dS ds \right) = \\ &= \cos(e) \left[S \log(r + s - S \cos(e)) + s \log(r + S - s \cos(e)) - \frac{Pp(\text{solid angle})}{\sin(e)} \right] \end{aligned} \quad (3.3.12)$$

This decomposition comes from the analogy with the Newtonian potential for a parallelogram built on the two segments as described in [31], providing an exact solution for the Neumann formula for each possible mutual position of the two filaments. Further simplifications of

the formula are reported in the same work. However, it must be noticed that, in order to perform this integration, the system must be analytically described in rigorous manner, requiring important computational efforts. The most convenient approach for the application of these results is to treat the system numerically, allowing the right input for the formula to be automatically defined. In this thesis, a general code for each geometry has been reported, despite the experimental verification has been done only for square coils.

3.3.2 Matlab Implementation

All the formulas commented above make the integration affordable despite complex geometries characterizing the apparatus. More precisely, they can be very useful when implemented in a calculator and, in order to allow the correct calculation, the data must be rearranged so that the computer is able to deal with them. For this kind of application, the Matlab environment represents one of the most user-friendly tools, for which both the geometrical model and the equations have been arranged. Similarly to the general approach treated in section 3.2, the physical dimensions of the prototype - which is described in 3.1 - play a fundamental role in the calculation and then they must be stored and provided as input for the code. Indeed, in the Campbell's original paper [31], different formulas for the mutual inductance of two wires are reported, depending on the orientation of the segments with respect to each other. In order to follow this approach, the windings must be split into straight segments storing the start and end points. It is then important to fix a common reference frame for all the coils involved; each geometrical object is expressed in the cartesian formulation with respect to it. An accurate model of the coil has been established, considering all the three dimensional developments of the structure giving rise to a very complex algorithm. To have the possibility to check the results of this first part of the code, the stored winding has been plotted, as it is possible to see in figure 3.3.1. For what concerns the receiver circuit, a spatial variation must be integrated in the model. Assuming the same geometry for the receiver coil, the calculation of the mutual inductance as a function of position requires the code to be extended considering different positions for the receiver winding. As already mentioned in

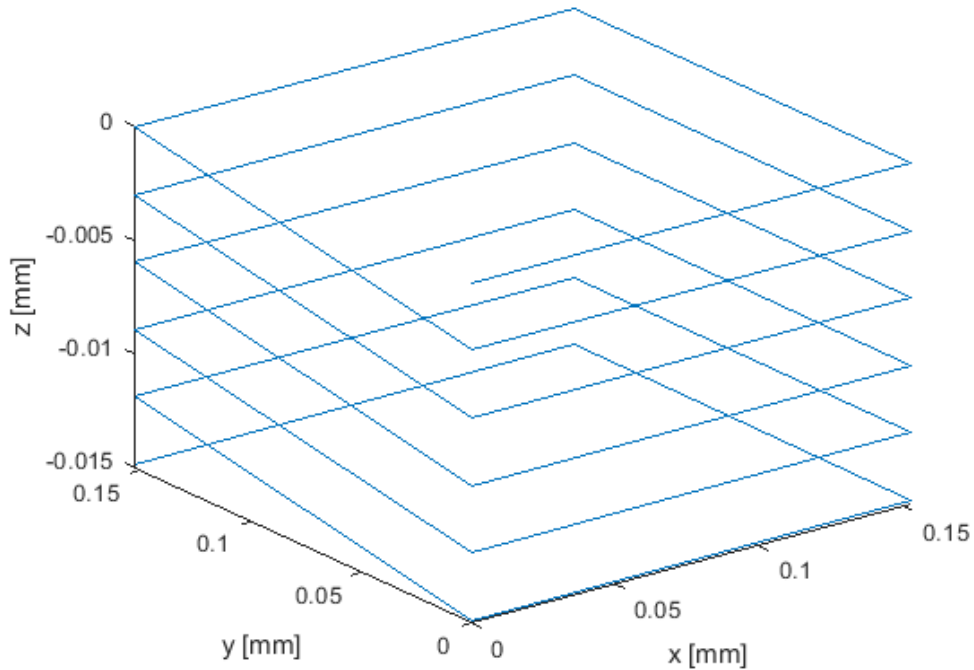


Figure 3.3.1: Representation of the coil in Matlab environment.

section 3.2.2, the calculation of the coefficient $M_i(x)$ has been performed considering only a spatial variation along the x coordinate, namely for the receiver moving along the array. It is important to highlight that the mutual inductance is defined for a pair of current loops a time only, and this code has been written to calculate it once, exploiting the resulting function for all the mutual couplings. In this way, the algorithm has been optimized, reducing the computational efforts required. In figure 3.3.1 different loops that represent the receiver circuit for different values of the coordinate x , each with a different color, are plotted. In this example, a discretization of 25mm has been enforced. The next step of the simulation is the calculation of the mutual inductance of any two filaments in a three dimensional space, which has been performed implementing the Campbell's formula (3.3.10) reported above. As already mentioned, several simplified formulas have been shown in that article, obtained from the Neumann integral. Those expressions, together with (3.3.8), are the ones implemented in this code, whereas the definition a common reference frame was necessary for each pair of segments in order to correctly apply the method. In particular, three cases are really useful

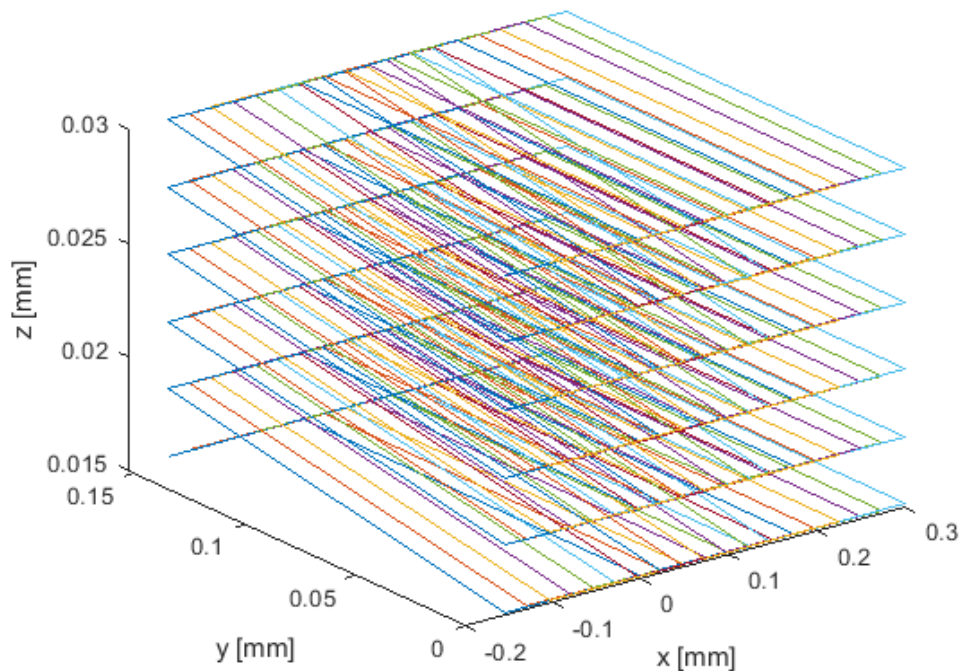


Figure 3.3.2: Representation of the receiver coil in different positions.

for the aim of this work:

- The mutual Neumann integral between any two straight filaments making with each other the angle e (general case), reported in the first equation of [31].
- The mutual Neumann integral between any two straight filaments for the special case of filaments mutually parallel, reported in the third equation of [31].
- The self Neumann integral of a single filament defined in (3.3.8), presented in [29].

It is important to notice that, being the problem formulated for a general relative position of the pair of segments, no approximations have been done in the definition of the geometric model of the coil, reproducing the real situation. This requires to deal with complicated concepts of analytical geometry, especially for what concerns three-dimensional angles. Indeed, in the formula (3.3.12) the calculation of solid angles is required and this problem has been

overcame thanks to the specific arrangement suggested in [31](formula number 10), implemented in a dedicated Matlab function. Similarly, also the other specific formulas have been grouped in functions and recalled in the main file, resulting in a clearer and leaner interface. In particular, besides the geometrical modeling, one single function has been developed for the calculation of the mutual inductance, that has been cycled for each position of the receiver circuit, providing the appropriate input filaments. As a result, a vector containing the inductance coefficients is obtained, with a size that depends on the number of positions considered for the receiver. This formulation corresponds to the definition of a discrete function, in which the number of elements that composes the length x acts as a discretization of that variable. The continuous version can be obtained by means of the automatic interpolation performed by Matlab that provides $M_i(x)$ for different z displacements, as reported in the following figures. According to the number of elements in which the length x has been split, the accuracy with which the curve approximates the reality can improve, helping the whole model to become very accurate. For this example, a discretization step of 5mm has been chosen, being this a value that provides an integer number of positions for the receiver. This results in a more symmetric graph. As last observation, it is interesting to analyze the function with the x domain extended three times, in order to appreciate the behaviour for those positions. Intuitively, the mutual inductance decreases as the receiver moves away from the transmitter coil, reaching asymptotically the value zero for large misalignment. The plot in figure 3.3.4 shows that behaviour, that apparently matches the predictions but, with a focus on the area at the bottom of the “bell” it is possible to appreciate the presence of negative values, as shown in the zoomed image of the same figure. This peculiarity reflects the same anomaly detected in the results of the FEM simulation, discussed in 3.2.2. The same considerations hold, but could be for sure an interesting peculiarity to be experimentally proved or disproved, thus opening a wider discussion.

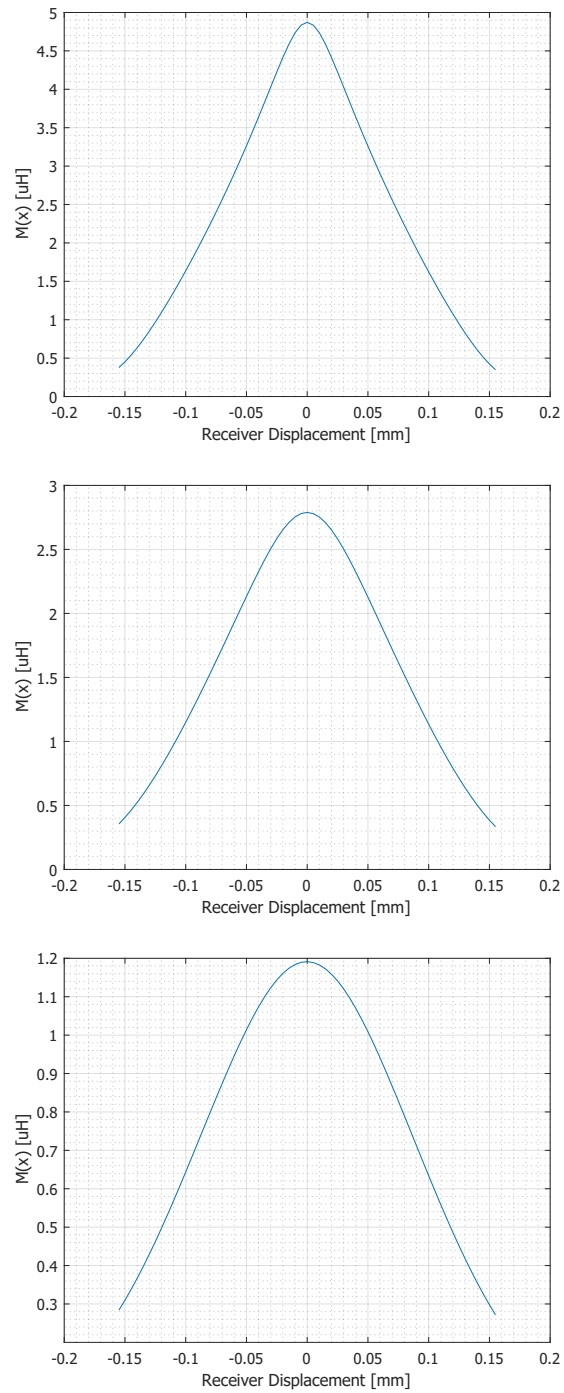


Figure 3.3.3: Mutual inductance coefficients as a function of the x displacement for different values of z : $z = 10\text{mm}$ for the first plot, $z = 40\text{mm}$ for the second plot and $z = 90\text{mm}$ for the third.

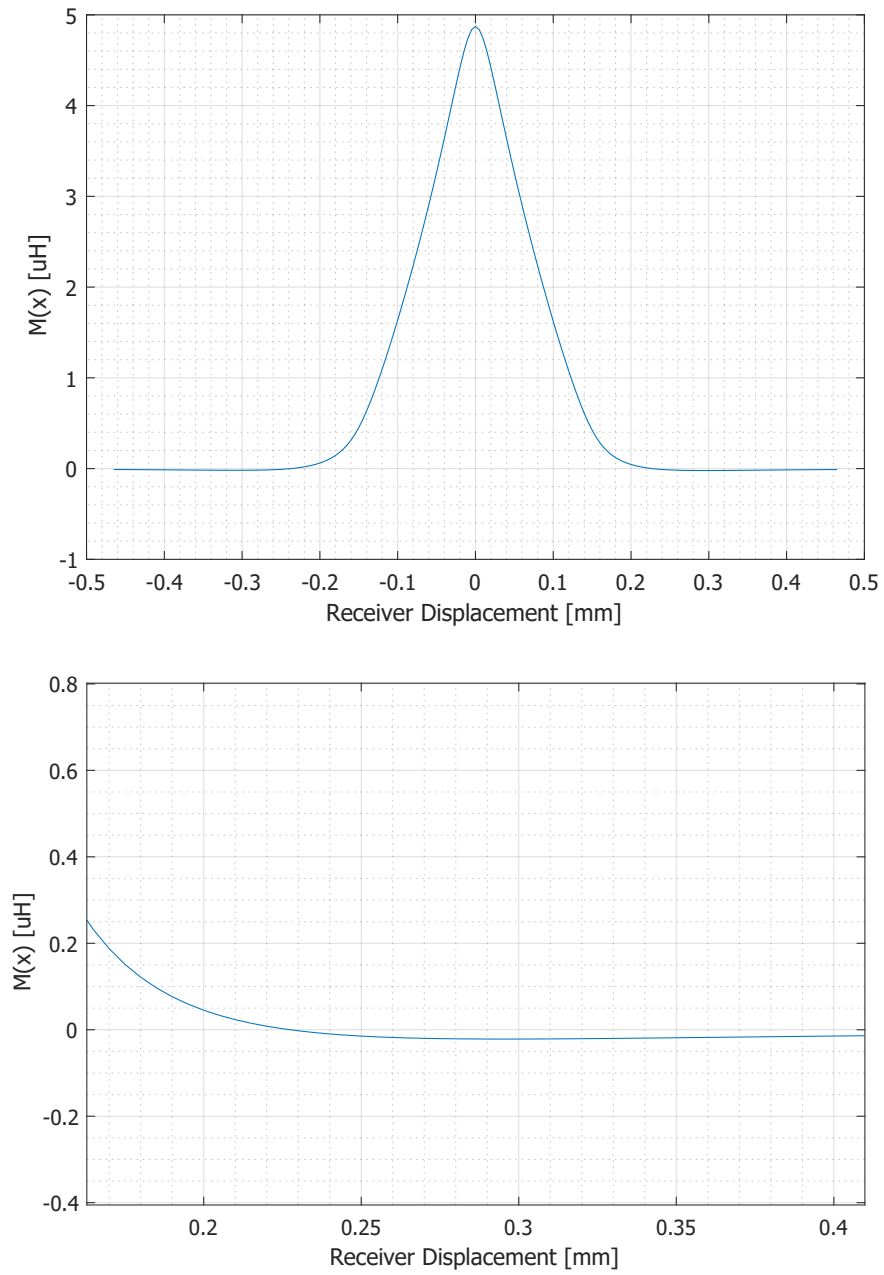


Figure 3.3.4: Mutual inductance for the extended x domain.

Table 3.4.1: Mutual inductance results comparison.

M [μH]		Matlab code	FEM simulation	Experimental
$M_{i,r}(x) _{x=0}$	$z = 10mm$	4.87	4.94	4.8
	$z = 40mm$	2.76	2.81	2.7
	$z = 90mm$	1.19	1.11	1.2
Self-inductance L [μH]		11.9	11.19	12.5

3.4 Result comparison

The definition of a correct mutual inductance coefficient is a crucial point for reaching the final goal of the work and in this frame, the results have been checked with as many tools as possible. In particular, being the rest of the analysis performed in Matlab environment, the discrete function is handled as described in section 3.3.2, leading to the necessity of validate that model. In order to do this, FEM simulations and experimental results - already available - have been exploited. As mentioned in the paragraphs above, the mutual inductance depends on the position of the receiver and the distance of this latter from the array. These dependencies are described by the variable x and z respectively. In the table 3.4.1 some cases are reported considering the maximum value of $M_{i,r}$ for different distances from the array, since the experimental values were measured only in perfect alignment conditions.

The estimation obtained with the Matlab code differs with respect to the experiments for some percent, resulting greater when the receiver is closer to the array and smaller when it moves away. The numerical simulations provides values that are smaller compared to both the other techniques. The last parameter presents the self-inductance, whose values do not match between each other as expected. The main reason of this error can lie in the approximation introduced by the analytical formulation and the inaccuracies occurred during the measurements. Indeed, for what concerns the Matlab model, it exploits the Campbell formulation of the Neumann integral, which assumes to deal with segments of negligible diameter. This hypothesis is not verified when the mutual inductance is computed for pairs of segments that belong to the same edge of the coil, being their distance small compared with the cross section of the wire. This inevitably leads to an error, especially in the case

of the self-inductance, as it is possible to guess. The error introduced by the finite element method software can be traced back to the simulation error, which is basically due to the discretization and linearization of the field problem. The experimental measurements have been performed on the same prototype studied in this work and are described in 5, whose results are considered reliable.

Chapter 4

Current Calculation

In this short chapter the current calculation method is explained, starting from the analytical description of the problem until the presentation of the results with the proper comments. This part of the work represents an original contribution, being all the currents of the apparatus be determined, namely the currents circulating in each resonator for each position of the receiver circuit. This step is necessary for the complete characterization of the system, being involved in the evaluation of the electromechanical interactions between the circuits and thermal stress of them, phenomena that cannot be neglected in high power applications. Indeed, in the last decade, the interest in high efficiency systems for wireless power transfer has driven the research in this field towards the study of alternative methods together with the optimization of the component involved. For this reason, resonant arrays are now exploited as improvement of the classical coupled coils, that usually work in resonance in order to extend the allowed displacement and need to be designed to tolerate increasing power, especially if they are used in electric vehicle charging. The currents play the crucial role, being the variable that leads the design requirements for what concerns power systems and characterize the quality of this latter. The transmitted power is indeed evaluated by means of proper measurements on the receiver current, which usually closes on a load. All these aspects are taken into account in the numerical simulations presented in this work, allowing the assessed values to be completely matched. It must be underlined that the model can be

developed thanks to the definition of the mutual inductance function in the previous chapter.

4.1 Theoretical model

Even though different models have been defined depending on the dimension of the receiver, the prototype available in the laboratory is composed of equal wound coils with an identical receiver and then the following analysis refers to that system. According to the theory approached in chapter 2 for the case of a receiver identical to the array resonators 2.1, the receiver can interact with only two cells of the array a time, leading to the definition of the matrix (2.1.10). In order to find the currents circulating in the coils the system (2.1.8) must be solved, where $\hat{\mathbf{I}}$ and $\hat{\mathbf{V}}$ are the currents and voltages vectors of the array, respectively. In particular, the voltages at terminals of the coils or the capacitor - that are equal since they are L-C series circuits - are null if the perfect magnetic resonance imposed by the source is achieved. The only exception is for the first terminal, which is directly supplied by the voltage generator presenting \hat{V}_s at its terminals. The vector is then defined as:

$$\hat{\mathbf{V}}^T = [\hat{V}_s \ 0 \ \dots \ 0] \quad (4.1.1)$$

For what concerns the vector $\hat{\mathbf{I}}$, it contains all and only the currents in each cell, whose values strictly depend on the interaction between the coils, especially with a moving receiver and then it holds:

$$\hat{\mathbf{I}}^T(x, z) = [\hat{I}_1(x, z) \ \hat{I}_2(x, z) \ \dots \ \hat{I}_n \hat{I}_2(x, z)] \quad (4.1.2)$$

The interaction with the receiver circuit is described by means of the function $M_{i,r}(x, z) |_{z=const}$ obtained in chapter 3, which makes the impedance matrix dependent on the receiver displacement, namely $\hat{\mathbf{Z}}_{\mathbf{m}} = \hat{\mathbf{Z}}_{\mathbf{m}}(x, z) |_{z=const}$. The rigorous notation for Ohm's law in matrix form becomes

$$\hat{\mathbf{V}} = \hat{\mathbf{Z}}_{\mathbf{m}}(x, z) |_{z=const} \hat{\mathbf{I}}(x, z) |_{z=const} \quad (4.1.3)$$

The solution implies to invert the matrix $\hat{\mathbf{Z}}_{\mathbf{m}}$, obtaining

$$\hat{\mathbf{I}}(x, z) |_{z=const} = \hat{\mathbf{Z}}_{\mathbf{m}}^{-1}(x, z) |_{z=const} \hat{\mathbf{V}} \quad (4.1.4)$$

In this way all the currents circulating in the resonators are determined for each value of the displacement x (and eventually z). The prototype is composed of six resonators wound on square wood blocks with identical receiver - as described in 5 - and then the expression of the impedance matrix, written for a the case in which the receiver covers the i^{th} and $(i+1)^{\text{th}}$ cells at a given distance z , assumes the form:

$$\hat{\mathbf{Z}}_{\mathbf{m},i,i+1}(x) = \begin{bmatrix} \hat{Z} + R_s & j\omega M & 0 & 0 & 0 & 0 \\ j\omega M & \hat{Z} & j\omega M & 0 & 0 & 0 \\ 0 & j\omega M & \hat{Z} + \hat{Z}_{d_i}(x) & j\omega M + \hat{Z}_{d_{i,i+1}}(x) & 0 & 0 \\ 0 & 0 & j\omega M + \hat{Z}_{d_{i+1,i}}(x) & \hat{Z} + \hat{Z}_{d_{i+1}}(x) & j\omega M & 0 \\ 0 & 0 & 0 & j\omega M & \hat{Z} & j\omega M \\ 0 & 0 & 0 & 0 & j\omega M & \hat{Z} + \hat{Z}'_T \end{bmatrix} \quad (4.1.5)$$

where \hat{Z} is the proper impedance of a cell and is equal for all elements and the coefficient M is the mutual inductance between two adjacent resonators of the array (also this parameter is equal for all coupled cells of the array). The impedance defects introduced because of the presence of the resonator receiver are written in a generic formulation in the following equations:

$$\begin{aligned} \hat{Z}_{d_i}(x) &= \omega^2 \frac{M_{i,r}^2(x)}{\hat{Z}_r} \\ \hat{Z}_{d_{i+1}}(x) &= \omega^2 \frac{M_{i+1,r}^2(x)}{\hat{Z}_r} \\ \hat{Z}_{d_{i,i+1}}(x) &= \hat{Z}_{d_{i+1,i}}(x) = \omega^2 \frac{M_{i,r}(x)M_{r,i+1}(x)}{\hat{Z}_r} \end{aligned} \quad (4.1.6)$$

where $M_{i,r}(x) = M_{r,i}(x)$ and $M_{i+1,r}(x) = M_{r,i+1}(x)$ are the functions describing the mutual inductance between the receiver and the cells that it faces. The resistance R_s is internal resistance of the supply apparatus, which usually must be considered to make the representation rigorous and the impedance \hat{Z}_T is the matching load for the magnetoinductive wave generated along the array. Indeed, since this system behaves as magnetoinductive waveguide, if the array is terminated in the proper load, standing waves can be eliminated, as reported in [32]. It is clear that when the receiver moves and covers different cells, the impedance matrix has to be updated, thereby changing its topology. In order to allow the code to build - and then solve - the above mentioned system with an automatic procedure, the impedance matrix has been split in two contributions, where the former is constant and the latter depends on the displacement. In particular, the first matrix corresponds to the impedance matrix of the array without any receiver, which has been already studied in [27] and for the system of six elements is:

$$\hat{\mathbf{Z}}_{\mathbf{marray}} = \begin{bmatrix} \hat{Z} + R_s & j\omega M & 0 & 0 & 0 & 0 \\ j\omega M & \hat{Z} & j\omega M & 0 & 0 & 0 \\ 0 & j\omega M & \hat{Z} & j\omega M & 0 & 0 \\ 0 & 0 & j\omega M & \hat{Z} & j\omega M & 0 \\ 0 & 0 & 0 & j\omega M & \hat{Z} & j\omega M \\ 0 & 0 & 0 & 0 & j\omega M & \hat{Z} + \hat{Z}'_T \end{bmatrix}. \quad (4.1.7)$$

As it is possible to observe, $\hat{\mathbf{Z}}_{\mathbf{marray}}$ is a tridiagonal matrix of the Toeplitz type and this property allow wide considerations, including the possibility to define a closed formula for the calculation of the currents, as reported in [27]. Unfortunately, the presence of the receiver breaks these symmetries, thereby making it impossible to find close-form expressions for the currents. Indeed, the defects must be incorporated adding the terms described in (4.1.6) to

(4.1.7), process that can be shown as the addition of a matrix devoted to the defects:

$$\hat{\mathbf{Z}}_{\mathbf{m}_{d_{i,i+1}}}(x) = \begin{bmatrix} 0 & 0 & 0 & 0 & 0 & 0 \\ 0 & 0 & 0 & 0 & 0 & 0 \\ 0 & 0 & \hat{Z}_{d_i}(x) & \hat{Z}_{d_{i,i+1}}(x) & 0 & 0 \\ 0 & 0 & \hat{Z}_{d_{i+1,i}}(x) & \hat{Z}_{d_{i+1}}(x) & 0 & 0 \\ 0 & 0 & 0 & 0 & 0 & 0 \\ 0 & 0 & 0 & 0 & 0 & 0 \end{bmatrix} \quad (4.1.8)$$

The result is expressed as sum of the two contributions, as shown in the relation

$$\hat{\mathbf{Z}}_{\mathbf{m}}(x) = \hat{\mathbf{Z}}_{\mathbf{m}_{\text{array}}} + \hat{\mathbf{Z}}_{\mathbf{m}_{d_{i,i+1}}}(x) \quad (4.1.9)$$

The implementation of this algorithm is done in Matlab, with the possibility to exploit the storage of the data as regards the geometry and the inductances, being all the previous operation done in the same environment. In order to make this procedure automatic, the additional terms are added by means of a proper “for” loop able to identify the correct position in which the defect must inserted, whereas the constant matrix $\hat{\mathbf{Z}}_{\mathbf{m}_{\text{array}}}$ is written exploiting its symmetry property, since Matlab provides special tools to handle this mathematical objects (Toeplitz functions have been used). The resulting code gives rise to a series of different impedance matrices, one for each position of the array, since the data are stored as discrete functions of the displacement. Depending on the position of the receiver, the defects are evaluated on the basis of mutual inductance, provided by the previous calculations. Being the structure periodic, the same function $M(x)$ can be exploited with any resonator of the array which interacts with the receiver, even if, in line of principle, it should be defined for each pair of currents - and then of coupled circuits. In that case, the mutual inductance curve would be shaped as the “bell” shown in the previous chapter and lay down to zero when the circuits do not overlap. The procedure implemented allows the same data to be exploited since the counter that acts as x variable is incremented each time displacement is changed

with the proper space shift, allowing the code to be leaner and more efficient. Once the impedance matrix has been defined for each position, it is possible to solve the system and then obtain the currents, as described above. This operation has to be repeated of course for each matrix, namely for each value of the displacement obtaining a series of current arrays, whose number depends on the discretization of that x dimension. It must be noticed that the discretization step with which the impedance matrices are calculated must be the same of the one adopted in the inductance calculation procedure, in order to be sure that for each x position for which the system is solved, a value of mutual inductance has been calculated. This consideration rises because of the presence of discretized functions, which requires one to be careful in handle them; a lot of errors, indeed, are due to the wrong correspondence of the values stored in the structures, that became very complex when incorporating several “layers”.

4.2 Numerical Implementation and Results

The implementation of the model described in the precedent paragraph allowed an easy evaluation on the currents, with the possibility to repeat the calculation several times and for different geometries. The results achieved for the available array prototype are reported in the following, with special focus on the receiver current. The current arrays obtained from the solution of the system (4.1.3) returns as many current arrays as the positions of the receiver. Each of them contains six phasors representing the sinusoidal currents circulating in the coils, assumed to be isofrequential at the resonant frequency of the system. The magnitude of the resonator currents are plotted with respect to the position of the receiver circuit in separated graphs and the resulting curve has been shaped by means of the automatic interpolating function available in Matlab. The results reported in the following comes from the numerical simulations only and the input values for the analysis have to be taken into account to avoid meaningless discussions. In order to well understand the discussion and to ensure a complete visualization of the physical phenomena involved, the basic theory of magnetoinductive waves must be resorted to, as described in the first chapter. The analysis

aims to describe the behavior of the system with reference to the currents and the energy, validating the above described model which will be exploited for the purpose exposed at the beginning of this chapter.

4.2.1 Input Variables

As it can be guessed, the input parameters affect strongly the behaviour of the apparatus, thus they must be chosen according to the electrical characteristics of this latter together with the aim of the analysis. These parameters - reported in the list below - represent the input of the Matlab functions written ad hoc to solve the system, incorporating also the definition of the impedance matrix:

- Supply voltage $\hat{V}_s = \frac{10}{\sqrt{3}} V$
- Internal resistance of the power supply $R_S = 50 \Omega$
- Resonant frequency $f_{res} = \frac{1}{2\pi\sqrt{LC}} = 146.95 kHz$
- Matching termination impedance $\hat{Z}_T = 1.5 \Omega$
- Discretization step for both mutual inductance and current calculations $x_{step} = 5 mm$
- Receiver load $R_R = 5 \Omega$

Several simulations have been done varying these parameters, in order to better define the performance of the system in different operating conditions, but the main discussion has been done with reference to the numerical results that reproduces the experimental condition of the laboratory.

4.2.2 Simulation for low distance receiver

The graphs reported below show the behavior of the currents considering that the position of the receiver varies along the length of the array and the distance from it is assumed to be $10mm$ in the z direction, namely the receiver is placed directly over the array - meaning that the distance between the faced resonators is due to the wooden substrate. In order to clarify the exposure of the results, it must be underlined that the scale for the current amplitude has been set using as reference the maximum and minimum values of the current in the considered cases. For what concerns the x axis, it is has been indexed with the magnitude of the receiver displacement and, considering that the resonators are $153mm$ long, it is possible to identify the location of the cells of the array.

1 First Resonator of the Array The plot of the current of the first resonator of the array is reported in figure 4.2.1 and shows a nearly constant behavior for the entire length of the structure, with some negative peaks in correspondence to the odd cells. Indeed the minima occur for the values $0.31mm$ and $0.62mm$, which correspond to the perfect alignment condition with the third and fifth cell. The presence of maxima and minima seem to be negligible in the whole scale, whereas it can be appreciated with the appropriate relative scale. In figure 4.2.2 the y -axis has been zoomed, highlighting that the current oscillates between $0.128A$ and $0.1402A$ initially and damping effects occur as the receivers moves along the array. A reasonable explanation lies in the presence of the magnetoinductive wave which travels along the structure and then each cell sees a different peak.

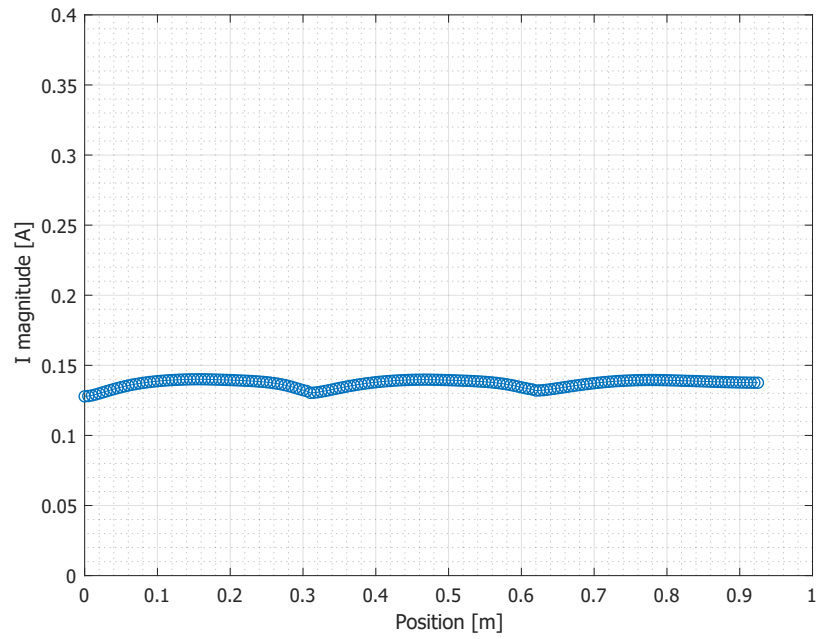


Figure 4.2.1: Magnitude of the current in the first resonator of the array.

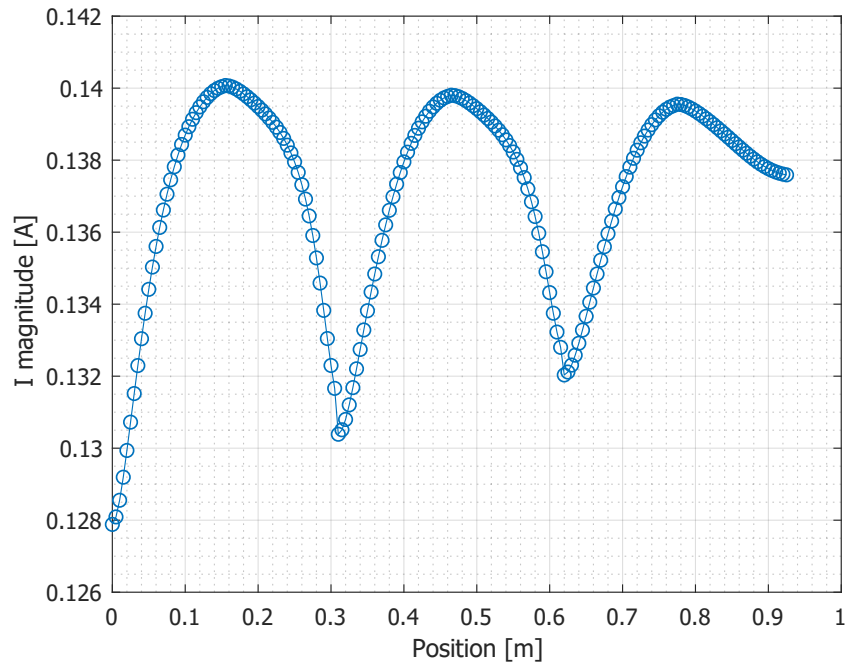


Figure 4.2.2: Magnitude of the current in the first resonator of the array in small scale.

2 Second Resonator of the Array The current in the second cell of the array with reference to the absolute scale is plotted in figure 4.2.3 and is likewise characterized by an oscillatory behaviour. However, in this case, the shape of the curve looks like mirrored with respect to the current in the first resonator - figure 4.2.1 , situation that can be traced back to the phase shift introduced by the inductive coupling with the adjacent resonators. The array cells are, indeed, coupled trough the pure imaginary impedance $j\omega M$, that delays the currents of $\frac{\pi}{2}$ radians, as it is proved in [27]. The presence of the receiver provides further coupling, which induces an extra shift in the phase of $\frac{\pi}{2}$ radians, causing the phase inversion of the currents, as shown. Besides, it must be noticed that a strong peak of $0.38A$ occurs when the receiver is aligned with the next resonator, namely the third. The same behaviour repeats when the receiver is aligned with the fifth cell, namely giving life to a periodicity which is typical for this apparatus, even if it is usually smoother.

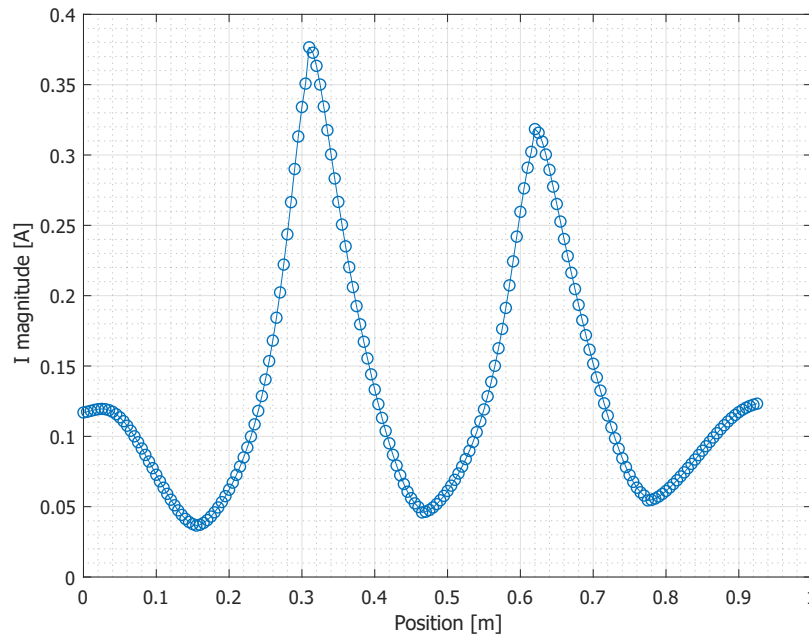


Figure 4.2.3: Magnitude of the current in the second resonator of the array.

3 Third Resonator of the Array Similarly to what happens for the first resonator, the evolution of the current profile shown in figure 4.2.4 for the third cell remains nearly constant for displacements that are greater than 0.459mm , namely for the receiver placed over the third cell and following ones. Indeed, a strong negative peak occurs when the receiver is aligned with the second cell. The average magnitude of the currents is slightly smaller with respect to the one in the first cell, mainly due to Joule losses caused by the resistance of the wire.

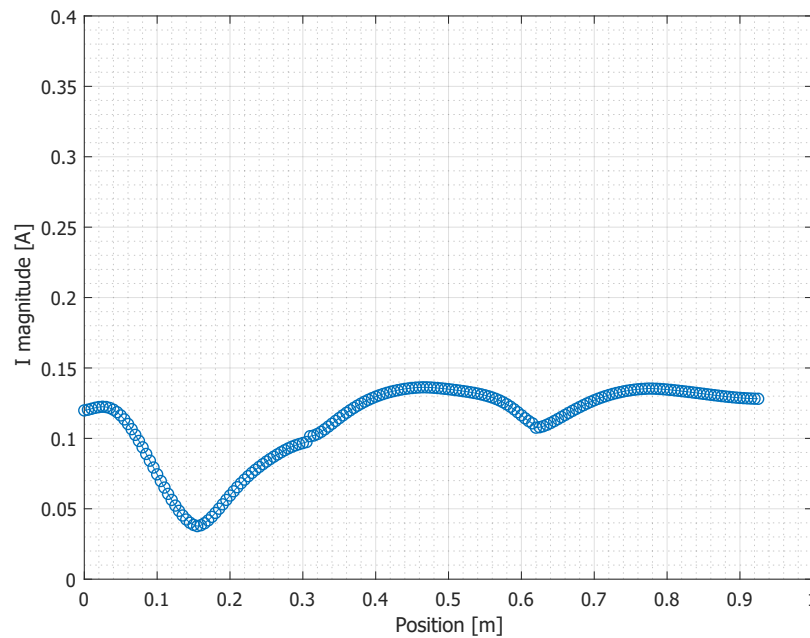


Figure 4.2.4: Magnitude of the current in the third resonator of the array.

4 Fourth Resonator of the Array Looking at figure 4.2.5, it is possible to appreciate another trend which suggests the presence of periodicity. In this case the curve reflects the one obtained for the second cell, reported in figure 4.2.3, both in shape and in magnitude. It is interesting to notice that the peak expected in correspondence of the alignment of the receiver with the third cell is completely absent, indicating that the currents of the array cells closer to the power source present more peaks with an higher magnitude. The slight fall in the value of these maxima with respect to the case of figure 4.2.3 can be due to the dissipating effects of the winding resistance, while the absence of them for the far resonator of the array has to be traced back to the presence of the receiver, which modifies the structure of the magnetoinductive waveguide and the associated phenomena.

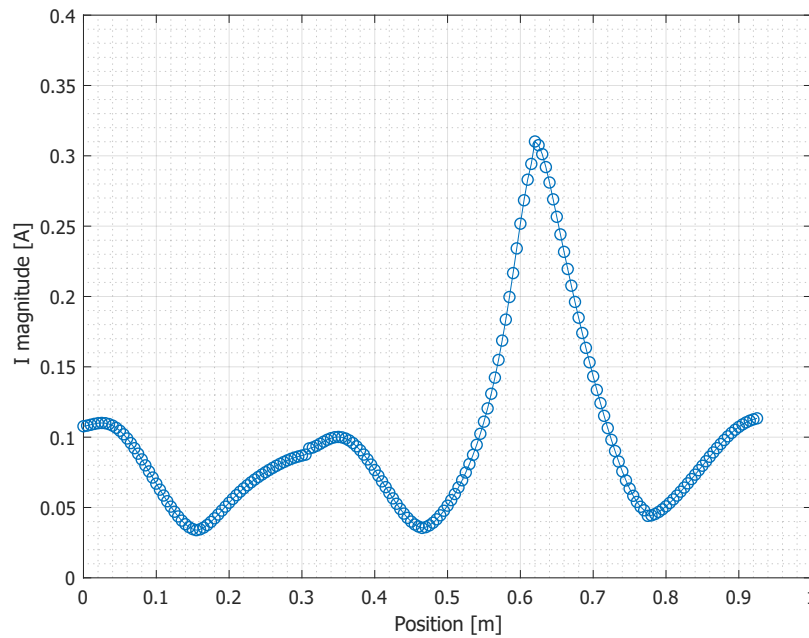


Figure 4.2.5: Magnitude of the current in the fourth resonator of the array.

5 Fifth Resonator of the Array The characteristic behaviour for the fifth resonator described in figure 4.2.6 is similar to the others identified for the odd cells, presenting an almost constant trend with periodic negative peaks in case of presence of the resonator on the previous odd elements. What surprises is the magnitude of the currents of the array cells after the position of the receiver, which present the same values unless a little decrease due to joule losses. It seems that the receiver causes current deeps until it reaches the considered cell (i.e., the fifth cell) and overcomes it, situation for which the behavior remains stable.

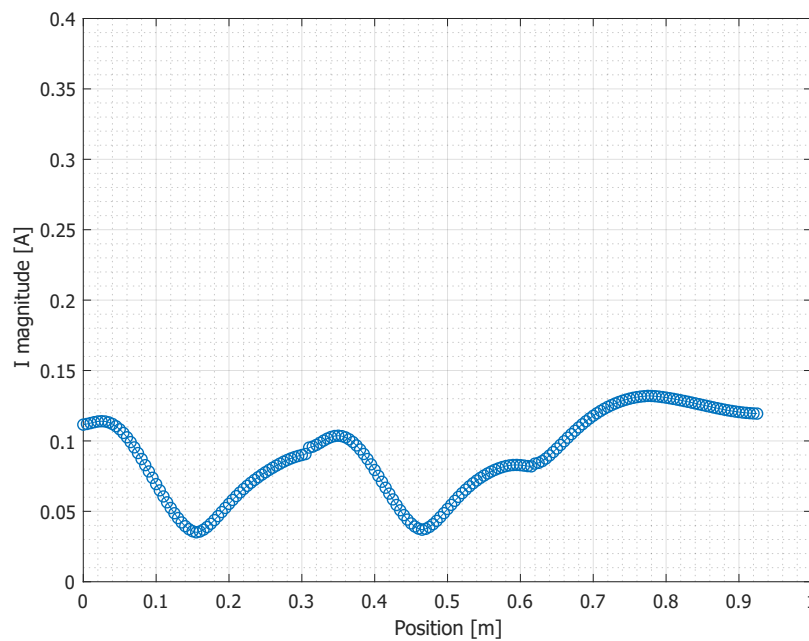


Figure 4.2.6: Magnitude of the current in the fifth resonator of the array.

6 Sixth Resonator of the Array The last resonator of the considered array is labeled with an even number and then the current is expected to reflect the ones for the other even elements. The typical trend is described in section 4.2.2 and the results satisfy the prediction, being the curve oscillating between $0.095A$ and $0.03A$. The constant behaviour is not reached, since it requires that the receiver overcomes the considered cell, which is in this case the last. Looking at the average current, it is decreased as consequences of the insertion of the termination impedance \hat{Z}_T to match the line, which adds to the winding resistance dissipating the power that reaches the cell.

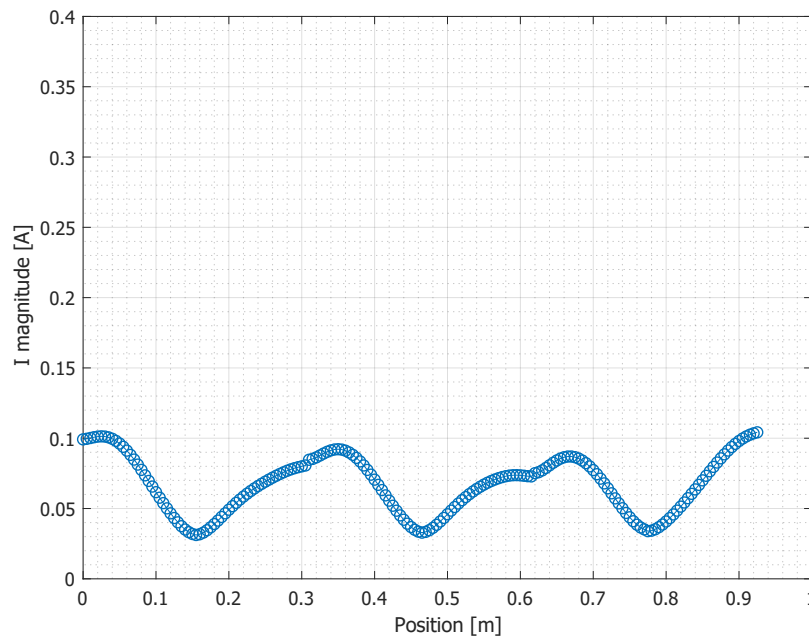


Figure 4.2.7: Magnitude of the current in the sixth resonator of the array.

Receiver Another part of the system that is important to analyze is the receiver circuit placed over the array, whose behavior represents the reference for the discussion about the performances of the system. Indeed, the applications of this kind of apparatuses in the field electrical engineering are usually devoted to the transmission of energy wirelessly, where the main goal is to feed the load connected to the receiver circuit with the highest amount of power possible. The receiver winding is terminated on the series between a capacitor - that allow the circuit to resonate - and a load resistance R_R that acts as a dissipative load. The resulting current is plotted in figure 4.2.8, where the absolute scale - defined at the begin of the analysis - has been adopted. The value of this current remains lower with respect to the others circulating in the array for the entire sweep that has been simulated, presenting maxima in correspondence of the alignment with the odd cells and minima for the positions for which the receiver is aligned with the even ones. This peculiarity suggests the optimum positions in which the receiver can pick up the maximum amount of power and the others in which is not convenient to operate, namely the odd and even ones respectively.

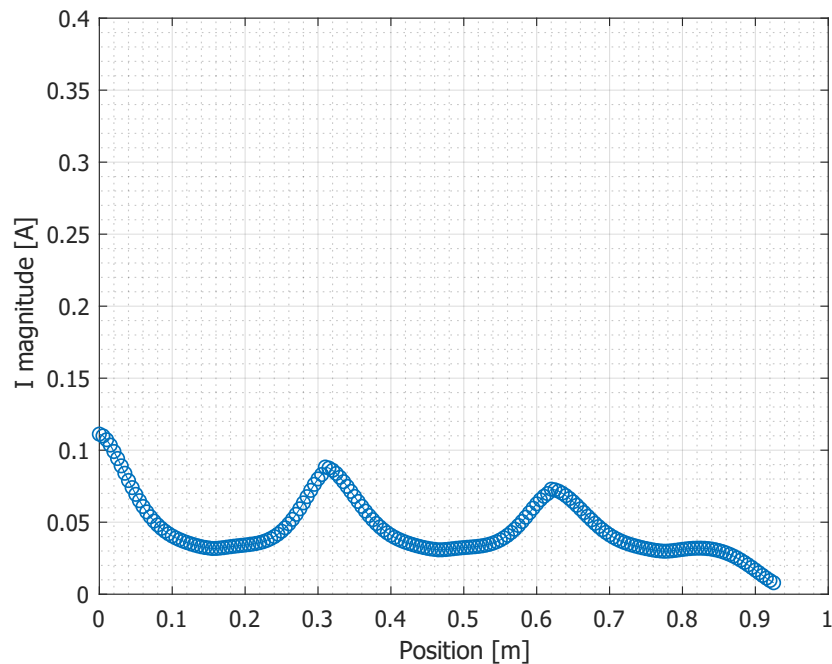


Figure 4.2.8: Magnitude of the current in the receiver circuit.

Currents comparison Another interesting observation can be done comparing the currents of the array cells with the one of the receiver and in order to do this, two groups of plots have been reported in the figures. On the left and right columns, blue lines describe the currents circulating in the odd and even resonators, respectively. The receiver current is drawn in red and obviously is the same for all plots: it has been replicated in each plot to allow fast comparison, useful to gain a whole visualization of the phenomenon. For this analysis only the qualitative trend is considered, being the numerical values the same described in the paragraphs above. As already addressed before, the presence of the receiver strongly affects the current values for the resonators of the array and it is possible to identify typical current trends - with reference to the position - that are common for each cell. In particular, the same behavior holds for the currents of the array cells for a position of the receiver between them and the power source, namely for those which have not already faced the receiver. This consideration can be done for each resonator of the array, except the first one, which is directly connected to the voltage source and for which this condition never holds. On the left side of each $\hat{I}_i - x$ curve reported in the figure 4.2.9 the phenomenon just explained can be appreciated, being all those lines identically shaped. Furthermore, it is possible to state that the trends of the last cell and receiver currents as function of the displacement tend to overlap, as it is clearly visible in the last plot of the right column in figure 4.2.9, whose shapes present only a small difference that can be due to the difference in the circuit topology.

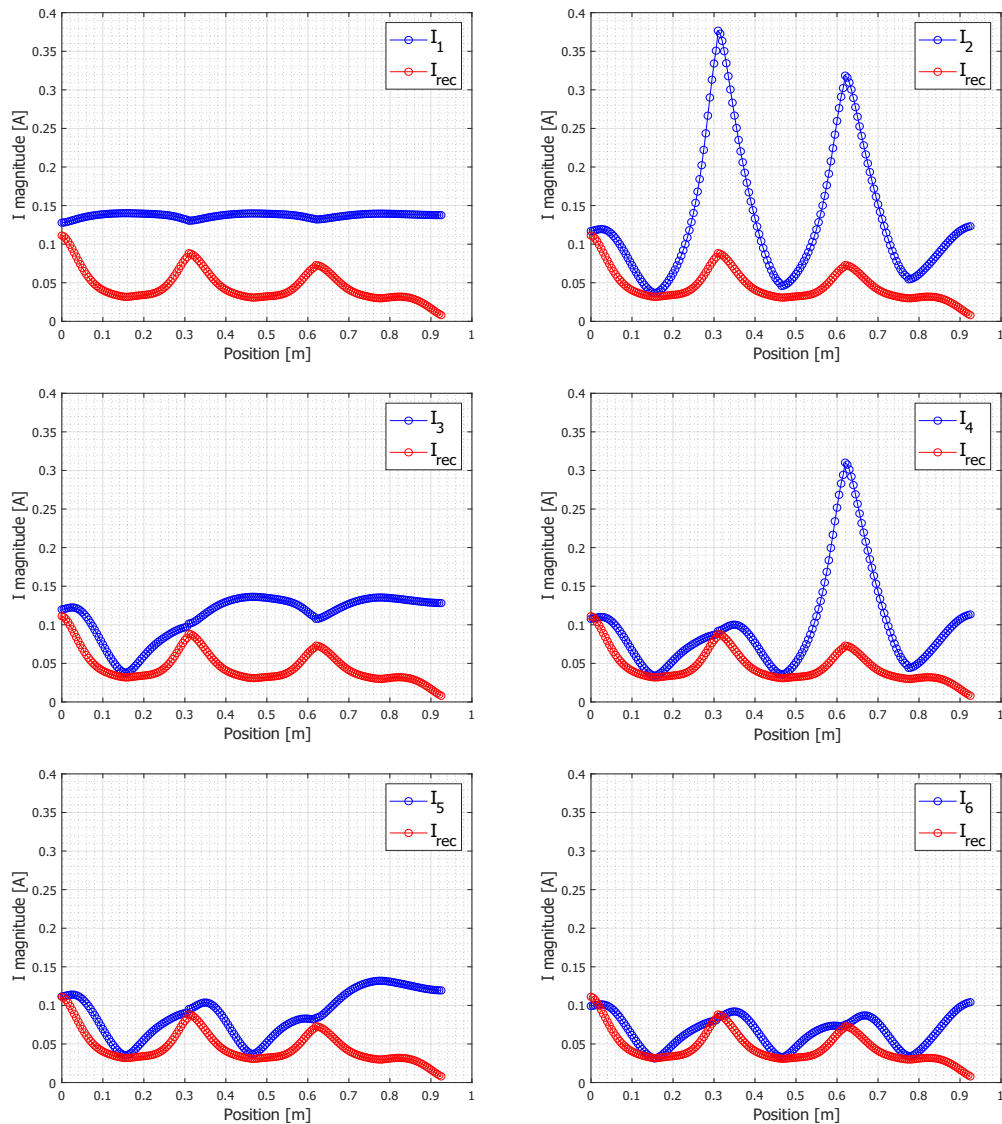


Figure 4.2.9: Comparison of the receiver current with the currents of an array with 6 resonators for $z = 10mm$.

As further prove of this consideration, a similar apparatus with an higher number of resonators has been analyzed and the results reported in figure 4.2.10. The characteristics are identical to the array exploited for the other simulations (described in 4.2.2), namely the same inputs that have been described in 4.2.1. The presence of additional cells makes the chain of resonators longer and all the considerations just described are still present. This confirms the validity of the precedent discussion, with the possibility to better visualize the

periodicity that has been predicted. Indeed, it is now easier to see different trends and their evolution, especially for what concerns the peaks that characterize the even elements, that are present in an higher number. Being the magnitude of this current about 2.5 times the average one experienced in the odd cells, the risk of an overload is seriously practical and the higher it is the stronger is the stress that the components have to bear, both electrical and thermal. For the second cell the number of this maximum has been estimated to be $\frac{n}{2} - 1$ and then 2 in case of 6 resonators while 3 if 8 elements are considered. Unfortunately, those peaks occur in correspondence of the alignment of the receiver with the odd cells, that are the positions that allow the maximum transfer of energy, as it is possible to understand observing the value of the receiver currents (red line of the graphs). For what concerns the currents in the odd cells, they have been already discussed previously and defined to be almost constant. However, some maxima and minima are present and their difference increases in the last even resonator, whose current remains at values similar to the one of the receiver for most of the positions simulated. In this case the situation is mirrored with respect to even cells, being the position of the minimum currents observed for the position of maximum power transmission, namely the maximum for the receiver current. This consideration could be totally forgotten, being the whole trend nearly constant. Another important analysis refers to the choice of the receiver load as it can affect both the receiver and the array currents, causing singular effects. The value set for this simulations is the one adopted in the study reported in[27] and allow an observation related to the perfect alignment position of the receiver. In particular, it is possible to state that each time the receiver is aligned with one of the array cells, the magnitude of its current has the same value of the one of the resonator which is facing. For example, considering the currents $|\hat{I}_1|$ and $|\hat{I}_{rec}|$ at first, their values are nearly similar and the same holds for $|\hat{I}_2|$ and $|\hat{I}_{rec}|$ for a displacement of $153mm$, namely when the receiver completely covers the second element. This peculiarity can be noticed for each graph and is possible only with the proper receiver load.

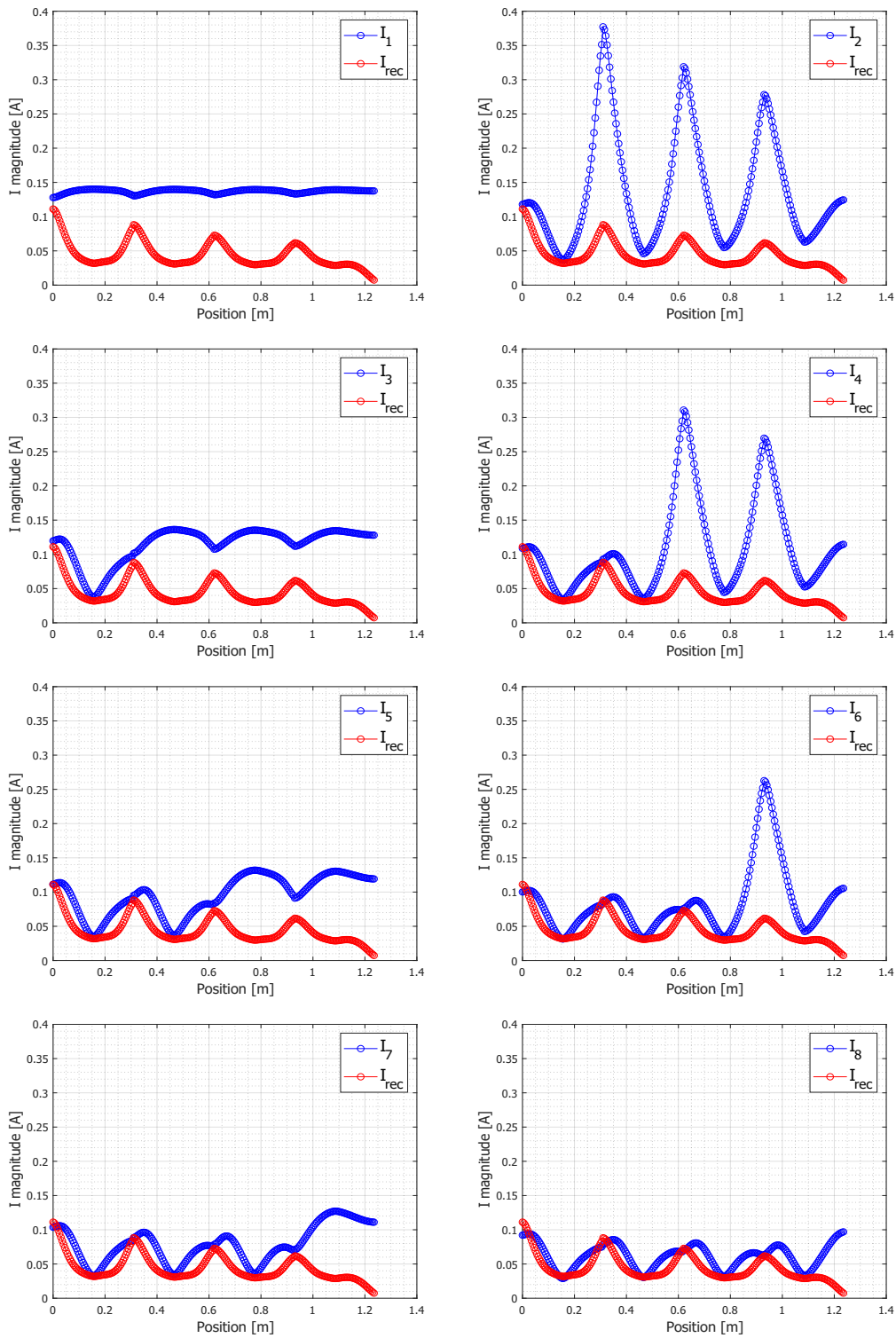


Figure 4.2.10: Comparison of the receiver current with the currents of an array with 8 resonators $z = 10mm$.

4.2.3 Simulation for large distance receiver

One of the most critical points in this kind of systems is the distance of the receiver from the array, which could strongly affect the performances of the apparatus. In wireless power transfer applications it represents the main challenge, together with the quality of the energy which is transferred that reflects on the current. In order to complete the analysis of the performance of the array, a couple of simulations with an increased distance of the receiver have been performed and the results are shown in the following graphs. In order to standardize the analysis, the value for the z coordinate has been set equal to $40mm$ and $90mm$, according to the calculations of the mutual inductances described in the previous chapter, for which the values of the function $M_{i,r}(x, z) |_{z=const}$ have been experimentally and numerically validated. In figure 4.2.11 is reported the current behaviors in case of a receiver $40mm$ far from the array. In this first case, the current trend is again similar to the one obtained for the minimum distance. All the curves appear smoothed, especially the ones concerning even cells, whose values present the most important peaks that now overcame the average value obtained for the odd cells 1.8 times only (it was 2.5 in the previous case). The currents in the odd cells feature the same evolution, with an increased gap with respect to the value of the receiver current. Indeed, looking at the figure 4.2.9, it is possible to notice that the minimum values of all currents remain nearly the same, whereas all the maxima are strongly reduced or almost disappear. The second variation applied, namely $z = 90mm$, emphasizes the characteristics shown by the precedent simulation. As can be see in figure 4.2.12, the peaks in the receiver actually disappeared, while the average value for the array currents is almost the same. The receiver current appears now further reduced, being around $0.025A$.

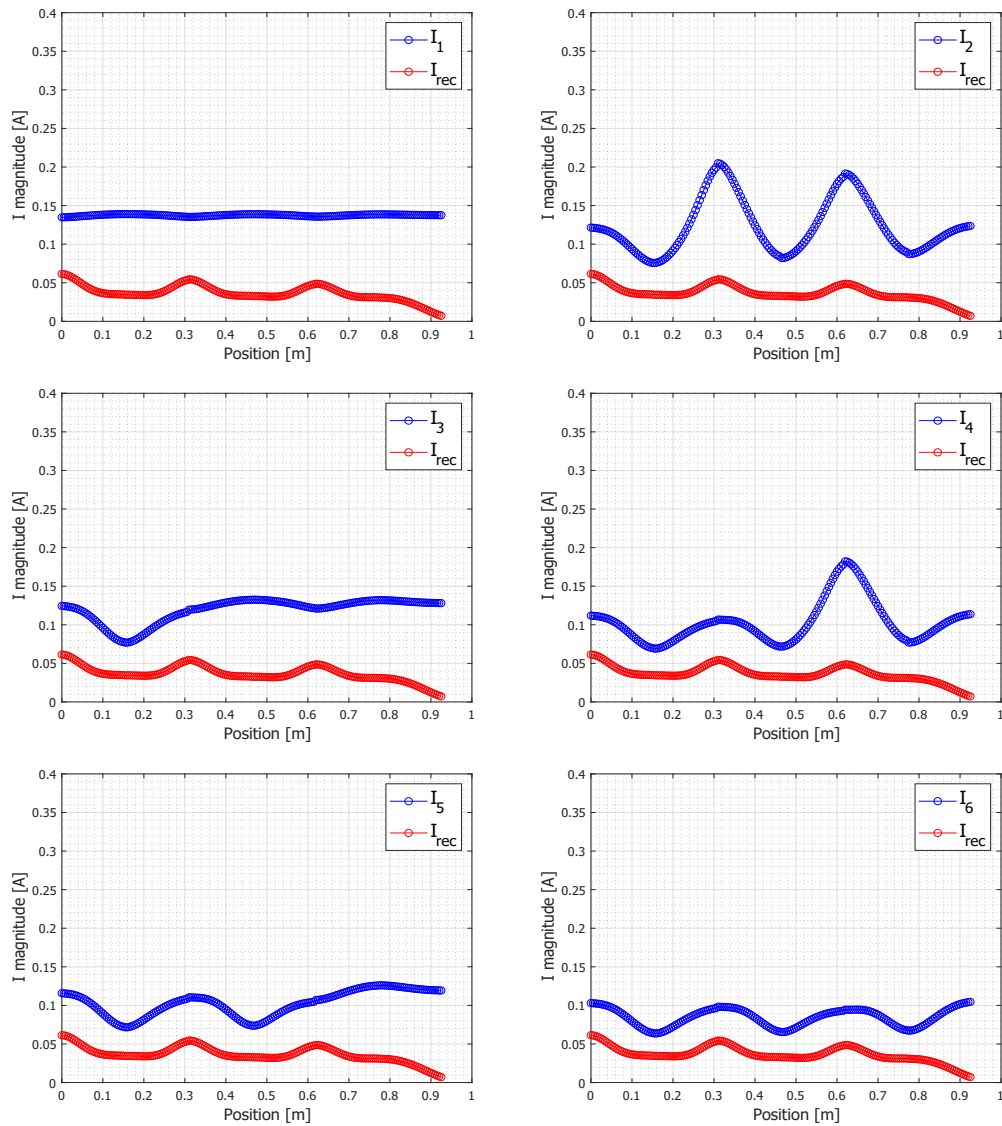


Figure 4.2.11: Comparison of the receiver current with the currents of an array with 6 resonators $z = 40mm$.

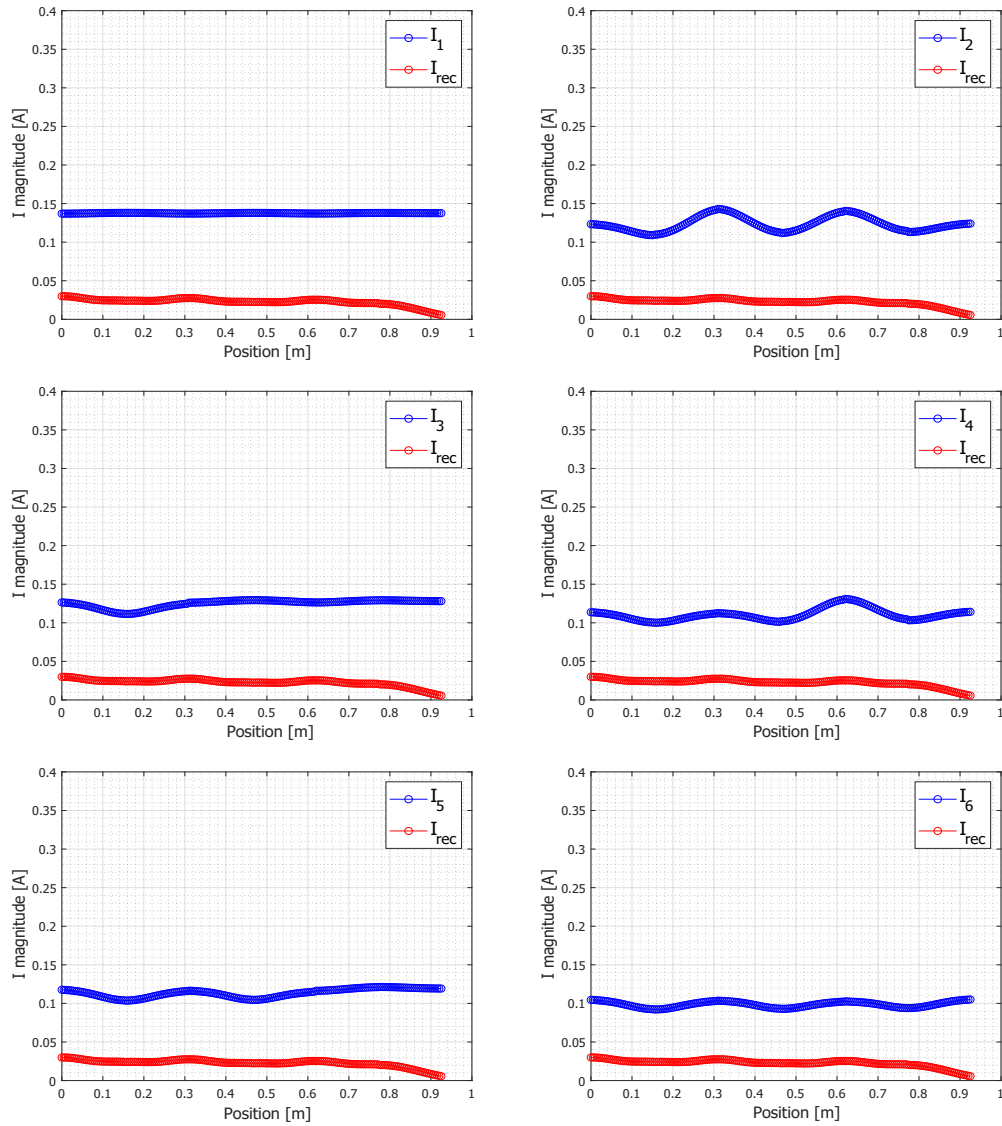


Figure 4.2.12: Comparison of the receiver current with the currents of an array with 6 resonators $z = 90mm$.

4.3 Conclusions

After the discussion of the results of the numerical simulations, the whole behavior in terms of currents has been described, helping the general understanding of the operation mode for this kind of apparatus. In particular, the previous paragraphs highlighted the unexpected trend of the currents for the even numbered cells, whereas the odd ones show a nearly constant magnitude for the current values. However, it is interesting to observe that each cell shows a similar behavior - of the current as a function of the receiver position - when the receiver covers cells that precede the one considered. In other words, each resonator of the array is affected in the same way until the receiver reaches it, as it is possible to see clearly in the graphs of figure 4.2.10, especially for the odd array resonators. This similarity is appreciable especially for the cells placed far from the power source, for which the receiver is placed between them and the power source for most of the simulations. In particular, the currents experience dramatic drops when the receiver covers the even numbered cells (preceding the one under analysis), whereas the same happens for the receiver current (red curve) resulting in important oscillations. This peculiarity can be addressed to the characteristics of the coupling between the receiver and the resonators, which results stronger with respect to the one experienced by the adjacent resonators of the array. Indeed, the maximum value of the mutual inductance for the minimum vertical displacement $M_{i,r}(x, z) |_{z=10mm}$ is equal to $4.8\mu H$ and then much greater than the value for adjacent array resonators, which is $1.5\mu H$. As a consequence, the major part of the magnetic flux produced by the array resonators is linked to the receiver rather than to the adjacent array cells and then the power tends to be absorbed by the receiver instead of propagating along the array structure. This phenomenon strongly depends on the mutual coupling $M_{i,r}(x, z) |_{z=10mm}$, which varies according to the position of the receiver along the array and the distance from this latter, reflecting its behaviour on the currents. As further proof, for an increased value of the mutual inductance between the receiver and the resonators, the currents appear more constant (and thus the power distributed more equally), as shown in figures 4.2.11 and 4.2.12. A receiver close to the power source can in this way compromise the possibility to feed further receivers that should

catch the power from the resonators of the array placed in the rest of the structure, even if this kind of study is beyond the aim of the thesis. Overall, it is difficult to define an analogy between the trends obtained for the array currents, even if it is possible to understand that complex phenomena related to the magnetoinductive wave are present. Indeed, this circuit interacts with the magnetic field generated in the coils of the structure, whose behaviour in case of an unloaded system, namely without the receiver, has been well described in [27]. In that case a wave - generated by the interaction between adjacent cells - propagates towards the last resonator and, if a perfect matching condition is realized, no reflections occur, as happens in our simulations. Once the receiver is placed above the cells, a voltage is induced in it, making a current flow and then a magnetic field interact with the magnetoinductive device inducing a reaction current. Its presence affects the magnitude and the phase of each current circulating in the array in different ways depending on the number of the cells and consequently the magnetic field, which is the crucial quantity for this kind of systems.

Chapter 5

Experimental Verification

In the previous chapters of this thesis lots of efforts have been spent to define a suitable model able to describe the behavior of an array of coupled resonators, in analogy with a one dimensional metamaterial structure. Until now, the analysis has been approached studying the currents circulating in the circuits by means of numerical simulations, whose results have been only partially confirmed. Indeed, the mutual inductance coefficients have been numerically evaluated by means of two equivalent approaches and then a comparison with the measured values reported in [27] has been done for the peak values, whereas the currents calculated in the previous chapter have not been validated yet. One of the main reasons that makes the analysis of the magnetic systems difficult to be approached is its dependence on the geometry, requiring to repeat the calculations for each variation that occurs. In this frame, it is possible to understand the difficulties encountered in the exploitation of the studies that can be found in literature, being them relevant to different apparatus. The only possibility that allow the theoretical model to be completely validated is to define and design an experimental prototype on which it is possible to lead all the tests and measurements required for the confirmation of the theoretical model. In this work, the apparatus exploited for the experimental verification is the the resonator array is the one available in the laboratory and has been fully describe in 5.1.3. If in the case of the mutual inductance only the maxima have been checked, the current trend as a function of the receiver displacement has been

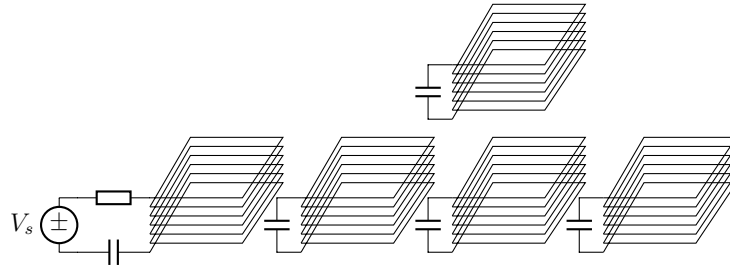


Figure 5.0.1: Representation of the resonator array with a receiver.

confirmed, providing an indirect validation also for the entire function $M_{i,r}(x, z) |_{z=const}$, being this latter the only unknown that affects the variables in the model.

5.1 Experimental Setup

The system that has been experimentally tested consists of an array of coupled coils working in resonance condition and by which is possible to transfer energy wirelessly. The apparatus geometry appears as a series of relay passive resonant circuits that are coupled thanks to the mutually linked flux and the resulting magnetic field allows the power to travel along coils. This particular behavior is appreciable for each system that presents a similar structure and, being them characterized by the same circuit model reported in 1.2.1, it is possible to treat this apparatus as a one dimensional magneto-inductive wave guide, also according to [26]. The type of resonators and their interactions are defined by the layout of the system and can be different depending on the application, whereas, in this research, the resonators have a square shape and are arranged over a surface, allowing a better coupling. Furthermore, resorting to the basic theory describing the behavior for this kind of objects, it is possible to increase the transmitted power through the coils thus improving the whole efficiency.

1.2.2. The size of the circuits depends both on the power transmitted - that affects the currents in the windings and then the size of the conductors - and the frequency of the supply voltage, whose fundamental component must oscillate at the resonant frequency in order to exploit the properties for metamaterials described in the chapter 1. In literature, being this kind of systems studied for the transmission of information, they usually operate

at very high frequencies, such as few tens of MHz, and very low power, namely just few watts. These characteristics lead to the choice of a single or multilayered flat resonator for the coils, that are printed on PCB and whose are supplied by signal generators reaching very high frequencies as reported in [33] and [9]. For what concerns high power applications, wound coils are usually employed, being both the voltage and the current higher with respect to the signal transmission apparatus. For the same reason, also the section of the conductors and the distance between them must increase, improving safety conditions. In this case the supply system is based on DC-AC power converters that can feed the circuit with a very high frequency voltage, even up to 300 kHz with the modern GaN and Sic switches. Working at these frequencies, the output stage is usually a square wave but the current circulating in the resonators is sinusoidal, since the resonant circuits behave as filter. According to [33] and [23], this is basically due to the high quality factor Q of the coils and allows simple power source configurations admissible.

5.1.1 Power Source

The aim of the analysis basically lies in the experimental validation of the numerical results and then of the theoretical model by which the performances are predicted. In this frame a low power test has been chosen, being it simpler to be implemented since it requires a small size signal generator while ensures a safer work environment. As consequence, a high frequency signal generator of the type “TG1010” has been used, manufactured by Thurlby Thandar Instruments. It is a 10MHz Programmable DDS Function Generator which has been connected to the terminals of the first resonator of the array.

5.1.2 Measurements Instrumentation

The results - given in terms of currents - have been obtained by means of proper measurements on the prototype. During the operations, both the currents and voltages have been monitored

by means of different probes of the oscilloscope Agilent “ Infiniium ” 54855A with a sampling capability of $2G\frac{Sa}{s}$ and bandwidth of $500MHz$. In particular:

- 4 Agilent voltage probes with attenuation ratio of 10:1
- 1 AC/DC current probe Tektronix TCP302 with variable attenuation ratio which signal has been processed through the amplifier Tektronix “TCPA 300”.

All the measured quantities were visualized and inspected connecting the probes to the oscilloscope, which is equipped with 4 different channels. In order to provide the right signal to be triggered, one of the 3 voltage probe connected to the instrument has been kept used for the voltage of the power source.

5.1.3 Array

Inductors The resonator array presented in this thesis is composed of 6 square coils made with stranded wire, being a cheap alternative to Litz wire. The stranded wire is an Alpha Wire PPE Hook Up Wire, $3.31mm^2$, 600 V 12 AWG composed of 65 tinned copper strands of 0.25mm diameter each, with a resulting conductor area of $3.31 mm^2$. Each wire was insulated with PPE (Polyphenylene Ether) and its total diameter was 2.97mm. The coils have been wound on a wood block of dimensions 153mm x 153mm x 29mm, where the indentation channel is 1.5mm deep and 18mm wide and in order to keep them tight around the wood core The wires have been wrapped on the channel with electrical black tape. The resulting winding presents six turns, as shown in figure 5.1.1.

The self-inductance of the coils has been numerically predicted as explained in the chapter 3, where a further comparison with the value obtained experimentally has been reported. In particular, the measurements have shown a value around $L = 12.6 \mu H$. The resonators were then placed side-by-side over a surface, as close as possible one to the other. The minimum separation distance is 0.6mm, defined by the insulation thickness of the wires, which is



Figure 5.1.1: Resonator prototype: stranded wire wound around square wood block.

0.3mm. In figure 5.1.1 the experimental prototype of the array of six resonators is shown, with the first resonator connected to the voltage generator and another equal resonator as load. It is interesting to notice that, despite the lower operating frequency, a large value of Q equal to 108 has been obtained, thanks to the large section of the conductor. Moreover, having a similar value of $|k| = 0.25$, it results $|kQ| = 27$ which is much higher than the value of 9.9 obtained for the planar multilayer coils studied in [27]. This leads to a lower attenuation, which is clearly observed in the efficiency measurements that is possible to find in Chapter 3 of [27], where for an array of 4 cells larger values are obtained in case of stranded wire resonators.

Capacitors The resonant frequency at which the system operates is usually chosen according to the applications and the features of the power supply, which represents the main limit in high power applications. Indeed, only in recent years the developments in the power switches allow output voltage frequency of hundreds of kHz to be achieved, as mentioned before. In the present case, it was chosen that the signal generator feeds the apparatus with a voltage at a frequency around 150 kHz , therefore defining the resonance for which the resonators are designed, which must be the highest possible as explained in chapter 1.



Figure 5.1.2: Experimental setup of an array of six resonators connected to the signal generator and loaded with an identical resonator acting as a receiver, placed over the last but one element.

Hence, the appropriate capacitance must be inserted in order to obtain the desired effect according to the commercial values available in the market. As consequence, two capacitors of $47nF$ in parallel were connected in series to the winding of each resonator, resulting in a total capacity of $94nF$. As it is well known, being the choice of the capacitor driven by the market availability, the desired value is difficult to be found, causing variations of the resonant frequency with respect to the calculated value. Furthermore, stray capacitances can affect the design value and they are mainly due to the physical connections and the adjacent wires of the windings that act as capacitive plates.

Resistors The resistors connected to the receiver and to the last resonator of the array have resistances $R_{load} = 5\Omega$ and $\hat{Z}_T = R_T = 1.5\Omega$, respectively; they are Thick Film resistors, with a rated maximum power of 100W. Furthermore, to improve the thermal dissipation capability of this components, heatsinks have been mounted over them, although not necessary during the present validation.

Parameter assessment The accuracy of a measurement is strongly affected by all the elements involved in the real system and, for this reason, parasitic affects can compromise the experiment. This happens as consequence of the nonideal behavior that characterizes the components and proper measurements must be performed in order to evaluate the effective values of the parameters. The experimental evaluation of the self-inductance, intrinsic AC resistance, added capacitance and resonant frequency of each resonator were determined through measurements using a Vector Network Analyser (VNA) and are reported in the following. Note that the results have been obtained as average of the maximum and minimum measured value for each parameter. In detail:

- The Self inductance of a coil L results $L = 12.6 \pm 0.1 \mu H$
- The whole capacitance of each cell results $C = 93.1 \pm 0.2 nF$
- The whole resistance of each cell results $R = 0.11 \pm 0.01 \Omega$
- The effective resonant frequency $f_0 = \frac{1}{2\pi\sqrt{LC}} = 147.0 \pm 0.5 kHz$

The mutual inductance between adjacent coils of the array must be derived from the measurement of the input impedance that the network analyzer sees when is connected to two coupled resonators, exploiting the following formulation

$$\hat{Z}_{in} = R + \frac{(\omega_0 M)^2}{R} \quad (5.1.1)$$

where \hat{Z}_{in} represents the impedance measured by the VNA and R is the whole resistance of the winding. Performing this computation, is possible to find the value $M = -1.55 \pm 0.05 \mu H$ for the mutual inductance, valid for each pair of coupled resonators of this type lying on the same plane in an horizontal configuration.

Receiver In order to analyze the capability of this apparatus of transmitting power wirelessly, a receiver has been placed over the array. In particular, for all the analyses - either

theoretical and experimental - a resonant coil identical to the ones used to create the array has been exploited as receiver, with the only difference that a resistive load has been added to the series of the coil and the capacitor. Being the receiver placed directly over the array, the minimum distance between the faced resonators is $10mm$ due to the wooden substrate. The measured mutual inductance between the receiver and an array resonator in case of perfect alignment has been obtained applying the formula (5.1.1) to the measurements conducted using the VNA, with which different vertical displaced couplings have been tested, In particular,

- A value of $M_{i,r} = 4.8 \mu H$ for the minimum distance $z = 10mm$
- A value of $M_{i,r} = 2.7 \mu H$ for the distance $z = 40mm$
- a value of $M_{i,r} = 1.2 \mu H$ for the distance $z = 90mm$.

5.2 Results

In this section the results of the measurements performed on the prototype are presented, discussed and compared with the values numerically estimated. In particular, the currents in the receiver and the resonators of the array have been validated. All the tests have been conducted with the same setup and the techniques explained above, sampling the currents for different position of the receiver placed over the array. The entire length of the structure has been swept with steps of $1mm$, reporting in the following plot the points for which notable changes in the current magnitude occurred. According to the previous chapter, the scale for the y-axis - namely the one for the current - has been chosen as the wider of the ones needed for all the circuits, helping to visualize the scale of the whole phenomenon; it ranges from 0 to $0.4A$. As first, in figure 5.2.1, the currents measured and calculated for the first resonator are plotted in blue and red, respectively, allowing a direct comparison of the two trends.

As it is possible to see, the measured values give life to a curve which accurately reflects the one calculated by means of the numerical model, presenting only a small reduction in

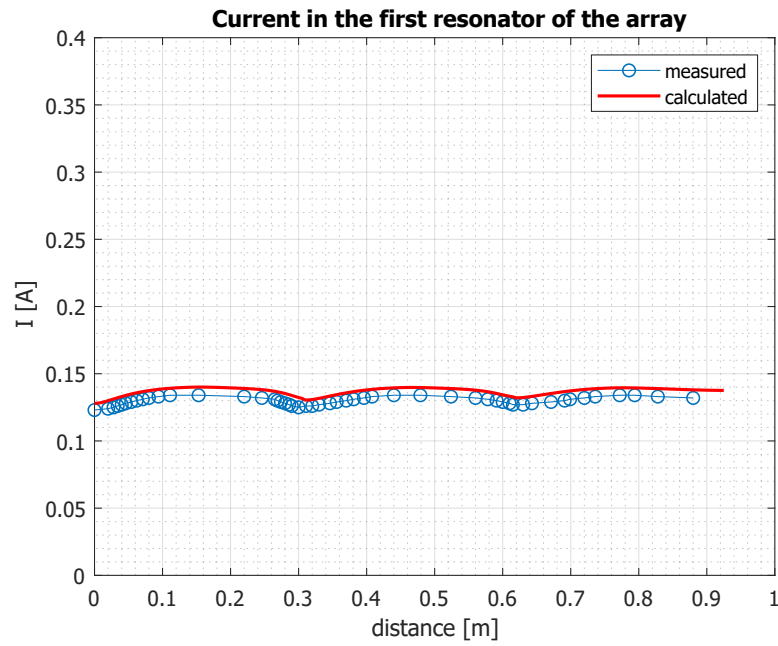


Figure 5.2.1: Comparison of the measured and calculated currents for the first resonator of the array.

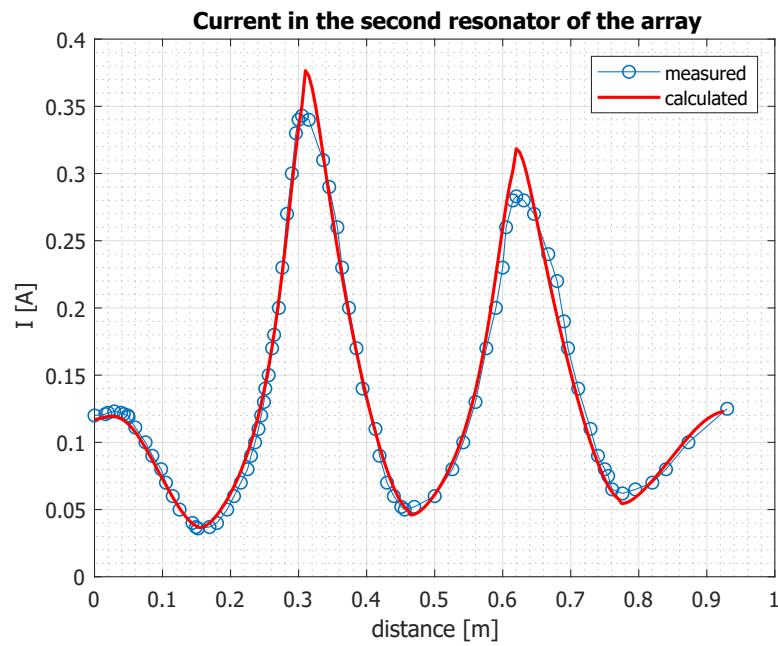


Figure 5.2.2: Comparison of the measured and calculated currents for the first resonator of the array.

the magnitude of $0.005A$ for the point of maximum and $0.004A$ for the point of minimum with respect to the predicted values, resulting in errors of 5.5% and 5% respectively. The experimental trend appears more constant as the receiver displacement varies. However, these features make the experimental curve appear scaled down of a constant quantity and this difference can be traced back to the inaccuracy of the instruments as well as the error due to nonideal characteristics of the components. Indeed, as it is well known, there are two main categories of sources of uncertainty to be associated with the result of a measurement: sources that give rise to random uncertainty contributions and sources that give rise to systematic contributions to uncertainty. When repeated measurements of a quantity value are performed, the instrument reading may vary, particularly in its last decimal digits. This is due to the noise or disturbances that add during the measurement process, which can be of different types. In the same way, systematic errors can affect all the measurements and often their source is very difficult to find. The graph in figure 5.2.2 reports the trend of the measured and calculated currents for the second resonator of the array, confirming the prediction made and discussed in the paragraph above. Furthermore, it shows a similar characteristic for the error as happened in the first case described, despite its value is strongly amplified both for the peaks and the minimums. Indeed, for the point of maximum current - for which the error was maximum in the previous case - the numerical values double the ones experimentally assessed, resulting in a 9% of error, whereas for the minimum the error is reduced to some percent. In particular, this latter varies from the value of 1.5% for the first minimum that presents a numerical overestimation, whereas in the remaining two minima the error is around 3% being the experimental curve underestimated. The next focus is on the third resonator of the array, for which the current trend is reported in figure 5.2.3. Also in this case a small percentage of error is present making the experimental curve slightly shifted down with respect to the numerical one, but the error is distributed differently. Indeed, for most of the positions covered by the receiver, the values of the simulated and measured currents differ for only some percent and the comparison is characterized by a whole overestimation of the assessed values by the numerical code. A strange behavior can be noticed in the correspondence of the point of perfect alignment of the receiver with the

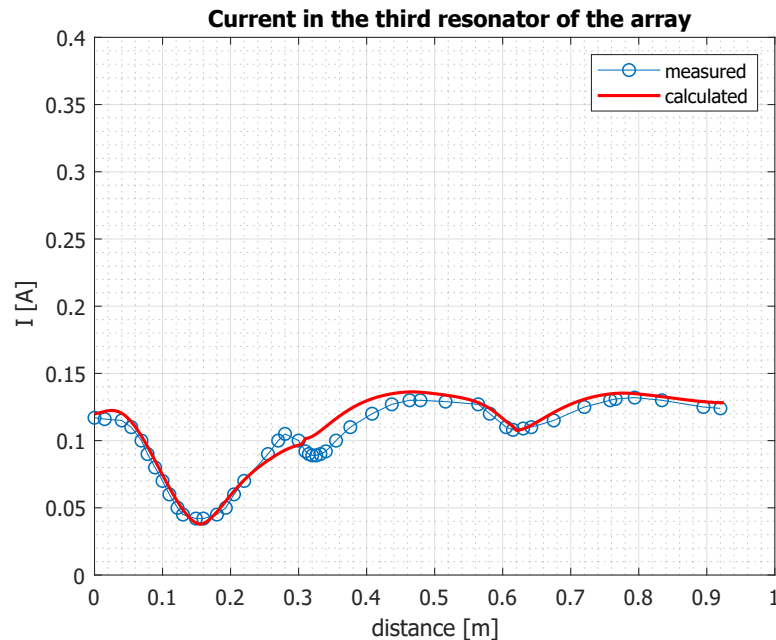


Figure 5.2.3: Comparison of the measured and calculated currents for the third resonator of the array.

third resonator, namely the one under analysis in this paragraph, which leads to a strong increase of the difference between the curves. In particular, for that position, an inflection in the current occurs and this detail has been found for both the measured and simulated values, even if it is more severe for the blue curve (i.e., the measurements). The error reached is around 15% with an underestimation of the experimental current on the left side of the inflection and an overestimation on the right side. The main reason that can justify the value of this error can be traced back to the impossibility of a real system to present a behavior so discontinuous as happened for the numerical red curve and some instabilities due to parasitic effects can alter the currents in the real prototype.

The current trend for the fourth resonator summarizes all the characteristics discussed for the previous case. Indeed, as it is possible to see in figure 5.2.4, the two curves present nearly equal values for positions of the receiver preceding the one representing the perfect alignment with the third cell, for which the above discussed current inflection again occurs. As a consequence, the error increases and presents a similar value (about 12%) as that for the previous resonator. According to the prediction, once the receiver overcomes an even

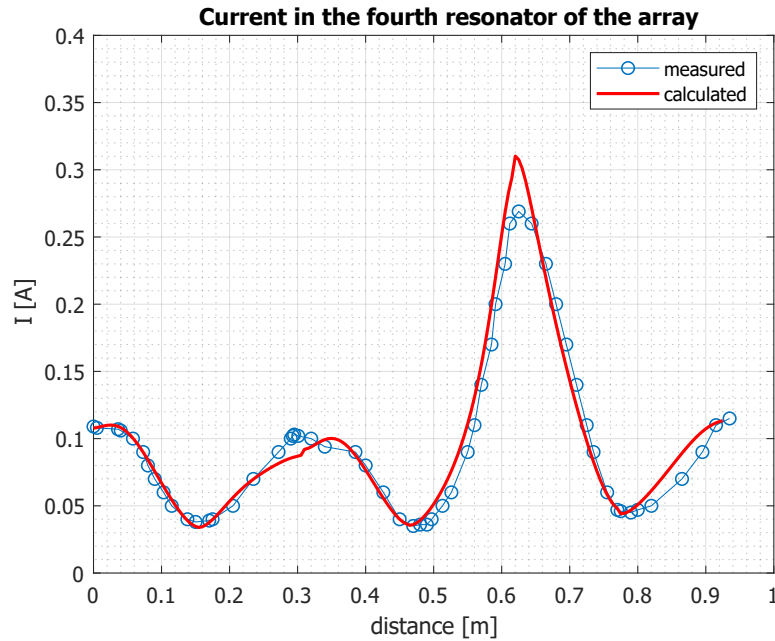


Figure 5.2.4: Comparison of the measured and calculated currents for the fourth resonator of the array.

numbered cell, the current experiences severe peaks, whose number depends on the length of the array and the experimental curve confirms this trend, despite an important error of a 13% in correspondence of the alignment with the subsequent resonator (in this case the fifth). The next picture reports the current values for the fifth resonator of the array and it is presented in figure 5.2.5. The experimental curve follows the one numerically estimated, even if large differences are present, especially when the receiver covers the odd numbered cells. These positions correspond to the points of maximum for the currents and the error reaches 15%, similarly to what happens for the other cells, whereas the minimum values of the measured and estimated currents correspond.

The current behavior for the last resonator of the array, namely the sixth one, is reported in figure 5.2.6 and the consideration just discussed for the previous cells applies again. This last element of the array is connected to the load that matches the array and it does not ever experience higher currents due to its characteristics. Indeed, the higher load due to the matching impedance decreases the current circulating in the coils and, furthermore, the receiver absorbs most of the power which travels along the structure, being it always placed

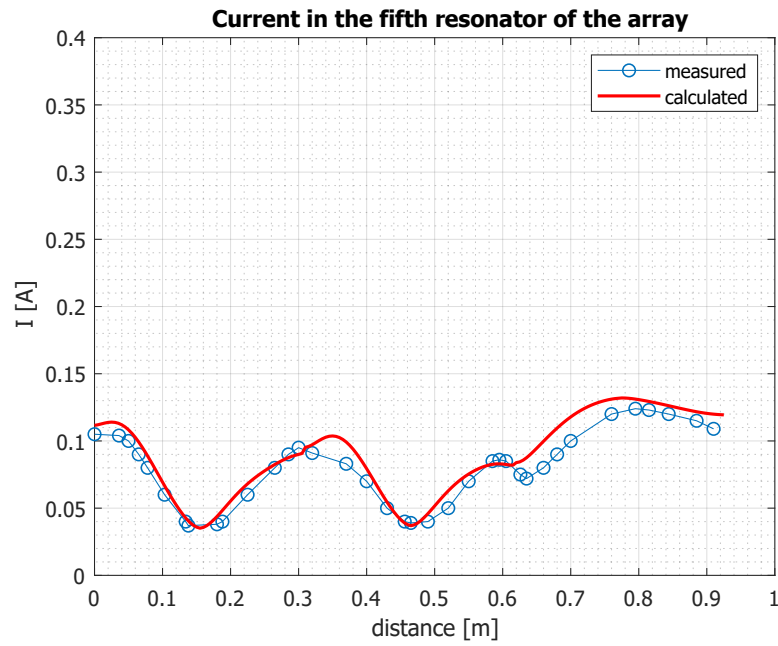


Figure 5.2.5: Comparison of the measured and calculated currents for the fifth resonator of the array.

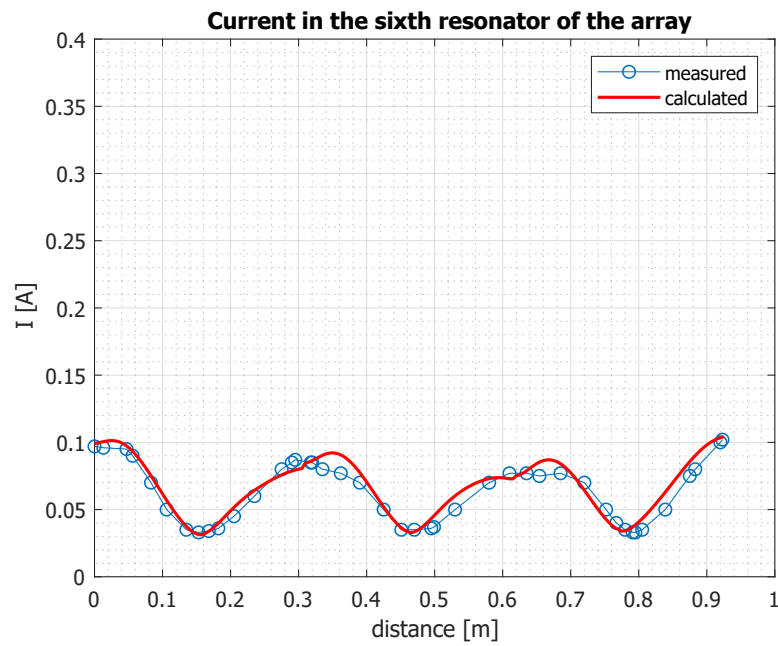


Figure 5.2.6: Comparison of the measured and calculated currents for the sixth resonator of the array.

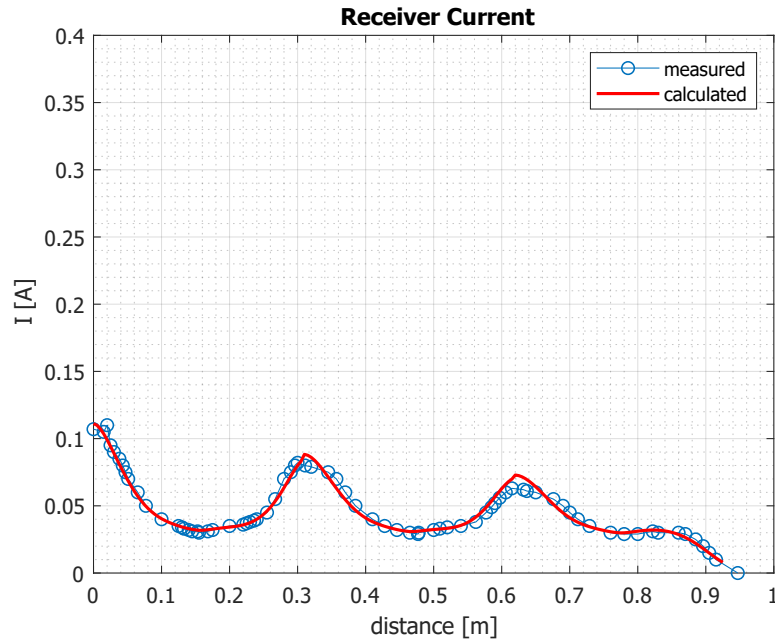


Figure 5.2.7: Comparison of the measured and calculated currents for the receiver.

between the power source and this last cell. It is now interesting to analyze the behavior of the receiver current, which has been plotted in figure 5.2.7 with the scale chosen as explained above. The two trends are nearly equal, with a percentage difference for the currents around 15% for the peaks and 8% for the minima of the functions. Once again, the characteristic of this error mirrors the one found for the other two cases, giving life to interesting discussion. No simple phenomena can be addressed as causes for this mismatching and they can be traced back to the damping effect due to the nonideal behavior of the components. Indeed, electric and dielectric losses act as parasitic resistance which determines the peaks to be damped and the whole behavior to appear shifted down of a variable quantity, thereby including dissipative effects that is difficult to model theoretically. In this frame, it is also possible to state that the more the resonator is placed far from the power source, the more the parasitic effects and nonidealities affect the error. Indeed, the only controlled quantity of the system is the voltage applied to the first resonator, for which the value is fixed by the generator and the rest of the apparatus operates thanks to the magnetic couplings. Considering an ordinary cell, the circulating current is powered by the induced voltage, which in turns depends on currents in the previous resonators and all the parameters that cannot be modeled. It is clear

that the error affecting the variables propagates, increasing its value, whereas the presence of enforced quantities could increase the possibility to stabilize it and improve the control of the apparatus operation.

Chapter 6

Force Calculation

6.1 Introduction

In the last 10 years, the interest in arrays of relay resonators or metamaterials exploited for wireless power transfer application has gain a lot of interest in the scientific and industrial world, as introduced at the beginning of this thesis. The research in this field is now trying to increase the transferred power with a continuous reduction in the dimensions of the apparatus, resulting in important improvements for what concerns performances and efficiency. In this frame, all the side phenomena that are involved in the transfer of energy - which are usually neglected - can affect the operation of the system, leading to a deviation from the predicted behavior. In particular, thermal and mechanical stresses could strongly modify the working condition and in some case completely compromise the operations, thereby requiring the an appropriate study. In the present chapter the focus is on the forces of electromagnetic origin acting on the the receiver circuit, that have been predicted and numerically evaluated, whit a consequent discussion of the results. The model considers the mechanical stress for each position of the receiver in stationary-space condition, whereas a dynamic action of this latter produces effects that can drop the hypothesis of sinusoidal condition (even if it could reveal the possibility to exploit mechanical work). The system considered in this thesis has been

already described several time but, for purpose of the the analysis presented in this chapter, a brief discussion about the mechanical configuration of the apparatus is necessary. Basically, the coils that constitute the inductive element off the array lies an a plane, placed side by side and are considered fixed with respect to the absolute reference system respect to which all the formulations are referred, thereby enforcing mechanical constraints for each direction. No mechanical degrees of freedom are allowed for the array coils. For what concerns the receiver, it is free to translate along the length of the array, whereas it can move away from this latter, resulting its position dependent on the x and y coordinates only. This consideration highlights the reason why the force calculation has been performed only for the receiver coil, for which the generated mechanical stresses can lead to unwanted deviation of its position.

6.2 Forces of electromagnetic origin

In physics the force experienced by a test charge q moving with velocity v is described as

$$\vec{f} = q\vec{E} + q\vec{v} \times \vec{B} \quad (6.2.1)$$

where \vec{E} is the electric field and \vec{B} the magnetic field present in that region. This equation is referred as Lorentz force and provides a definition of \vec{E} and \vec{B} . As it is possible to see the total force is given by two contributions: the first of electric origin which acts on a static charge and the second of magnetic origin, that depends moving charges. This latter is then related to a current, which is expressed as $q\vec{v}$ in case of a single charge. In the continuum theory the quantity involved refers to densities of charges and currents, namely ρ_f and \vec{J}_f respectively. As consequences forces are stated in terms of force density as

$$\vec{F} = \rho_f \vec{E} + \vec{J}_f \times \vec{B} \quad (6.2.2)$$

In this study, the physical phenomenon is based on a magnetic interaction of two coils and the energy is transmitted trough the magnetic field, thereby excluding the presence of an

electric field. Hence in the magnetic system considered the force density becomes

$$\bar{F} = \bar{J} \times \bar{B} \quad (6.2.3)$$

As already explained, the devices devote to this applications are basically constituted on magnetically coupled windings and then the force must be evaluated on the current-carrying conductors. In those cases the current can be assumed to be concentrated on the axis of the conductors and each time this hypothesis holds the current can be considered equally distributed in space, leading to the assumption of filiform current. The relationship between the current element can be expressed by means of the equation

$$\bar{J}dv = I\bar{dl} \quad (6.2.4)$$

where I is the amount of current considered uniformly distributed along the infinitesimal oriented length \bar{dl} . Thus, the force acting on the current element $I\bar{dl}$ in a magnetic field \bar{B} can be found as

$$d\bar{F} = I\bar{dl} \times \bar{B} \quad (6.2.5)$$

Considering the current I circulating in a closed path l (or a circuit) the force on the circuit can be calculated as

$$\bar{F} = \oint_l I\bar{dl} \times \bar{B} \quad (6.2.6)$$

and then, if I is constant along l it holds

$$\bar{F} = I \oint_l \bar{dl} \times \bar{B} \quad (6.2.7)$$

This formulation provides an alternative definition for \bar{B} , being defined as the force per unit of current element. It is important to underline that the magnetic field produced by the current element does not exert force on the element itself and then it must be to another element, namely to an external source.

6.2.1 Virtual work approach

This statement can appear obvious considering the force on a infinitesimal current element interacting with the magnetic field produced by itself, being it defined through the cross product between them. The magnetic field, in turns, lies along the direction given by the cross product between unitary vectors of the current element generating the field and the distance between the wire and the field point, leading to a resulting induction vector which is perpendicular to the generating current. It is clear that the resulting force provides a null contribution. However, the whole force acting on the circuit is obtained as the integral of this infinitesimal contribution and the interaction of different element of the same circuit could give life to non negligible mechanical effects, even if they are crossed by the same current. Indeed, the magnetic field that they generate has different direction depending on the orientation of the portion of circuit considered making this latter stressed by a force which originated by its current only. At this point, it is important to define the aim of the study which define the hypothesis and the limit of the model created. Indeed, as explained in the rows above, a winding is interested by force originated by the magnetic field produced by its current, which stress the object modifying its structure, resulting the main subject of the analysis if this latter aim to study the mechanical deformation of the coil. Instead, assuming the whole winding indeformable, it is possible to prove that the magnetic field produced by the current in the circuit does not produce any effects on the circuit itself. As result, the only mechanical interaction that originates is due to the a magnetic field external to the winding and the basic law for the statics can be resorted without any further consideration. The prove of this last statement can be approached by means the a virtual energy balance, namely the application of virtual work principle to the energy balance performed for the apparatus, which is reported in the following. As remind, it is important to underline the generality of this approach, being the virtual work a product of the application of the principle of least action to the study of forces and movement of a mechanical system. Indeed, among all the possible displacements that a system may follow, called virtual displacements, one will minimize the action. This displacement is therefore the displacement followed by the particle according to the principle of least action. The work of a force on a system along a virtual

displacement is known as the virtual work. The theorem states that, for a system in static equilibrium, to every virtual infinitesimal displacement in the phase space is associated a null mechanical work. In this context, it is possible to speak of virtual work, the mechanical work of a force relative to an infinitesimal virtual displacement (an instantaneous change of coordinates). First of all, the energy balance must be written for the magnetic system composed on coupled circuits, in the frame of virtual variations.

$$\delta W_g = \delta W_J + \delta W_m + \delta L \quad (6.2.8)$$

where

- δW_g represents the whole virtual energy provided by the generators
- δW_J represents the whole virtual energy dissipated due to Joule effects
- δW_m represents the virtual variation of magnetic energy
- δL represents the virtual work of the magnetic field forces

In order to refer the balance to the array of resonators, the generalized Ohm's law have to be resorted and applied to the apparatus. Then, for the a generic coil holds

$$v_i = R_i i_i + \frac{d\Phi_{ci}}{dt} \quad (6.2.9)$$

from which the power can be written as

$$v_i i_i = R_i i_i^2 + i_i \frac{d\Phi_{ci}}{dt} \quad (6.2.10)$$

and then

$$v_i i_i dt - R_i i_i^2 dt = i_i d\Phi_{ci} \quad (6.2.11)$$

Considering now all the n circuits by which the system is composed the virtual balance is defined as follows:

$$\sum_{i=1}^n v_i i_i \delta t - \sum_{i=1}^n R_i i_i^2 \delta t = \sum_{i=1}^n i_i \delta \Phi_{ci} \quad (6.2.12)$$

where the terms on the left side correspond to the virtual energy of the source δW_g and the energy dissipated due to Joule effect δW_J respectively. Now, replacing the 6.2.12 in 6.2.8, is possible to state

$$\sum_{i=1}^n i_i \delta \Phi_{ci} = \delta W_m + \delta L \quad (6.2.13)$$

Knowing that

$$W_m = \frac{1}{2} \sum_{i=1}^n \Phi_{ci} i_i \quad (6.2.14)$$

and assuming that the analysis is performed for constant value of the currents, the energy is expressed as

$$\delta W_m |_{i_i=const} = \frac{1}{2} \sum_{i=1}^n \Phi_{ci} i_i |_{i_i=const} \quad (6.2.15)$$

Considering an arbitrary virtual displacement $\delta \eta_r$ of the circuit r^{th} , it is possible to associate it to the virtual work system δL and then, replacing 6.2.15 in the equation 6.2.13, it results i

$$F_{\eta_r} \delta \eta_r |_{i_i=const} = \frac{1}{2} \sum_{i=1}^n \Phi_{ci} i_i |_{i_i=const} \quad (6.2.16)$$

where F_{η_r} is the force exerted on the circuit r^{th} by the magnetic field, in the direction of the displacement $\delta \eta_r$. The same equation can be written as

$$F_{\eta_r} |_{i_i=const} = \frac{1}{2} \sum_{i=1}^n i_i \frac{\partial \Phi_{ci}}{\partial \eta_r} |_{i_i=const} \quad (6.2.17)$$

and then, considering the relation between the resulting flux linked with the circuits i^{th} Φ_{ci} and the current by which it is produced

$$\Phi_{ci} = \Phi_{i,j} = M_{i,j} i_j \quad (6.2.18)$$

it is possible to express the 6.2.17 as

$$F_{\eta_r} |_{i_i=const} = \frac{1}{2} \sum_{i=1}^n i_i i_j \frac{\partial M_{i,j}}{\partial \eta_r} |_{i_i=const} \quad (6.2.19)$$

Theorem The magnetic field produced by a current does not exert any force on that current.

Proof In the hypothesis of consider a unique circuit in which the current i_1 circulates producing the magnetic field \bar{B}_1 and for which the self-inductance coefficient is $L = M_{1,1}$, the equation 6.2.19 become

$$F_{\eta_1} |_{i_1=const} = \frac{1}{2} i_1^2 \frac{\partial L}{\partial \eta_1} |_{i_1=const} \quad (6.2.20)$$

Being the inductance coefficients dependent on the geometry of the object only and supposing that no deformation occurs for the considered circuit in the virtual displacement η_r , then L does not vary and its derivative is null.

$$\frac{\partial L}{\partial \eta_1} |_{i_1=const} = 0 \quad (6.2.21)$$

As consequence, the force acting the current i_1 is null for an arbitrary virtual displacement.

$$F_{\eta_1} |_{i_1=const} = 0 \quad (6.2.22)$$

6.2.2 Magnetic field generated by the array

The force that acts on the receiver is due to the interaction of the current that circulates in the coil with the magnetic induction field in which the receiver lies, that can be assumed to be generated by the array currents only, thereby neglecting all the contributions due to external to the apparatus. Furthermore, being the system magnetically linear, it is possible

to consider the resulting magnetic field as the sum of the contribution of each array cell, leading to the following expression:

$$\bar{B}(\bar{p}) = \bar{B}_1(\bar{p}) + \dots + \bar{B}_i(\bar{p}) + \dots + \bar{B}_n(\bar{p}) \quad (6.2.23)$$

where $\bar{B}(\bar{p})$ is the total magnetic induction field evaluated in any point \bar{p} of the free space and $\bar{B}_i(\bar{p})$ is the magnetic induction field calculated in \bar{p} due to the current of the resonator i^{th} . Now, a focus on the methods for the evaluation of the magnetic induction of a single coil must be resorted and arranged in order too make the calculation as simple as possible. The classical approach refers to the force generated by moving charges and exploits the expression of the coulombian electric field generated by those charges. In terms of currents, it results in the well known Biot-Savart elementary formula, which allows the calculation of the magnetic field generated by a current element in a point \bar{p} of the space as follows

$$d\bar{B}(\bar{p}) = \frac{\mu_0 I}{4\pi r^2} d\bar{l} \times \bar{u}_p \quad (6.2.24)$$

where I is the current circulating in the element $d\bar{l}$, r^2 is the distance between the point \bar{p} and the element, \bar{u}_p the unitary vector of starting from the element $d\bar{l}$ and pointing the field point \bar{p} . The resulting field is the sum of the contribution of each current element and it can be obtained integrating along the circuit γ holding

$$\bar{B}(\bar{p}) = \frac{\mu_0 I}{4\pi} \int_{\gamma} \frac{d\bar{l} \times \bar{u}_p}{r^2} \quad (6.2.25)$$

The application of this formula for an infinite straight wire lead to the magnitude of the magnetic induction field for any point of the space

$$B(\bar{p}) = \frac{\mu_0 I}{4\pi r} \quad (6.2.26)$$

whereas for a finite straight wire of length l it results in the easy expression reported in

$$B(\bar{p}) = \frac{\mu_0 I}{4\pi r} (\sin\alpha + \sin\beta) \quad (6.2.27)$$

in which α and β are the angles centered in \bar{p} and formed by the distance r and the segments from \bar{p} to the two extremes of the wire. The direction of the magnetic induction field found with the laws (6.2.26) and (6.2.27) is expressed by means of the unitary vector defined a

$$\bar{u}_B = \bar{u}_l \times \bar{u}_p \quad (6.2.28)$$

where \bar{u}_l is the unitary vector for the direction of the current, which corresponds to the direction of the element \bar{dl} in this approximation. It is important to underline that this two expression for the magnetic field in a point of the space has a general validity, since they results from the direct integration of the 6.2.24.

6.2.3 Final formulation for the calculation of the fore action on the receiver

Thanks to its simplicity, the formula 6.2.27 can be exploited for the evaluation of the magnetic field generated by the coils of the array resonators and in order to do this, the force acting on a single element \bar{dl}_r of the receiver winding is found replacing the equation 6.2.27 in 6.2.5

$$\begin{aligned} \bar{dF}(\bar{p}) &= I_r \bar{dl}_r \times \left[I_i \frac{\mu_0}{4\pi r} (\sin\alpha + \sin\beta) \bar{u}_l \times \bar{u}_p \right] \\ &= \frac{\mu_0}{4\pi r} I_r I_i (\sin\alpha + \sin\beta) \bar{dl}_r \times \bar{u}_l \times \bar{u}_p \end{aligned} \quad (6.2.29)$$

The total force acting on the coil is then obtained as the sum of the elementary contributions \bar{dF} , namely it is expressed as the integral along the curve γ wich follows the path described by the circuit, leading t

$$\bar{F} = \int_{\gamma} \bar{dF} \quad (6.2.30)$$

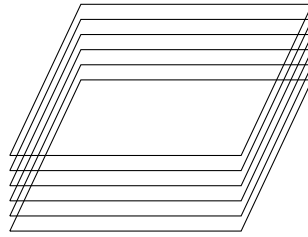


Figure 6.3.1: Representation of the coil exploited in the simulation.

6.3 Numerical model

The theoretical formulation of the problem has been developed in section 6.2 which shows the general approach for the mechanical action on a wire surrounded by a magnetic field, thus experiencing a force of electromagnetic origin. With reference to the array of resonators (equipped with a receiver) studied in this thesis, it is possible to observe that the overall magnetic field is the result of the action of each current present in the system, which in turn is characterized by a force. Even if any current element is not affected by a force induced by the magnetic field it generates, there is always a strong field due to the simultaneous presence of other sources and important attention must be paid in dealing with these quantities. The numerical implementation of this method has been done again in the Matlab environment, as it is for the rest of the analysis, allowing the exploitation of the results of the precedent codes and then leading to the definition of a whole model for the entire apparatus. The first step of the calculation is devoted to the evaluation of the magnetic field generated by the coils, which is based on the implementation of the formula (6.2.27). In particular, being the resonator coil composed of polygonal shaped turns (square in this case) it is easy to decompose it in straight filaments, each of them providing a contribution to the field at a point. In this way, that formula is directly applicable considering each segment and the point, whereas the total contribution for the field at a point can be obtained as the sum of these contributions. For a resonant array the currents have been calculated for each circuit involved in the apparatus and are exploited for the field and force calculations. It is important to notice that their behaviour is sinusoidal in time and all the analysis refers to steady-state conditions even if it has been repeated for different positions of the receiver incorporating in it the dependence

from the x -coordinate. This implies that the currents are considered as phasors, resulting in the following expression for the magnetic field magnitude of a single coil

$$\hat{B}_i(\bar{p})(x) = \sum_{k=1}^{N_{seg}} \frac{\mu_0 \hat{I}_i(x)}{4\pi r_k(\bar{p})} (\sin(\alpha_k(\bar{p})) + \sin(\beta_k(\bar{p}))) \bar{u}_k(\bar{p})(x) \quad (6.3.1)$$

The sum of vectorial quantities requires the direction of each contribution $\bar{u}_{B_i}(\bar{p})(x)$, that has been calculated according to (6.2.28) exploiting the Matlab functions already built in the code for the previous calculations. Those valuable algorithms allow the geometric model to be approached in a very general way, with the possibility to handle all the geometric objects defined in cartesian coordinates and find the related parameters such as angles, solid angles and distances. As last step for the calculation of the magnetic induction generated by the array, the influence of each resonator must be taken into account, summing for all the cells that are present, leading to

$$\begin{aligned} \hat{B}(\bar{p})(x) &= \sum_{i=1}^n \sum_{k=1}^{N_{seg}} \frac{\mu_0 \hat{I}_i(x)}{4\pi r_{i,k}(\bar{p})} (\sin(\alpha_{i,k}(\bar{p})) + \sin(\beta_{i,k}(\bar{p}))) \bar{u}_{i,k}(\bar{p})(x) \\ &= \frac{\mu_0}{4\pi} \sum_{i=1}^n \hat{I}_i(x) \sum_{k=1}^{N_{seg}} \frac{(\sin(\alpha_{i,k}(\bar{p})) + \sin(\beta_{i,k}(\bar{p})))}{r_{i,k}(\bar{p})} \bar{u}_{i,k}(\bar{p})(x) \end{aligned} \quad (6.3.2)$$

The remaining part of the code is devoted to the calculation of the force, for which the approach is defined in (6.2.7). In this case it is not possible to avoid the numerical integration as happened for the magnetic field, being the formula (6.2.27) the result of an exact integration. Then, the continuous model must be approached numerically, requiring the mathematical operator to be linearized. The basic methodology which is usually adopted for this kind of procedures requires the discretization of the integration region in elements that must be defined as small as possible - being them referred to as the infinitesimal quantity - with the following sum of each of them. Inside the length element \bar{dl}_r , the magnetic field is considered uniform, making it possible to assume that the force experienced by a current element is only due to the magnetic field in the center of it and then the element of force is found. This procedure represents the discretization of the formula (6.2.5), which can be

written for a general point of the space as

$$\begin{aligned}\hat{F}(\bar{p})(x) &= \hat{I}_r(x) \bar{d}l_r(\bar{p}) \times \hat{B}(\bar{p})(x) \\ &= \hat{I}_r(x) \hat{B}(\bar{p})(x) \bar{u}_r(\bar{p}) \times \bar{u}_B(\bar{p})\end{aligned}\quad (6.3.3)$$

It is clear that the dimension of the current element that discretizes the receiver winding is set depending on the number of points on that circuit for which the force is calculated. In order to get the whole force acting on the coil, the contributions of each point have to be summed together, leading to the expression (6.3.4), which represents the discrete form of (6.2.30).

$$\hat{F}_r(x) = \sum_{j=1}^{N_{discretizations}} \hat{F}(\bar{p}_{r_j})(x) \quad (6.3.4)$$

where in this case the points \bar{p}_r belongs to the curve representing the receiver circuit. It is important to underline that the length of the current elements of the receiver circuit determines the error made in the numerical approximation of the integral and it is controlled by varying the number of points \bar{p}_r that contribute to the sum.

6.4 Results

The implementation of this algorithm required few hundreds of code rows, whereas the amount of time needed for a calculation depended on the number of sections in which the length of the circuit has been discretized, namely the length of the current elements. In order to improve the accuracy of the results, different simulations have been performed varying this length, even if several runs have been crashed due to insufficient memory. The machine used for the calculations was equipped with 32GB of RAM memory, whereas at least 16GB were required for the complete calculus. The computational effort needed for the evaluation of the force has strongly increased with respect to the rest of the code, which was devoted to the calculation of the mutual inductance and the currents. Another impact factor that

contributes to make the simulation strategy very complex and computationally heavy is the dependence of the parameters on the space coordinate (x coordinate), condition that affects all the physical quantities involved in the model. Indeed, all the results has been stored point by point depending on the receiver position, namely performing a sort of discretization for the distance of this latter which has been measured from the position of perfect alignment with the first resonator of the array. The step for the variation of the x coordinate is set during the mutual inductance calculation and its value defines the accuracy of the parameter and therefore, it causes an error that propagates and affects also the results of the next calculations. The force on a coil is the result of the interaction of its current with a magnetic field, which is in turn determined by another current present in the system. Both of them are determined numerically and then are affected by an error, that must be combined with the one introduced by the integration process needed for the force evaluation. In order to understand the impact of this last approximation, different simulations have been performed changing the number of the discretized current elements \bar{dl} and are reported in the following. Before starting the discussion, the parameters of the system must be defined. In particular, the simulations have been performed for different values of \bar{dl} , whereas the other parameters were:

- number of resonators $n = 6$
- the square coils are the ones described in chapter 5.
- vertical displacement of the receiver with respect to the array $z = 10mm$
- current values calculated in chapter

Simulation 1 The first result reported has been obtained from the integration of the force element (6.3.3), which has been implemented as (6.3.3). The number of discretizations of each segment that composes the coil has been set equal to 153, corresponding to a current element which is $1mm$ long. All the simulations have taken few hours and consist of the sequence of the mutual inductance, currents and force calculations. The figures plot the whole force acting

on the receiver which is due to the magnetic field of the entire array, for each direction of the coordinate system. It is interesting to note that all the calculations have been done assuming steady state conditions for the whole system, allowing the representation of the electrical and mechanical state variables as phasors in a Steinmetz plane. The resulting force is a vector of the 3-D space, whose magnitude is a sinusoidal function of the time, since it is originated from sinusoidal currents. This means that, for each point of the space, the force oscillates around its average value and then the magnitude of each complex function has been plotted with respect to the displacement of the receiver. In figure 6.4.1 is reported the x component of the force, namely the force acting in the direction of the receiver (coincident with the array axis) pointing towards the last cell of the array. Its behavior is strongly nonlinear, nearly shaky and it is very difficult to be described by a function. Despite its shape, the curve clearly shows severe peaks in correspondence with the position of perfect alignment with the first and third cells, namely for the positions about 0 m and 0.3 m. The reason can be found looking at the currents circulating in the cells covered by receiver reported in 4.2.9 and the receiver itself for a certain position, being the force directly associated to the currents. It must be observed that many mathematical operators manipulate the currents, which are both functions of the time and space and then the result is very difficult to be predicted in this way. However, the presence of severe peaks in the current of the second resonator can induce a relatively high value of the magnetic field in the array resulting in peaks of force, since the receiver current is characterized by maxima for the same positions. For what concerns the first relative maximum (occurred for $x = 0$), it is possible to state that it is due to the high value of the current in the first cell, which remains stable for the entire sweep along the array. The interesting event is represented by the minimum of the force in correspondence of the position $x = 0.62m$, namely when the receiver coil covers the fifth cell, for which the force becomes very small. This phenomenon appears very complicated to explain because the currents in the even numbered resonators experience very high values for this position (receiver aligned with the fifth cell), while the odd numbered ones show the same constant value. Intuitively, this leads to predict a second important peak for the forces, whereas its plot shows a minimum. The cause can be traced back to the phase shift

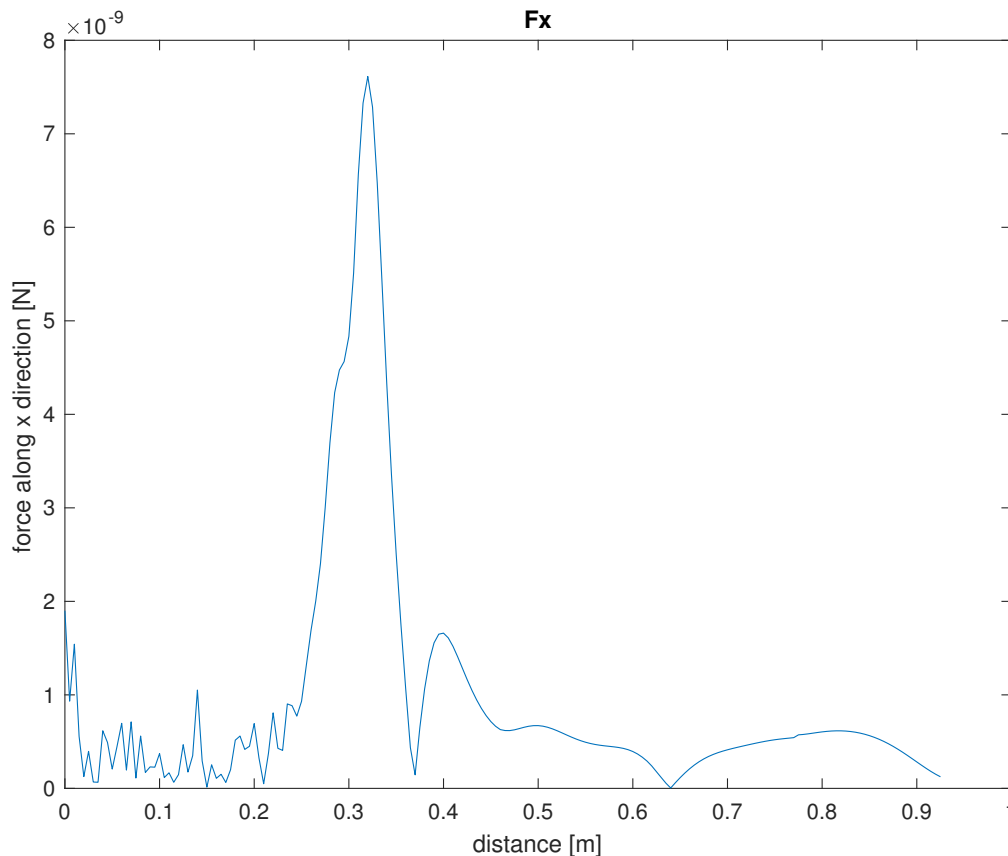


Figure 6.4.1: Force on the receiver along the x direction as function of the receiver displacement with a discretization for the current element of $0.5mm$.

experienced by the currents as consequence of the further inductive coupling introduced by the receiver. Indeed, the force is obtained as cross product between a current and a magnetic field, this latter in turn obtained by means of another cross product applied to similar quantities. This mathematical procedure leads to an extension of the complex space in which the phasors are defined, which became of the type \mathbb{C}^2 , thereby requiring to deal with quaternions and making the analytical approach very complicated. Despite all these considerations, the magnitude of the force along the array length is of the order of nN , difficult to be appreciated in physical reality. Such small values could be more subjected to numerical errors, especially in correspondence of the drastic variations that are very close to be considered discontinuities as well as they can cause an instability for the fitting polynomial (automatically set by the function “plot” on Matlab). For what concerns the force lying on the other two directions y and z of the space, they have been plotted in figure 6.4.2 and

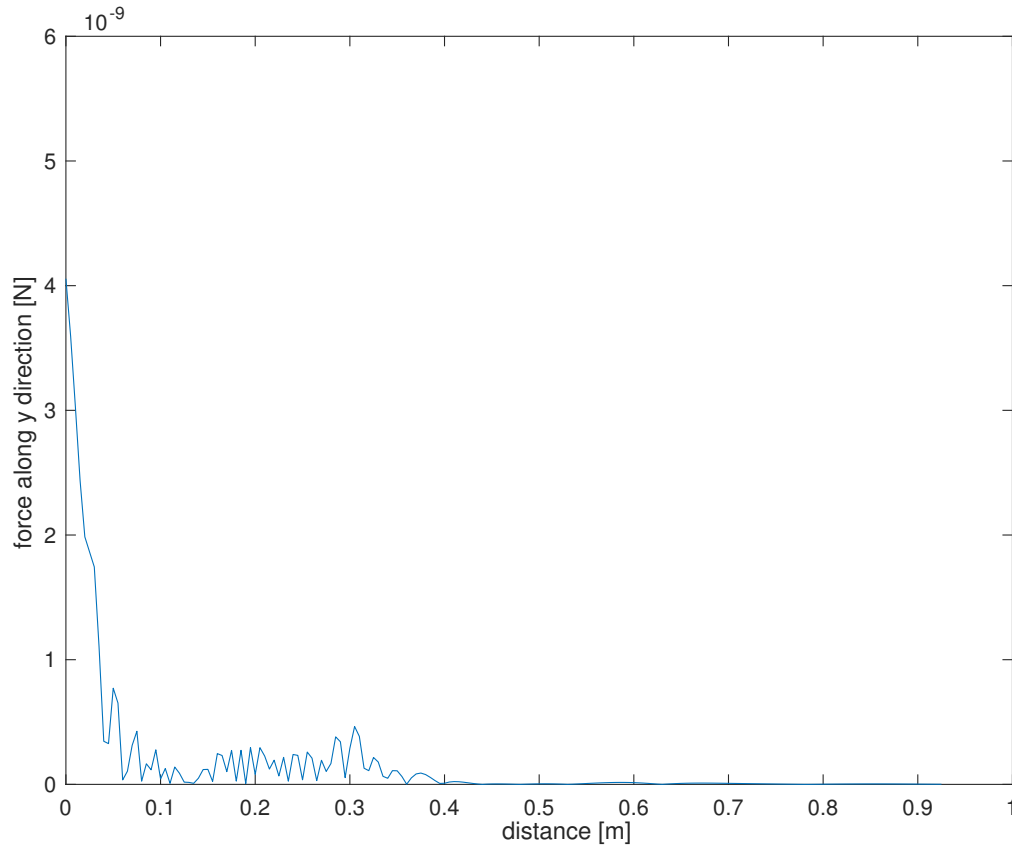


Figure 6.4.2: Force on the receiver along the y direction as function of the receiver displacement with a discretization for the current element of $0.5mm$.

6.4.3 respectively. The receiver experiences a force in the y direction only when it covers the first resonator of the array, whereas for all other position no relevant force has been found. In particular, little contributions originate for receiver displacements ranging from $0mm$ to $0.4mm$, namely in correspondence of the first 3 cells, becoming completely null for the rest of the structure. It must be noticed that when the receiver is placed at the beginning of the array there is no further source of magnetic field being capable to induce forces on it, leading to an y component of the force with a peak value of $4nN$, whereas in the other positions $F_y(x)$ appears overall compensated among the current elements. A perfect compensation occurs for the z component, meaning that the receiver is not subject to vertical thrust.

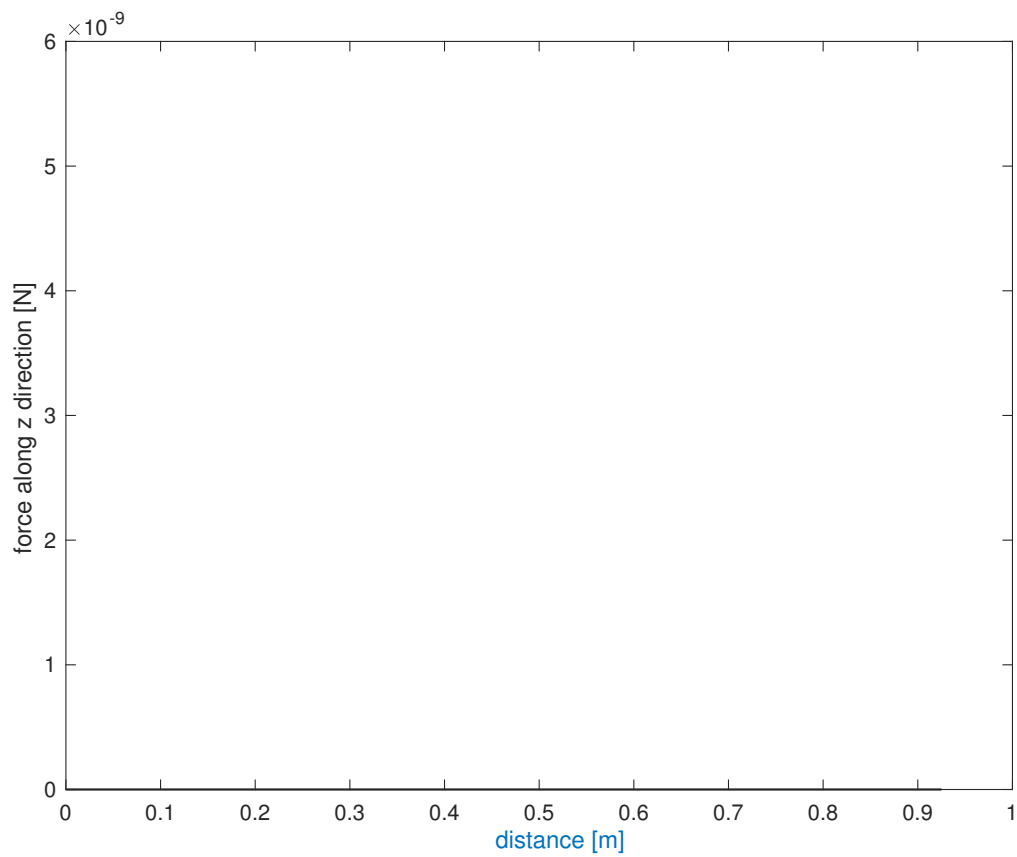


Figure 6.4.3: Force on the receiver along the z direction as function of the receiver displacement with a discretization for the current element of 0.5mm .

Simulation 2 The results of the numerical integration could be improved reducing the length of the current elements involved, as explained above, even if small integration elements could lead to round errors when their value is closed to the machine precision. The plots in the following figures have been obtained with a dl value of $0.1mm$, whereas about 36 hours have been taken by the calculator to complete the whole simulation. The component of the force on the receiver along the x direction has been plotted in figure 6.4.4 and shows a nearly equal trend even if the values experienced a strong reduction. Indeed, the main peak is reduced of 15% with respect to the value reported in 6.4.1, as it is for the rest of the points. Furthermore, an oscillation around that maximum occurred, probably due to a numerical round. Along the other directions the force calculated in this simulation is nearly identical to the one reported in 6.4 for each position of the receiver circuit.

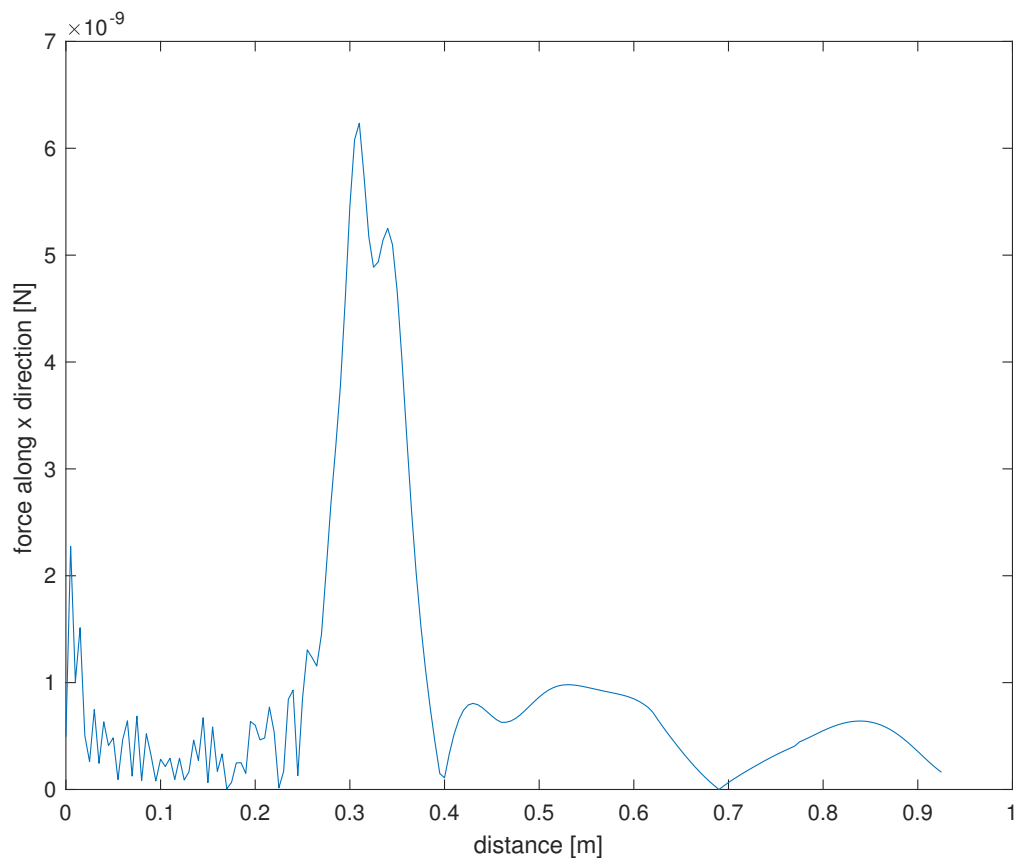


Figure 6.4.4: Force on the receiver along the x direction as function of the receiver displacement with a discretization for the current element of $0.1mm$.

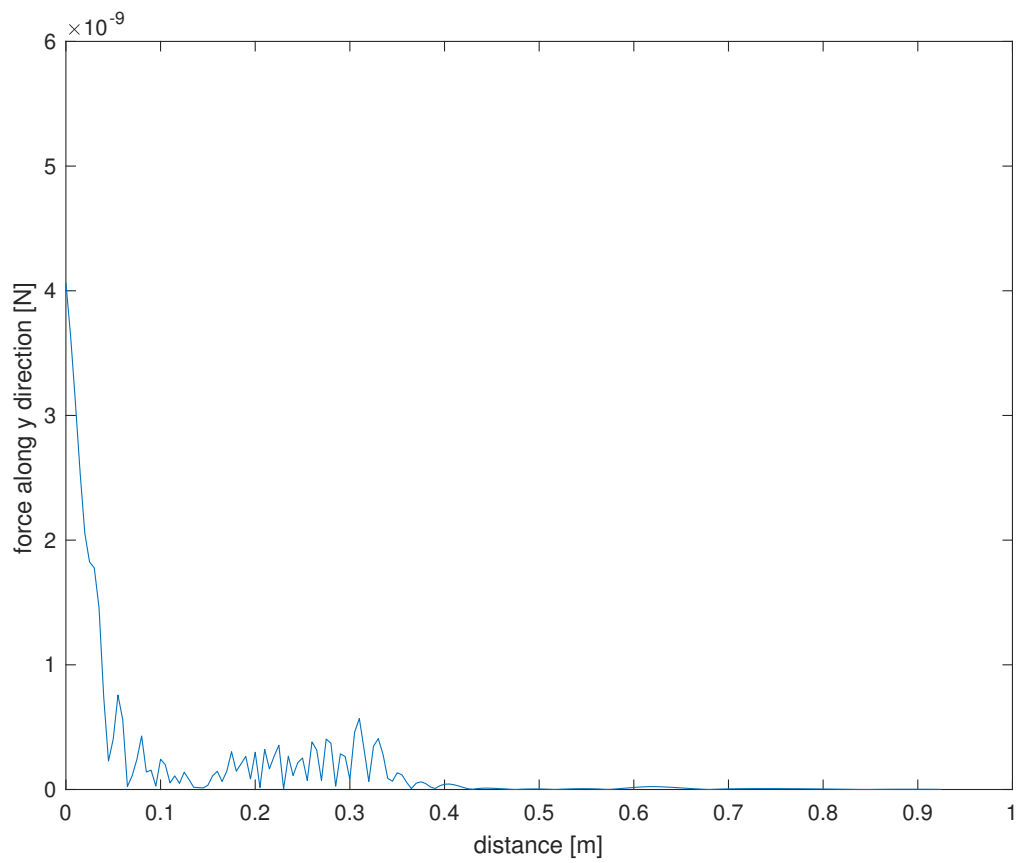


Figure 6.4.5: Force on the receiver along the y direction as function of the receiver displacement with a discretization for the current element of $0.1mm$.

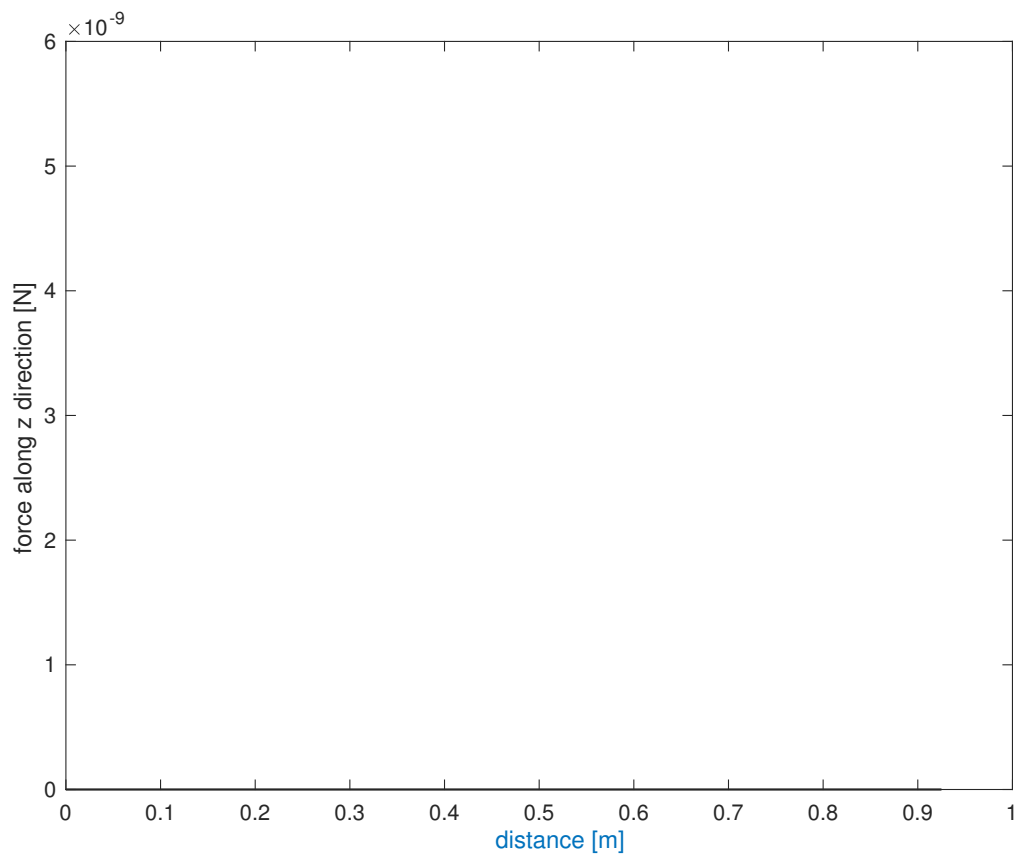


Figure 6.4.6: Force on the receiver along the z direction as function of the receiver displacement with a discretization for the current element of $0.1mm$.

Chapter 7

Conclusions

In this thesis the analysis of a resonator array for wireless power transfer has been deepened, developing a generalized circuit model for the system able to take into account different positions and configurations of the receiver and providing a supplementing mechanical characterization in static conditions. The study began with the definition of the Ohm's law that describes all the circuits of the array in a matrix formulation, by which the whole impedance matrix has been derived with assumption of neglecting all the terms describing the interaction of nonadjacent cells. This led to a tridiagonal matrix with equal elements along the diagonal, whereas the presence of the receiver introduces new terms that must be summed in the corresponding position. The same methodology has been followed also for different sizes of the receiver coil, which can cover more than one cell, leading to the general case in which all the resonators of the array face the receiver circuit. For this latter, the matrix resulted full of terms, whereas all the symmetries disappeared and no closed formulas are available for the solution of the system. The currents, indeed, have been obtained inverting the whole impedance matrix numerically, which has been done by means of a computer code valid for any geometry of the receiver circuit, resulting in a relatively fast algorithm able to solve the matrix Ohm's law simulating the behaviour of the apparatus. In order to evaluate the correct values for the impedances, a precise calculation of the mutual inductance coefficients was necessary and their results allowed the whole model to be generalized for each

position of the receiver along the array and represent the first part of the whole algorithm. The mutual inductance coefficients were calculated exploiting the so called “partial inductance approach” , whereas, a further validation of these coefficients has been done with a FEM software, which led to slightly different results due to the approximations that the two different methods assume. Indeed, it is possible to observe that following the field approach all the equations are defined and solved in the entire space, thereby ensuring to consider the electromagnetic interaction as a whole. However, the discretization of the domain necessarily lead to an error with affects the whole simulation. The partial inductance method, instead, considers the conductors as filaments, thereby assuming the current concentrated on the axis of each wire. In this way, it is possible to exploit the well known Neumann integral, at the cost of losing the information regarding the real extension of the object in the space. This approximation becomes quite weak when the coupled bodies are very close to each other, as it is attested by the error on the self-inductance. Indeed, the results obtained with the two methods present the greater error for the self-inductance, being its calculation based on the mutual interaction of the coil wires, whose are clearly at small distance. Despite this difference, both the solutions showed a change of sign of the mutual inductance between the receiver and a cell when the position of the former is about to leave the latter moving along the array, thereby indicating that the prevailing coil flux enters the surface bounded by the receiver circuit from the top instead than from the bottom. For greater distances the interaction becomes null, as expected. The following part of the code exploits the function $M(x)$ to build the impedance matrix and calculate the currents, whose behaviour turned out to be very surprising. Indeed, there is some periodicity in the currents trends defined as function of the receiver displacement, leading to different considerations. As first, it is important to notice that the currents circulating in the even numbered resonators of the array experience important peaks that could lead to severe overload compromising the operation of the system, whereas the ones for the odd numbered resonators are nearly constant. Furthermore, it is important to highlight that the current circulating in the array resonators which follows the one covered by the receiver experience very low values of the current and the same behaviour in the space. This means that most of the power is absorbed by the receiver circuit due to

the better coupling and then important Joule losses are saved. All these results have been experimentally validated with very low errors (around 5 to 10 percent) with measurements on the prototype. For what concerns the force calculation, a nontrivial integration has been performed numerically, requiring important computational effort even if no surprising results have been obtained. Indeed, the resulting force is in the order of nN , meaning that no notable mechanical stress affects the system, especially in case of low transmitted power. Before concluding, it must be noticed that the error affecting the currents is only due to the approximation with which the function $M(x)$ has been calculated, whereas the force calculation required an integration process that is very complicated to be performed, being its accuracy determined by the dimension of the current element that should be very small, theoretically almost nil. Overall, the analysis provides an important contribution to the model for this kind of apparatuses, that are becoming more and more important as solutions to improve the efficiency of the inductive power transfer.

7.1 Future perspective

The model presented in this thesis has been experimentally verified only for small power operations, whereas the high power performances should be simulated for a comprehensive validation even if no further phenomena are expected to affect its accuracy. Furthermore, this work refers to a system in which the receiver is fed in stationary positions, whereas all the physical quantities are assumed to be in steady state conditions. The natural improvement of the model is devoted to the analysis of the system for a dynamic change of the receiver position, which implies the motional effect to be included in the model. Indeed, the induced electromotive force in the receiver presents another contribution which is due to the variation of the coupling conditions, that are described by the mutual inductance and it is possible to prove that it is related to the velocity with which the receiver is moving. This kind of system can be exploited for the so called “dynamic charging”, which represents the actual challenge in WPT systems devoted to electric vehicle charging. To conclude, it must be noticed that the mathematical model of a physical system represents the first step needed

to fully understand its behaviour and then exploit its properties. All the engineered devices must be accurately designed and this study lays the foundations for the definition of a general methodology which takes into account all the key parameters that affect the performance of the system, with the subsequent aim of optimizing the whole apparatus.

Acknowledgments

I would like to express my truly gratefulness to my Principal Supervisor Prof. Leonardo Sandrolini for the constant guidance, encouragement and especially for his patience. I offer my sincere appreciation for the learning opportunities he offered me. Besides my Supervisor, I would like to thank my Co-supervisors Prof. Ugo Reggiani and Dr. Josè Alberto for their timely help and support. This work is the result of a continuous exchange of knowledge. For their continuous support, I am truly grateful.

I would like also to express my sincere appreciation to all the professors of the University of Bologna - Department of Electrical and Information Engineering, for their support towards the successful completion of my studies. Especially, I would like to truly thank Prof. Angelo Tani and his colleagues Dr. Michele Mengoni and Dr. Gabriele Rizzoli, who allowed me to widen my research from various perspectives. To Dr. Marco Landini, I would like to express my sincere appreciation for his invaluable guidance and support in the not trivial field of electromagnetism. This research could not have been accomplished without his assistance.

I would like to thank my “colleagues” at the University of Bologna for having become friends and traveling companions. In particular to Riccardo, who provided me the most useful and relevant advice that allowed me to complete this work in the best way possible.

The most grateful thanks go to my family, specially my mother and my father, that always encouraged me to try to reach my goals. You have made me what I am today and for this reason, I can only thank you. Finally, I express my deepest and heartfelt gratitude to

Carlotta. Your unwavering support and encouragement allowed me to overcome all the the obstacles, providing me unending inspiration.

To all those who are by my side every day, to all those who have been there and who will be there. Thanks.

Bibliography

- [1] G. A. Covic and J. T. Boys, “Inductive Power Transfer,” *Proceedings of the IEEE*, vol. 101, no. 6, pp. 1276–1289, jun 2013. [Online]. Available: <http://ieeexplore.ieee.org/document/6492113/>
- [2] W. C. Brown, “The history of wireless power transmission,” *Solar Energy*, vol. 56, no. 1, pp. 3–21, jan 1996. [Online]. Available: <https://www.sciencedirect.com/science/article/abs/pii/0038092X9500080B>
- [3] J.C.Maxwell, “A Teatrise on Electricity and Magnetism,” 1873.
- [4] N.Tesla, “System of transmission of electrical energy.” sep 1897. [Online]. Available: <https://patents.google.com/patent/US645576>
- [5] Z. Bi, T. Kan, C. C. Mi, Y. Zhang, Z. Zhao, and G. A. Keoleian, “A review of wireless power transfer for electric vehicles: Prospects to enhance sustainable mobility,” *Applied Energy*, vol. 179, pp. 413–425, oct 2016. [Online]. Available: <https://linkinghub.elsevier.com/retrieve/pii/S0306261916309448>
- [6] Z. Yang, W. Liu, and E. Basham, “Inductor Modeling in Wireless Links for Implantable Electronics,” *IEEE Transactions on Magnetics*, vol. 43, no. 10, pp. 3851–3860, oct 2007. [Online]. Available: <http://ieeexplore.ieee.org/document/4303216/>
- [7] Jaechun Lee and Sangwook Nam, “Fundamental Aspects of Near-Field Coupling Small Antennas for Wireless Power Transfer,” *IEEE Transactions on Antennas*

- and Propagation*, vol. 58, no. 11, pp. 3442–3449, nov 2010. [Online]. Available: <http://ieeexplore.ieee.org/document/5559351/>
- [8] Yungtaek Jang and M. Jovanovic, “A contactless electrical energy transmission system for portable-telephone battery chargers,” *IEEE Transactions on Industrial Electronics*, vol. 50, no. 3, pp. 520–527, jun 2003. [Online]. Available: <http://ieeexplore.ieee.org/document/1203003/>
- [9] R.-F. Xue, K.-W. Cheng, and M. Je, “High-Efficiency Wireless Power Transfer for Biomedical Implants by Optimal Resonant Load Transformation,” *IEEE Transactions on Circuits and Systems I: Regular Papers*, vol. 60, no. 4, pp. 867–874, apr 2013. [Online]. Available: <http://ieeexplore.ieee.org/document/6257504/>
- [10] A. Kurs, A. Karalis, R. Moffatt, J. D. Joannopoulos, P. Fisher, and M. Soljacic, “Wireless power transfer via strongly coupled magnetic resonances.” *Science (New York, N.Y.)*, vol. 317, no. 5834, pp. 83–6, jul 2007. [Online]. Available: <http://www.ncbi.nlm.nih.gov/pubmed/17556549>
- [11] Siqi Li and C. C. Mi, “Wireless Power Transfer for Electric Vehicle Applications,” *IEEE Journal of Emerging and Selected Topics in Power Electronics*, vol. 3, no. 1, pp. 4–17, mar 2015. [Online]. Available: <http://ieeexplore.ieee.org/document/6804648/>
- [12] A. P. Sample, D. A. Meyer, and J. R. Smith, “Analysis, Experimental Results, and Range Adaptation of Magnetically Coupled Resonators for Wireless Power Transfer,” *IEEE Transactions on Industrial Electronics*, vol. 58, no. 2, pp. 544–554, feb 2011. [Online]. Available: <http://ieeexplore.ieee.org/document/5437250/>
- [13] S. L. Ho, J. Wang, W. N. Fu, and M. Sun, “A Comparative Study Between Novel Witricity and Traditional Inductive Magnetic Coupling in Wireless Charging,” *IEEE Transactions on Magnetics*, vol. 47, no. 5, pp. 1522–1525, may 2011. [Online]. Available: <http://ieeexplore.ieee.org/document/5754800/>
- [14] S. Cheon, Y.-H. Kim, S.-Y. Kang, M. L. Lee, J.-M. Lee, and T. Zyung, “Circuit-Model-Based Analysis of a Wireless Energy-Transfer System via Coupled

- Magnetic Resonances,” *IEEE Transactions on Industrial Electronics*, vol. 58, no. 7, pp. 2906–2914, jul 2011. [Online]. Available: <http://ieeexplore.ieee.org/document/5560805/>
- [15] W.-S. Lee, W.-I. Son, K.-S. Oh, and J.-W. Yu, “Contactless Energy Transfer Systems Using Antiparallel Resonant Loops,” *IEEE Transactions on Industrial Electronics*, vol. 60, no. 1, pp. 350–359, jan 2013. [Online]. Available: <http://ieeexplore.ieee.org/document/6093746/>
- [16] T. P. Duong and J.-W. Lee, “Experimental Results of High-Efficiency Resonant Coupling Wireless Power Transfer Using a Variable Coupling Method,” *IEEE Microwave and Wireless Components Letters*, vol. 21, no. 8, pp. 442–444, aug 2011. [Online]. Available: <http://ieeexplore.ieee.org/document/5940188/>
- [17] T. C. Beh, M. Kato, T. Imura, S. Oh, and Y. Hori, “Automated Impedance Matching System for Robust Wireless Power Transfer via Magnetic Resonance Coupling,” *IEEE Transactions on Industrial Electronics*, vol. 60, no. 9, pp. 3689–3698, sep 2013. [Online]. Available: <http://ieeexplore.ieee.org/document/6226848/>
- [18] W. Niu, W. Gu, J. Chu, and A. Shen, “Coupled-mode analysis of frequency splitting phenomena in CPT systems,” *Electronics Letters*, vol. 48, no. 12, p. 723, 2012. [Online]. Available: <https://digital-library.theiet.org/content/journals/10.1049/el.2012.0953>
- [19] X. Wei, Z. Wang, and H. Dai, “A Critical Review of Wireless Power Transfer via Strongly Coupled Magnetic Resonances,” *Energies*, vol. 7, no. 7, pp. 4316–4341, jul 2014. [Online]. Available: <http://www.mdpi.com/1996-1073/7/7/4316>
- [20] E. Shamonina, V. Kalinin, K. Ringhofer, and L. Solymar, “Magneto-inductive waveguide,” *Electronics Letters*, vol. 38, no. 8, pp. 371–373, apr 2002. [Online]. Available: <https://digital-library.theiet.org/content/journals/10.1049/el{ }20020258>
- [21] E. S. Laszlo Solymar, *Waves in Metamaterials*, OUP Oxford, Ed., 2009.
- [22] C. J. Stevens, “Power Transfer via Metamaterials,” *Computers, Materials and Continua*, vol. 33, 2013.

- [23] —, “Magnetoinductive Waves and Wireless Power Transfer,” *IEEE Transactions on Power Electronics*, vol. 30, no. 11, pp. 6182–6190, nov 2015. [Online]. Available: <http://ieeexplore.ieee.org/document/6953328/>
- [24] R. Kshetrimayum, “A brief intro to metamaterials,” *IEEE Potentials*, vol. 23, no. 5, pp. 44–46, jan 2005. [Online]. Available: <http://ieeexplore.ieee.org/document/1368916/>
- [25] R. A. Shelby, D. R. Smith, S. C. Nemat-Nasser, and S. Schultz, “Microwave transmission through a two-dimensional, isotropic, left-handed metamaterial,” *Applied Physics Letters*, vol. 78, no. 4, pp. 489–491, jan 2001. [Online]. Available: <http://aip.scitation.org/doi/10.1063/1.1343489>
- [26] C. J. Stevens, “Some consequences of the properties of metamaterials for wireless power transfer,” in *2015 9th International Congress on Advanced Electromagnetic Materials in Microwaves and Optics (METAMATERIALS)*. IEEE, sep 2015, pp. 295–297. [Online]. Available: <http://ieeexplore.ieee.org/document/7342607/>
- [27] J. Alberto, “Mathematical Approach for an Accurate Solution of the Circuit Model of Resonator Arrays for Inductive Power Transfer,” Ph.D. dissertation, 2017.
- [28] G. Puccetti, C. Stevens, U. Reggiani, and L. Sandrolini, “Experimental and Numerical Investigation of Termination Impedance Effects in Wireless Power Transfer via Metamaterial,” *Energies*, vol. 8, no. 3, pp. 1882–1895, mar 2015. [Online]. Available: <http://www.mdpi.com/1996-1073/8/3/1882>
- [29] C. R. Paul, *Inductance : loop and partial*. Wiley, 2010.
- [30] F. S. Sandoval, A. Moazenzadeh, and U. Wallrabe, “Comprehensive Modeling of Magnetoinductive Wave Devices for Wireless Power Transfer,” *IEEE Transactions on Power Electronics*, vol. 33, no. 10, pp. 8905–8915, oct 2018. [Online]. Available: <https://ieeexplore.ieee.org/document/8126835/>

- [31] G. A. Campbell, “Mutual Inductances of Circuits Composed of Straight Wires,” *Physical Review*, vol. 5, no. 6, pp. 452–458, jun 1915. [Online]. Available: <https://link.aps.org/doi/10.1103/PhysRev.5.452>
- [32] Fralett Suarez Sandoval ; Ali Moazenzadeh ; Ulrike Wallrabe, “Magnetoinductive waves for wireless power transfer: challenges and solutions.” [Online]. Available: <https://ieeexplore.ieee.org/document/8278699>
- [33] G.Puccetti, “Enhancement of inductive power transfer with flat spiral resonators,” Ph.D. dissertation, 2015. [Online]. Available: <http://amsdottorato.unibo.it/7115/>
- [34] J. Alberto, “Circuit model of a resonator array for a WPT system by means of a continued fraction,” in *2016 IEEE 2nd International Forum on Research and Technologies for Society and Industry Leveraging a better tomorrow (RTSI)*. IEEE, sep 2016, pp. 1–6. [Online]. Available: <http://ieeexplore.ieee.org/document/7740586/>
- [35] W. Zhong, C. K. Lee, and S. Y. R. Hui, “General Analysis on the Use of Tesla’s Resonators in Domino Forms for Wireless Power Transfer,” *IEEE Transactions on Industrial Electronics*, vol. 60, no. 1, pp. 261–270, jan 2013. [Online]. Available: <http://ieeexplore.ieee.org/document/6041026/>
- [36] C. J. Stevens, “Magnetoinductive Waves and Wireless Power Transfer,” *IEEE Transactions on Power Electronics*, vol. 30, no. 11, pp. 6182–6190, nov 2015. [Online]. Available: <http://ieeexplore.ieee.org/document/6953328/>
- [37] B. T. Ranum, N. W. D. E. Rahayu, and A. Munir, “Development of wireless power transfer receiver for mobile device charging,” in *The 2nd IEEE Conference on Power Engineering and Renewable Energy (ICPERE) 2014*. IEEE, dec 2014, pp. 48–51. [Online]. Available: <http://ieeexplore.ieee.org/document/7067237/>
- [38] J. Alberto, U. Reggiani, L. Sandrolini, and H. Albuquerque, “ACCURATE CALCULATION OF THE POWER TRANSFER AND EFFICIENCY IN RESONATOR ARRAYS FOR INDUCTIVE POWER TRANSFER,” *Progress In*

- Electromagnetics Research B*, vol. 83, pp. 61–76, 2019. [Online]. Available: <http://www.jpier.org/PIERB/pier.php?paper=18120406>
- [39] J. Alberto, G. Puccetti, G. Grandi, U. Reggiani, and L. Sandrolini, “Experimental study on the termination impedance effects of a resonator array for inductive power transfer in the hundred kHz range,” in *2015 IEEE Wireless Power Transfer Conference (WPTC)*. IEEE, may 2015, pp. 1–4. [Online]. Available: <http://ieeexplore.ieee.org/document/7139136/>
- [40] E. Verband der Elektrotechnik and Institute of Electrical and Electronics Engineers., *MikroSystemTechnik 2017; Congress : 23-25 October 2017*. [Online]. Available: <https://ieeexplore.ieee.org/document/8278699>
- [41] S. Mohan, M. d. M. H. I. J. of solid ..., and undefined 1999, “Simple accurate expressions for planar spiral inductances,” *ieeexplore.ieee.org*. [Online]. Available: <https://ieeexplore.ieee.org/abstract/document/792620/>
- [42] F. S. Sandoval, A. Moazenzadeh, S. M. T. Delgado, and U. Wallrabe, “Double-spiral coils and live impedance modulation for efficient wireless power transfer via magnetoinductive waves,” in *2016 IEEE Wireless Power Transfer Conference (WPTC)*. IEEE, may 2016, pp. 1–4. [Online]. Available: <http://ieeexplore.ieee.org/document/7498834/>
- [43] M. Sadiku, *Elements of electromagnetics*. Oxford Univ Press, 2007.